
*Preparation and Properties of
Electrospun Polyacrylonitrile Fiber
Assemblies*

DISSERTATION

zur Erlangung des akademischen Grades eines
Doktors der Naturwissenschaften (Dr. rer. nat.)
in der Bayreuther Graduiertenschule für Mathematik und
Naturwissenschaften (BayNAT)
der Universität Bayreuth

vorgelegt von

Xiaojian Liao

Geboren in Ganzhou, Jiangxi Province, China

Bayreuth, 2020

This doctoral thesis was prepared at the department of *Macromolecular Chemistry II and Bavarian Polymer Institute* at the University of Bayreuth from 10/2015 until 12/2019 and was supervised by Prof. Dr. *Andreas Greiner*.

Date of submission: 16.01.2020

Date of defence: 15.06.2020

Acting director: Prof. Dr. Markus Lippitz

Doctoral committee:

Prof. Dr. Andreas Greiner	(reviewer)
Prof. Dr. Hans-Werner Schmidt	(reviewer)
Prof. Dr. Anna Köhler	(chairman)
Prof. Dr. Anna Schenk	
(additional reviewer: Prof. Dr. Stephan Förster)

Table of content

Table of content.....	1
List of publications	3
List of symbols and abbreviations.....	4
Summary/Zusammenfassung	8
Summary.....	8
Zusammenfassung.....	11
1 Introduction	14
1.1 High strength and toughness one dimensional fiber materials	14
1.1.1 Natural high strength and toughness fiber materials	15
1.1.2 Carbon-based high strength and toughness fiber materials.....	20
1.1.3 Polymer-based high strength and toughness fiber materials	25
1.2 Electrospinning.....	28
1.2.1 Electrospinning principles	29
1.2.2 Electrospinning materials.....	31
1.2.3 Electrospinning parameters	35
1.3 Electrospun fiber assemblies.....	36
1.3.1 1D electrospun fiber assemblies	37
1.3.2 2D electrospun fiber assemblies	43
1.3.3 3D electrospun fiber assemblies	44
1.4 Electrospun light-emitting fiber materials	48

Table of content

1.4.1 Processing of electrospun light-emitting fibers	48
1.4.2 Properties of electrospun light-emitting fibers	51
1.4.3 Applications of electrospun light-emitting fibers	53
1.5 Polyacrylonitrile	54
1.6 Thesis Objectives	57
1.7 References	59
2 Overview of the Thesis	72
2.1 High strength in combination with high toughness in robust and sustainable polymeric materials	73
2.2 Polarized blue photoluminescence of mesoscopically ordered electrospun non-conjugated polyacrylonitrile nanofibers	76
2.3 Impact of the Fiber Length Distribution on Porous Sponges Originating from Short Electrospun Fibers Made from Polymer Yarn	80
3 Publications	83
3.1 High strength in combination with high toughness in robust and sustainable polymeric materials	83
3.2 Impact of the Fiber Length Distribution on Porous Sponges Originating from Short Electrospun Fibers Made from Polymer Yarn	121
3.3 Polarized blue photoluminescence of mesoscopically ordered electrospun non-conjugated polyacrylonitrile nanofibers	134
4 Acknowledgements	160
5 (Eidesstattliche) Versicherungen und Erklärungen	163

List of publications

(1) X. Liao, M. Dulle, J. M. S. Silva, R. B. Wehrspohn, S. Agarwal, S. Förster, H. Hou, P. Smith, A. Greiner,

High strength in combination with high toughness in robust and sustainable polymeric materials,

Science, **2019**, 366(6471), 1376-1379.

(2) X. Liao, P. Hu, S. Agarwal, A. Greiner,

Impact of the Fiber Length Distribution on Porous Sponges Originating from Short Electrospun Fibers Made from Polymer Yarn,

Macromolecular Materials and Engineering, **2020**, 1900629.

(3) X. Liao, F. J. Kahle, B. Liu, H. Bässler, X. Zhang, A. Köhler, A. Greiner,

Polarized blue photoluminescence of mesoscopically ordered electrospun non-conjugated polyacrylonitrile nanofibers,

Materials Horizons, **2020**, 7(6), 1605-1612.

List of symbols and abbreviations

%	Percent
°C	Degree centigrade
1D	One-dimensional
2D	Two-dimensional
3D	Three-dimensional
AC	Alternate current
AIE	Aggregation-induced emission
Al	Aluminum
Ca	Calcium
Cd	Cadmium
cm	Centimeter
CNTF	Carbon nanotubes fiber
CNTs	Carbon nanotubes
Co	Cobalt
Cu	Copper
CV	Coefficient of variation
DC	Direct-current
EFYs	Electrospun fiber yarns
ELEF	Electrospun light-emitting fibers
Fe	Ferrum

List of symbols and abbreviations

GOF	Graphene oxide fiber
GPa	Gigapascal
GR	Graphene
graphene fiber	Graphene fiber
h	Hours
Hg	Mercury
J/g	Joule per gram
J/m ³	Joule per cubic metre
LC	Liquid crystals
Li	Lithium
MA	Major Ampullate
Mg	Magnesium
MI	Minor ampullate
mm	Micrometer
MPa	Megapascal
MPI	Vapor-phase Infiltration
Ni	Nickel
nm	Nanometer
OFET	Organic Field-effect Transistors
OLEDs	Organic Light-emitting Diodes
P3HT	Poly(3-hexylthiophen-2,5-diyl)

List of symbols and abbreviations

PAN	Polyacrylonitrile
PANi	Polyaniline
PA6	Polyamide 6
PA66	Polyamide 66
PCL	Poly(caprolactone)
PEG-BA	Poly(ethylene glycol) bisazide
PEO	Poly(ethylene oxide)
PES	Polyesters
PHBV	Poly(3-hydroxybutyrate-co-3-hydroxyvalerate)
PIs	Polyimides
PLA	Poly(lacticacid)
PLGA	Poly(lactic-co-glycolic acid)
PLQY	photoluminescence quantum yield
PMMA	Poly(methyl methacrylate)
PMIA	Poly(m-phenylene isophthalamide)
PPy	Polypyrrole
PS	Polystyrene
PVA	Poly(vinyl alcohol)
PVAc	Poly(vinyl acetate)
PVC	Poly(vinyl chloride)
PVDF	Poly(vinylidene fluoride)

List of symbols and abbreviations

QDs	Quantum dots
s	Second
S/m	Siemens per meter
SAXS	Small-angle X-ray Scattering
SEM	Scanning Electron Microscopy
SR	Stretch ratio
T _g	Glass transition temperature
Ti	Titanium
TPa	Terapascal
TTA	Triplet-triplet annihilation
UHMWPE	ultra-high molecular weight polyethylene
W	Watt
WAXS	Wide-angle X-ray Scattering
Zn	Zinc
μm	Micrometer

Summary/Zusammenfassung

Summary

The aim of this thesis was to prepare and investigate the electrospun fiber assemblies in different dimensions from one-dimensional (1D) fibrous yarns, two-dimensional (2D) fibrous membranes to three-dimensional (3D) fibrous sponges. The underlying concept was to organize the fiber alignment, hierarchical structures and interactions including the macroscopic fibril orientation in the yarns, the interconnection between the fibrils and the macromolecular orientation in the fibrils. Some designed strategies were carried out to pursue different performance in these electrospun fiber assemblies.

There is an intrinsic conflict in materials science between high strength and toughness, which is achieved in man-made single polymer nanofibers with ultrasmall diameter (less than 100 nm) by electrospinning. However, these single nanofibers are not robust enough to handle real-world applications. Natural fibers, such as dragline and recombinant spider silk, achieve the combination of high strength and toughness as well but their applicability is limited by either low availability or high prices for various applications. A straightforward concept to combine high strength and toughness was presented through the preparation of 1D polyacrylonitrile (PAN) fibers by yarn electrospinning, which creates fibers consisting of thousands of aligned fibrils in combination with a specified amount of an interconnecting linker – poly(ethylene glycol) bisazide (PEG-BA) (**Section 2.1**). Stretching at 160 °C with a stretch ratio of eight times could induce a high alignment of fibrils, and the adjacent annealing at 130 °C for 4 h under tension could lead to an azide cycloaddition reaction between the nitrile groups of PAN and bisazide groups of PEG-BA. The microstructures and crystal orientation of yarns with different stretch ratios at 160 °C were characterized by scanning electron microscopy (SEM), polarized Raman spectroscopy, wide/small-angle X-ray scattering and *in situ* X-ray diffraction measurements. The yarns obtained have a high tensile strength of 1236 ± 40 MPa, a modulus of 13.5 ± 1.1 GPa and a high toughness of 137 ± 21 J/g, which are similar properties to those of dragline spider silk.

Furthermore, designed 2D polarized photoluminescent fibrous membranes from non-conjugated polymer were prepared and investigated, as shown in the **Section 2.2**. We

designed three main rules for developing polarized photoluminescent materials from low-cost and easy-processable non-conjugated polymers or aggregation-induced emission (AIE) polymers: i) Electrospinning the non-conjugated or AIE polymer (PAN) into 2D fibrous membrane, ii) aligning the crystal arrangement by sufficient heat-stretching at 160 °C with a stretch ratio at 6 times, and iii) using functional cyano groups that show light-emitting when interactions between adjacent cyano groups lead to the formation of a more extended π -system. The obtained fibrous membrane exhibited a photoluminescence quantum yield of 30–32 %, which is remarkable for a simple non-conjugated polymer. Due to the contribution of $n-\pi^*$ transitions resulting from the nitrogen atoms in the cyano groups, intersystem crossing occurs that leads to the formation of highly mobile triplet states with quantum energy of about 2.5 eV and a lifetime up to 1 s. Meanwhile, these designed 2D fibrous membranes are also mechanically robust and flexible, with a high specific tensile strength of 534 ± 28 MPa*cm³/g and toughness of 79 ± 7 J/g. The combination of efficient polarized deep blue luminescence, room temperature phosphorescence, triplet-triplet annihilation (non-coherent photon upconversion), mechanical robustness and flexibility of these fibers opens up new avenues for applications of AIE polymers.

As shown in the **Section 2.3**, the pure PAN, highly aligned yarns, consisting of thousands of individual fibrils, were used to investigate the impact of the short fiber length distribution on the compressibility of the sponges. A new method for the preparation of short electrospun fiber dispersions with a controlled fiber length with low coefficient of variation (CV) was presented by cryo-microcutting of multifibrillar, highly oriented, pure PAN yarns. These short fibers exhibit tunable aspect ratios and narrow fiber length distribution, represented by the low CV values in the range of 15 to 20%. The 3D fibrous sponges obtained from these dispersions by freeze-drying showed similar pore size and pore size distribution but significantly higher compression strength and modulus for sponges with a low CV value of short fiber length. From this, we postulate that the mechanical properties of sponges could be tailored over a wide range by adjusting the fiber length, which provides an additional tool for the tuning of sponge properties in addition to chemical treatments.

In conclusion, the underlying context of this thesis is creating fiber assemblies with tailored properties through the organization of fiber alignment, hierarchical structures

and interactions of fibers in different dimensions. Three kinds of fiber assemblies with unique characteristics in different dimensions were prepared and investigated. The designed 1D fibrous yarns with highly alignment and connection of nanofibrils possess a combination of high strength and toughness. A mesoscopically ordered 2D fibrous membrane made from non-conjugated polymer exhibits polarized blue photoluminescence. The impact of the fiber length distribution on the compressibility of 3D porous sponges is analyzed quantitatively.

Zusammenfassung

Ziel dieser Arbeit war die Herstellung und Untersuchung von elektrogewebenen Fasern in verschiedenen dimensionalen Ausprägungen angefangen bei eindimensionalen (1D) faserhaltigen Garnen, zweidimensionalen (2D) faserhaltigen Membranen bis zu dreidimensionalen (3D) faserhaltigen Schwämmen. Das zugrunde liegende Konzept war hierbei die Organisation der hierarchischen Faserstrukturen und deren Interaktionen hinsichtlich makroskopischer Orientierung der Fibrillen in der Faser, der Verknüpfung der Fibrillen und der makromolekularen Orientierung der Fibrillen. Hierbei wurden einige speziell erstellte Strategien genutzt um verschiedene Eigenschaften in diesen elektrogewebenen Fasern zu erreichen.

Es gibt einen intrinsischen Konflikt innerhalb der Materialwissenschaften bezüglich hoher Festigkeit und Zähigkeit, welche durch elektrogewebene polymere Nanofasern mit sehr kleinen Durchmessern (weniger als 100 nm) erreicht werden können. Trotz allem sind diese einzelnen Nanofasern nicht robust genug, um tatsächlichen Anwendungen zu entsprechen. Ebenso kombinieren natürliche Fasern, wie der Abseilfaden der Spinne oder rekombinante Spinnenseide, hohe Festigkeit und Zähigkeit. Ihre Einsatzmöglichkeit ist jedoch aufgrund schlechter Verfügbarkeit oder hohen Preisen eingeschränkt. Ein einfaches Konzept um hohe Festigkeit und Zähigkeit zu erreichen wurde hier vorgestellt durch die Fertigung von 1D Polyacrylnitril (PAN) Garnen durch elektrogeweben. Wobei hier Garne aus tausenden von Einzelfasern in Kombination mit einer spezifischen Menge des Verknüpfers Polyethylenglycolbisazid (PEG-BA) (**Section 2.1**) hergestellt wurden. Durch Streckung bei 160 °C mit einem achtfachen Streckungsfaktor konnte eine hohe gleichseitige Ausrichtung der Fasern des Garns erreicht werden um anschließend bei 130 °C für 4h unter Spannung getempert zu werden. Dies führt zu einer Azid-Cycloaddition zwischen den Nitrilgruppen des PAN und den endständigen Azidgruppen von PEG-BA. Die Makrostrukturen und Kristallorientierung der Garne wurde bei unterschiedlichen Streckungsfaktoren bei 160 °C untersucht, durch die Methoden der Rasterelektronenmikroskopie (REM), der polarisierten Raman Spektroskopie, Weit- und Kleinwinkel Röntgenstreuung und *in situ* Röntgendiffraktometrie. Die Garne

haben einen hohen Zugwiderstand von 1236 ± 40 MPa, einen E-Modul von 13.5 ± 1.1 GPa und eine hohe Zähigkeit von 137 ± 21 J/g. Dies sind vergleichbare Eigenschaften zu denen des Abseilfadens aus Spinnenseide.

In **Section 2.2** wurden Fasermembranen von nicht konjugierten Polymere, welche 2D polarisierte Photolumineszenz zeigen, hergestellt und untersucht. Wir haben drei Hauptregeln für die Entwicklung von polarisierten Photolumineszenz Materialien von günstigen und einfach verarbeitbaren nicht konjugierten Polymeren oder Aggregation-induzierter Emission (AIE) Polymeren aufgestellt: i) Elektrospinnen von den nicht konjugierten oder AIE Polymeren zu 2D Fasermembranen, ii) anpassen der Anordnung der Kristallstruktur durch ausreichende Wärmestreckung bei 160 °C mit einem sechsfachen Streckfaktor und iii) Nutzung von funktionellen Cyanogruppen welche Lichtemittierung zeigen bei Interaktionen zwischen angrenzenden Cyanogruppen aufgrund der Ausbildung eines erweiterten π -Systems. Die Fasermembranen haben eine Photolumineszenz Quantenausbeute von $30-32$ %, dies ist ausgezeichnet für ein einfaches nicht konjugiertes Polymer. Aufgrund der Beteiligung des $n-\pi^*$ Übergangs durch die Stickstoffatome der Cyanogruppen erfolgen zwischen den Systemen Übertritte welche zu der Formierung von hoch mobilen Triplet Zuständen mit Quantenenergien von ungefähr 2.5 eV und einer Lebenszeit von bis zu 1 s führen. Dazu sind diese erzeugten 2D Fasermembranen mechanisch stabil und flexibel mit einer hohen spezifischen Zugfestigkeit von 534 ± 28 MPa*cm³/g und einer Zähigkeit von 79 ± 7 J/g. Die Kombination von effizienten polarisierten dunkel blauer Lumineszenz, sowie Phosphoreszenz bei Raumtemperatur, Triplet-triplet Auslöschung (nicht kohärente Photonen Ausbeute), mechanische Belastbarkeit und Flexibilität solcher Fasermembranen eröffnen eine Vielzahl von möglichen Anwendungen von AIE polymeren.

Darüber hinaus wurden hoch geordneten Garne bestehend aus tausenden von individuellen Fasern genutzt, um den Einfluss der Längenverteilung von Kurzfasern auf die Komprimierbarkeit der Schwämme zu untersuchen (**Section 2.3**). Eine neue Methode der Fertigung von kurzen elektrogewebenen Faserdispersionen mit kontrollierten Faserlängen mit niedrigen Variabilitätskoeffizienten über Cryo-Mikroschnitte der multifaserhaltigen, hoch orientierten reinen PAN Garnen wurde hierfür entwickelt. Diese Kurzfasern zeigen einstellbare Aspekt Verhältnisse und eine

schmale Faserlängenverteilung, dargestellt durch den niedrigen Variabilitätskoeffizienten mit Werten von 15.1 bis 20.0%. Die 3D Faserschwämme, welche über Gefriertrocknung der Faserdispersionen erhalten wurde, zeigten vergleichbare Porengrößen und Porengrößenverteilung aber signifikant höhere Kompressionsstärken und Moduln bei Schwämmen mit niedrigen CV Werten von kurzer Faserlänge. Dadurch können wir postulieren, dass die mechanischen Eigenschaften über einen großen Bereich von Faserschwämmen über Steuerung der Faserlänge eingestellt werden kann, wodurch ein weiteres Werkzeug zusätzlich zu der chemischen Behandlung für die Einstellung der Schwammeigenschaften erhalten wurde.

Der zugrundeliegende Kontext dieser Arbeit ist die Entwicklung von Faserverbänden mit massgeschneiderten Eigenschaften durch die Organisation von Faserausrichtung, hierarchischen Strukturen und Wechselwirkungen von Fasern in verschiedenen Dimensionen. Es konnten drei unterschiedliche Faserverbände mit einzigartigen Charakteristika in unterschiedlichen Dimensionen realisiert und untersucht werden. Durch eine gleiche Ausrichtung und ausgeprägte Konnektivität zwischen den einzelnen Nanofibrillen, weisen die erstellten 1D Fasergarne eine Kombination von hoher Festigkeit und Zähigkeit auf. Eine mesoskopisch geordnete 2D Fasermembran aus nicht-konjugierten Polymeren zeigen polarisierte blaue Photolumineszenz. Der Einfluss der Faserlängenverteilung auf die Kompressierbarkeit von 3D porösen Schwämmen wurde quantitativ untersucht. Hoffentlich ist es auf Basis dieser Arbeit möglich neue Materialien durch genau definierte elektrogewebene Faserverbände zu schaffen.

1 Introduction

The goal of this thesis is to prepare and investigate electrospun polyacrylonitrile fiber assemblies possessing unique characteristics in different dimensions, which require the exploration of the relationship between the macroscopic behaviors of fiber assemblies and the macromolecular orientation in the fibrils. The comprehensive overview of electrospinning fundamentals, on the one hand, and the electrospun fiber assemblies, on the other, will be addressed in this chapter. The electrospinning technique will include the principle, materials and methods which were used to generate submicrometer fibers. The following section will discuss the types, fabrication, properties and function of electrospun fiber assemblies with dimensions from one-dimensional (1D) fibrous materials, two-dimensional (2D) fibrous membranes and three-dimensional (3D) fibrous sponges. The interests in the 1D fibrous materials focus on the mechanical properties with the combination of high strength and high toughness, 2D fibrous materials on the functional properties and applications, and the new kind of 3D fibrous sponges investigate the impact the short fiber length distribution on their mechanical properties. The controlling of the characteristics and alignment of electrospun fiber and polymer are essential to designing the behavior of electrospun fiber assemblies. Therefore, the most relevant and recent advances related to the electrospun fiber assemblies, including high strength and toughness of 1D fibrous materials, photoluminescent 2D fibrous membranes and ultralight 3D uniform fibrous sponges, will be reviewed integrating the characteristics and alignment of electrospun fiber and polymer in this chapter. The thesis objective clarifies the aim of developing designed and promotional electrospun fiber assemblies in this context.

1.1 High strength and toughness one dimensional fiber materials

Modern applications, such as smart textiles, ultralight components of electric vehicles and flexible batteries, require materials which display a combination of high strength and toughness (average breaking energy of the samples) for sustainable performance. However, high strength and high toughness are generally mutually exclusive.¹ Thus, the development of high strength and tough materials, including the fibers, has traditionally been a motivation to compromise between strength and toughness.¹ Some of strategies in dealing with this conflict were reviewed from natural materials, carbon-based fibers to polymer nanofibers.

1.1.1 Natural high strength and toughness fiber materials

Recently, natural materials with the combination of strength and toughness, including wood, bone, teeth, fish scales, hairs, tendon, silk, and collagen, have been attracting many attentions.²⁻⁵ As 1D fiber materials, the natural silks from silkworms and spiders are two of the toughest materials known which possess high strength and toughness simultaneously.^{3,4} The spider dragline silk's strength reported of 1.1 GPa approaches that of typical high tensile engineering steel (1.3 GPa), but silks show a significantly lower relative density (1.3 g/cm³) than steel (7.8 g/cm³).³ Meanwhile, the average breaking energy for the sample threads, i.e. toughness, in control conditions was 165 ± 30 J/g.³ It is widely believed that the exceptional strength and toughness of silks arises from β -sheet nanocrystals that universally consist of highly conserved poly-(Gly-Ala) and poly-Ala domains. These β -sheet nanocrystals, bonded by means of assemblies of hydrogen bonds², provide rigid orderly domains and are embed in a semi-amorphous matrix consisting predominantly of less orderly β -structures, 3_1 helices and β -turns⁶⁻⁸ (**Figure 1.1 a**). The researchers think that as the silk fibers are exposed to stretch, these β -sheet nanocrystals reinforce the partially extended and oriented macromolecular chains by forming interlocking regions that transfer the load between chains under lateral loading, similar to the function in other mechanical proteins.^{2, 8, 9} Hence, β -sheet nanocrystals provide cohesion among the long polypeptide strands, enabling the amorphous domains to stretch significantly. As a result, the fracture of β -sheet nanocrystals occurs when there is large deformation and large loads.¹⁰

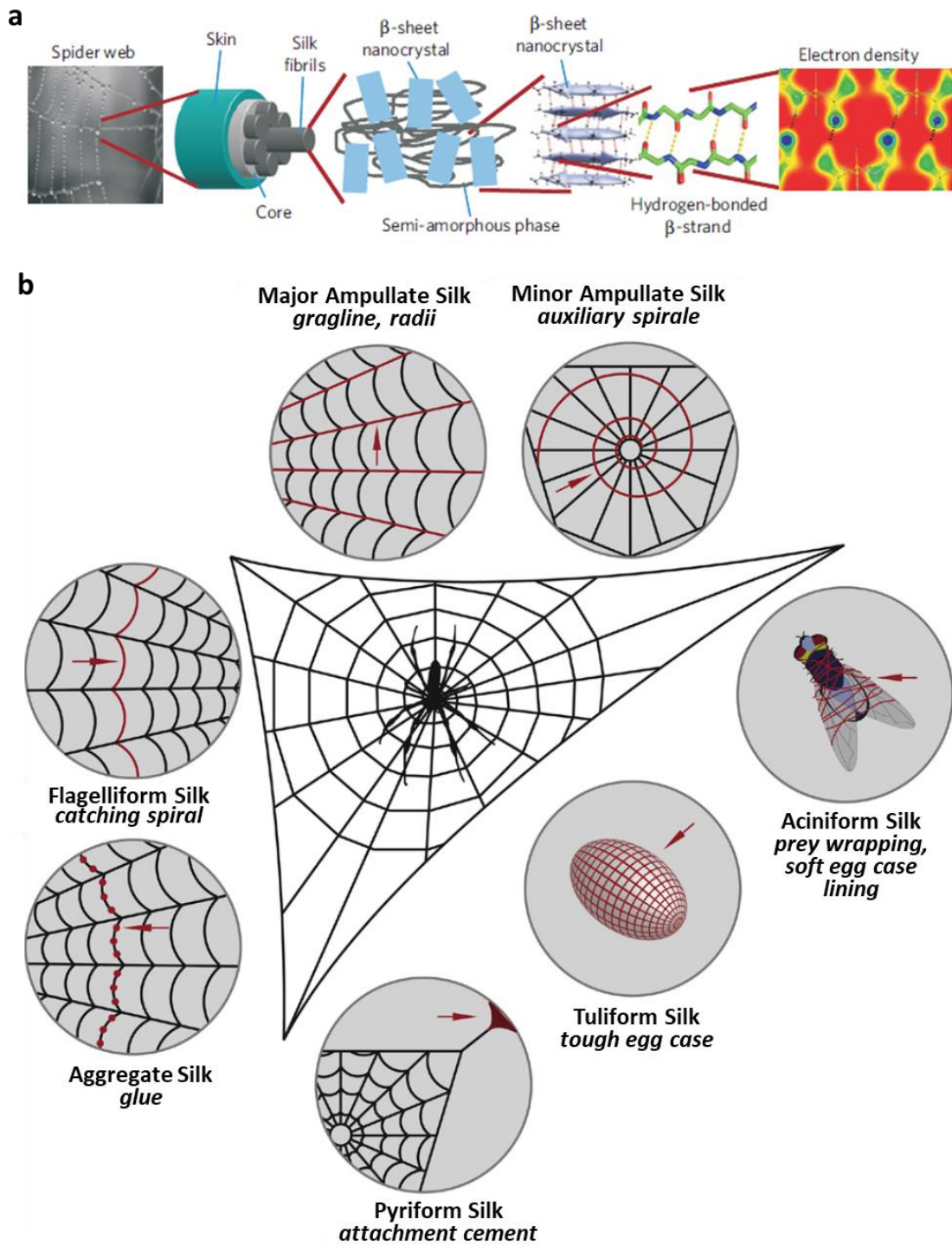


Figure 1.1. a, Schematic of the hierarchical spider silk structure that ranges from nano to macro including the electron density at the angstrom scale, hydrogen bonded β -strands, β -sheet nanocrystals, a hetero-nanocomposite of stiff nanocrystals embedded in a softer semi-amorphous phase and silk fibrils, which assemblies into macroscopical silk fibres. (Reprinted with permission from ref.². Copyright, 2010 Springer Nature.) b,

Schematic presentation of the six different types of spider silk fibers and one glue. (Reprinted with permission from ref.¹¹. Copyright, 2013 Elsevier Inc.)

Web spiders (*Aranea*), the most well-known order of the *Arachnida*, benefit from their silks every day. Scheibel *et al.* presented that some spiders, such as female orb-weavers, produced up to six different types of silks and one glue: Major ampullate/dragline silk, minor ampullate silk, flagelliform silk, pyriform silk, cylindrical/tubiform silk, aciniform silk and aggregate silk glue.¹¹ (**Figure 1.1 b**) Among these silks, the major ampullate/dragline silks show a good combination of high strength and toughness, as shown in the **Table 1.1**. F. Vollrath *et al.* investigated the mechanical properties of dragline golden silk produced under different spinning speeds (from 0.1 to 400 mm s⁻¹) and temperatures (from 5 to 40 °C). They argued that both trade-offs (between mechanical properties) and constraints (in the manufacturing process) have a large role in defining dragline spider silk.¹² B. Madsen *et al.* reported significant inter- and intraspecific differences in the mechanical characteristics of dragline silks collected from a range of spiders drawn from the *Argiopidae*, *Tetragnathidae*, *Theridiidae* and *Pisauridae*.¹³ They also studied the effect of the reeling speed on the mechanical properties of silk: (i) Breaking elongation decreased, (ii) breaking stress increased and (iii) Young's modulus increased with increasing reeling speed. However, different responses to the reeling speed treatments were observed in *N. edulis* and *Araneus diadematus* silks, which suggested differences in basic silk properties.¹³ M. Knez *et al.* designed a metal-incorporated protein matrix in the natural dragline spider silks by the multiple pulsed vapor-phase infiltration process to further improve the mechanical properties of the natural dragline spider silk (**Figure 1.2 a-e**). Different metals, such as zinc (Zn), titanium (Ti) or aluminum (Al) combined with water, were infiltrated into spider dragline silks and the resulting silks possessed a large enhancement in their mechanical properties. The tensile strength could increase to (4.2 ± 0.36) GPa and the toughness up to (1490 ± 22.0) J/m³. Importantly, this result (enhanced toughness of spider silk) could potentially serve as a model for a general approach to enhance the strength and toughness of other biomaterials.

Table 1.1. Mechanical properties of the different types of spider silk from different spiders. Values in the table are referenced by ref.¹¹.

Silk	Strength	Toughness	Modulus	Extensibility
	[MPa]	[MJ/m ³]	[GPa]	[%]
MA/Dragline <i>Argiope trifasciata</i>	1290	145	9.3	22
MI <i>Argiope trifasciata</i>	342	148	8.5	54
Flagelliform <i>Araneus diadematus</i>	500	150	0.003	270
Cylindriform <i>Argiope bruennichi</i>	390	128	9.1	40
Aciniform <i>Argiope trifasciata</i>	687	367	9.6	86

Typical commercial silkworm silk has moderate mechanical properties represented by a tensile strength of about 0.5 GPa, a toughness of about 60 J/g and a breaking elongation of about 15 %.⁴ Shao *et al.* fabricated the artificial reeling of silk from immobilized silkworms under steady and controlled conditions which produced fibers that are superior to naturally spun ones.⁴ They reported that the silkworm could produce stronger and more brittle fibers at faster spinning speeds, whereas slower speeds led to weaker and more extensible fibers. The final force-drawn silkworm fibers could compare favorably with *Nephila* spider dragline silk. Wang *et al.* obtained high strength silk fibers directly from silkworms by feeding them carbon nanotubes (CNTs) and graphene (GR) (**Figure 1.2 f and g**).^{14, 15} The CNTs or GR embedded silks by *in vivo* feeding can compare with the super silk fibers and even the spider fibers.

Furthermore, in order to increase the productivity of high strength silk fibers, lots of artificial silk fibers were developed by post-spinning recombinant spider silk proteins via metabolically engineered *E. coli* or transgenic goats. To date, the artificial silk fibers obtained have mechanical properties that were similar but still lower than those of

natural spider silk fibers.¹¹ Therefore, it is still a holy grail of silk research to fabricate high strength and tough artificial silk fibers similar to those found in natural silks.

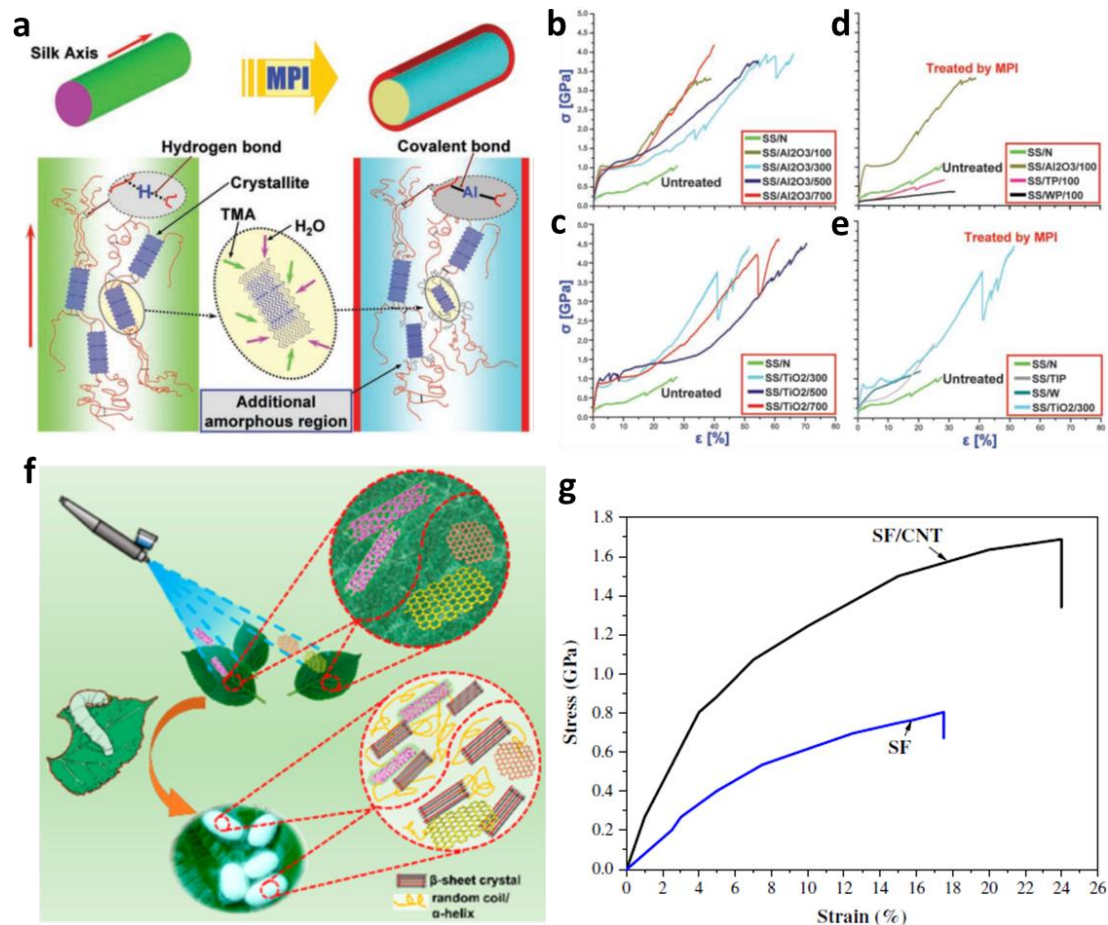


Figure 1.2. a, Schematic description of proposed molecular changes in the spider silk (SS) produced by the multiple pulsed vapor-phase infiltration (MPI). b-e, Tensile test curves of silk fiber samples treated by trimethylaluminum (TMA)/H₂O and (titanium(IV) isopropoxide) TIP/H₂O pulse exposure pairs and comparison to untreated samples and samples treated with various different processes. (Reprinted with permission from ref.¹⁶. Copyright, 2009 American Association for the Advancement of Science.) f, Schematic showing the natural process to incorporate CNTs or GR into silk by feeding silkworms with mulberry leaves spray-coated with CNTs or GR solutions. (Reprinted with permission from ref.¹⁴. Copyright, 2016 American Chemical Society.) g, A comparison of the stress and strain of silk fiber and CNT-embedded silk fiber. (Reprinted with permission from ref.¹⁵. Copyright, 2013 Elsevier B.V.)

1.1.2 Carbon-based high strength and toughness fiber materials

Carbon-based fibers are one of the most attractive materials in numerous applications. The carbon-based fibers generally include carbon fibers, CNT fibers (CNTF) and GR fiber (GRF) or GR oxide fiber (GOF).^{17, 18} The applications, such as flexible electronic fibrous conductors,¹⁹ actuators,²⁰ artificial muscles,²¹ solar cells,²² supercapacitors²³ and lithium ion batteries,²⁴ have been developed owing to their unique combination of light weight, superior conductivity, good flexibility, superb thermal conductivity, and good corrosion and oxidation resistivity.^{25, 26} Their excellent mechanical properties especially need to be pointed out: Carbon nanotubes with an inherent tensile strength higher than 100 GPa and a Young's modulus over 1 TPa,^{27, 28} and the GR with the highest mechanical strength of 130 GPa and modulus of 1100 GPa in the planar direction.^{25, 29, 30} Thus, lots of researchers have been searching for high strength and tough carbon-based fiber materials.

The CNT fiber is one of the typical 1D assembled fibers from numerous CNTs which was first proposed by Fan *et al.* in 2002.³¹ Until now, three main spinning processing, i.e. solution spinning,³²⁻³⁴ forest spinning^{35, 36} and aerogel spinning,^{37, 38} tailor CNTs fibers with different assembly structures and, consequently, different properties (**Figure 1.3**). Li *et al.* presented that: i) The CNTF made from solution spinning were short and densely packed; ii) CNTF made from forest spinning were relatively long (hundreds of micrometers), aligned but loosely packed; and iii) CNTF made from aerogel spinning were long (up to millimeters), entangled but also loosely packed.¹⁹³ Dalton *et al.* fabricated super-tough CNTs/PVA composite fibers with a tensile strength of 1.8 GPa and a super high toughness of 570 J/g by utilizing a solution spinning process(**Figure 1.3 j**).³² They found the largely amorphous PVA formed a coating on the nanotubes which could provide an important interphase region among CNTs and serve a similar function (extension in the amorphous regions between relatively rigid blocks) to the spider silk fibers. Thus, the super high toughness might be attributed to the slippage between individual nanotubes within bundles. Though the CNTs/PVA composite fiber shows a high strength and toughness, the electrical conductivity is so low that charge/discharge rates for fiber-based supercapacitors are limited. In 2004, Baughman *et al.* obtained single or multi-ply, torque-stabilized CNT yarns by introducing twist during spinning of multiwalled CNTs from nanotube forests, which

not only possess high strength but also maintain high conductivity.³⁵ With the development of this method, the tensile strength of these CNT yarns could reach 1.8 GPa (Figure 1.3 k).³⁶ Some CNT bundles with tensile strength over 80 GPa (corresponding to an engineering tensile strength of 43 GPa) were reported by Wei *et al.* in 2018. These were developed by aerogel spun processing and are the strongest fibers in the world (Figure 1.3 l).³⁷ The fabricated CNT bundles consist of a large number of components with parallel alignment, defect-free structures, continuous lengths (several centimeters long) and uniform initial strains.

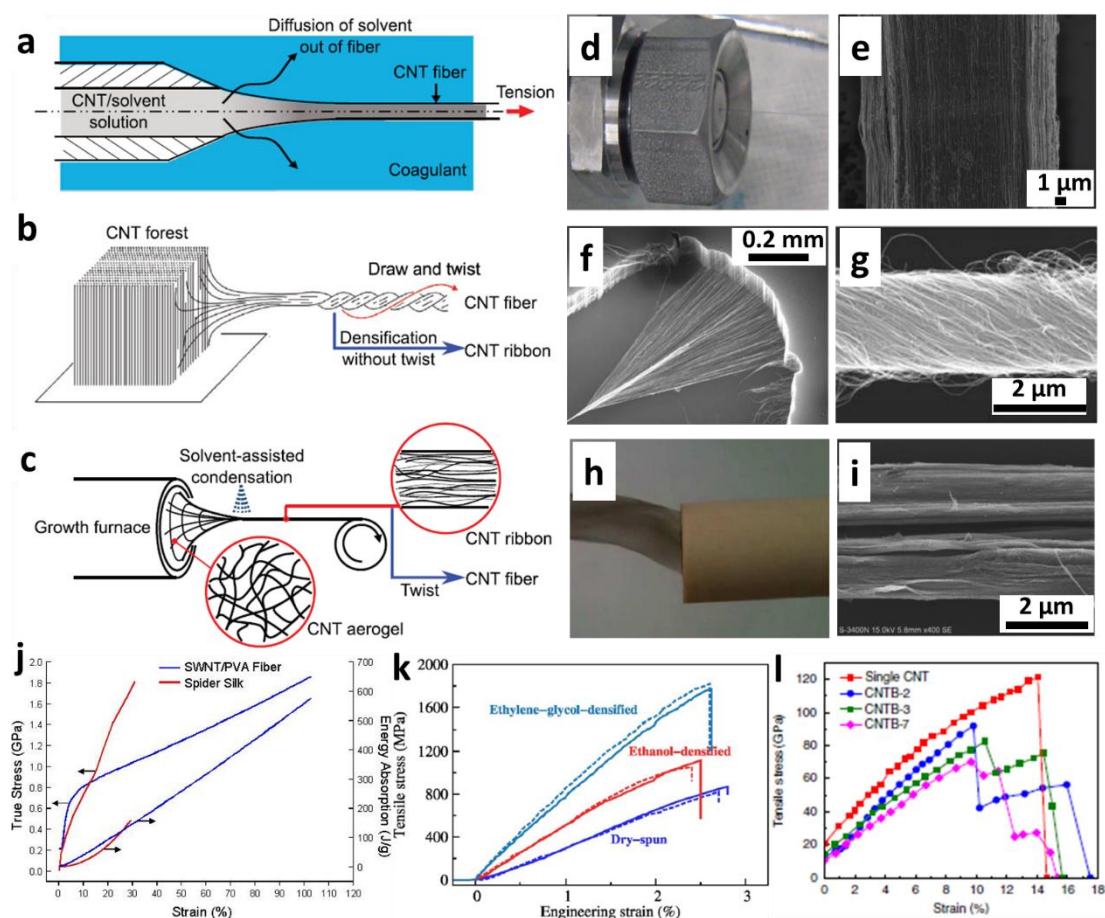


Figure 1.3. a–c, Three major methods to spin continuous CNTF; namely, coagulation-based solution spinning (a), spinning from a vertically aligned CNT forest (b), and spinning from an entangled CNT aerogel formed in the growth reactor (c). (Reprinted with permission from ref.¹⁷. Copyright, 2019 WILEY-VCH.) d, Close-up view of a single-filament solution spinning process of CNTF. e, CNTF SEM image showing the typical morphology of CNTF composed of about 100 nm thick fibrils aligned along the fiber axis. (Reprinted with permission from ref.³⁴. Copyright, 2013 American Association for

the Advancement of Science.) f, SEM images of a CNT yarn in the process of being simultaneously drawn and twisted during spinning from a nanotube forest outside the SEM. g, SEM images of singles CNTF. (Reprinted with permission from ref.³⁵. Copyright, 2004 American Association for the Advancement of Science.) h, Reaction solution is sprayed into a tube reactor and pyrolyzed to form CNTF via aerogel spinning. i, The surface SEM images of water-condensed CNTF. (Reprinted with permission from ref.³⁹. Copyright, 2014 Springer Nature.) j, Comparison of the mechanical properties of CNTs/PVA composite fibers (solution spinning) and *nephilia* spider silk. (Reprinted with permission from ref.³². Copyright, 2003 Springer Nature.) k, Stress-strain curves of as-spun, ethanol-densified, and ethylene-glycol-densified CNTF made from forest spinning. (Reprinted with permission from ref.³⁶. Copyright, 2014 WILEY-VCH.) l, Stress-strain curves for single CNTF and CNTF bundles with gauge lengths of about 1.5 mm. (Reprinted with permission from ref.³⁷. Copyright, 2018 Springer Nature.)

Meanwhile, the GR fiber (GF) or GR oxide fiber (GOF) are other attractive 1D carbon-based fiber assemblies. In 2011, researchers reported a simple approach to fabricate short GFs from chemical vapor deposition grown GR films. The GF obtained with porous and monolithic macrostructure show a typical electrical conductivity of ~ 1000 S/m but limited length.⁴⁰ Almost simultaneously, the meaningful and first continuous GF was invented by Gao *et al.* via a wet-spinning assembly of GR oxide (GO) liquid crystal dope, followed by chemical reduction in the lab, which opened the avenue to strong and multifunctional GF or GOF (**Figure 1.4 a**).⁴¹ This continuous wet-spun GF showed general mechanical properties with a tensile strength of 140 MPa, Young's modulus of 7.7 GPa and elongation at break of 6.8–10.1 %. Researchers have recently been trying to develop higher performance GFs by optimizing some key factors and posttreatment, such as the high quality spinning grade GO dope, suitable spinning nozzle, coagulation bath, heat stretching and high temperature reduction.¹⁸ Fruitful GFs have been developed, promising multifunctional uses in flexible electronics, conductors, supercapacitors, artificial muscle, solar cells and actuators. In 2016, scaled continuous GFs with outstanding mechanical properties (a tensile strength of 2.2 GPa and Young's modulus of 400 GPa) and excellent electrical conductivity (0.8×10^6 S m⁻¹) were produced by high-throughput wet-spinning of GO liquid crystals followed by graphitization utilized through a scale synergetic defect-engineering strategy (**Figure 1.4 b-f**).⁴² Some guest polymers (such as hyperbranched polyglycerol⁴³,

polyglycidylmethacrylate,⁴⁴ PAN⁴⁵ and PVA⁴⁶) and crosslinking with a metal ion⁴⁷ or sodium alginate⁴⁸ were used to enhance the mechanical properties of GFs. Though the GFs possess high strength and Young's modulus, the highly strong and tough GFs become another unresolved task due to the low toughness (most of them were less than 80 J/g). Furthermore, Sun *et al.* found that mixing CNTs and GO could not only improve the dispersion of both in the polymer matrix but also led to the synergetic enhancement of the strength of the CNTs/GO composite fibers.⁴⁹ They also presented the reduced GOF which exhibited higher toughness upon the removal of carboxyl and hydroxyl groups compared with GO fibers. Composite fibers with tunable toughness could be designed by mixing CNTs with GR in different ratios. Kim *et al.* also reported that increased toughness could be achieved by combining CNTs and reduced GO flakes in solution-spun polymer (PVA) fibers.⁵⁰ The optimized toughness could approach 1,000 J/g and a strength of about 550 MPa. An interconnected network of partially aligned reduced GO flakes and CNTs during PVA solution spinning was observed, which acted to deflect cracks, allowed energy-consuming polymer deformation and resulted in toughness enhancement. In order to overcome the limitation of the hybrid CNTs/GO fibers regarding low extensibility and the inability to operate in the wet-state condition, Kim *et al.* fabricated a high toughness and stretchable hybride and aligned GO/CNTs in a polyurethane matrix as elastic amorphous regions.⁵¹ This fiber possessed about 495 J/g of toughness, which exceeds the 165 J/g of spider silk. Notably, the fibers obtained could contract up to 60 % in response to water and humidity, which was similar to the supercontraction of the spider silk and showed its potential application as an artificial muscle which could be used in soft robotics and wearable devices.

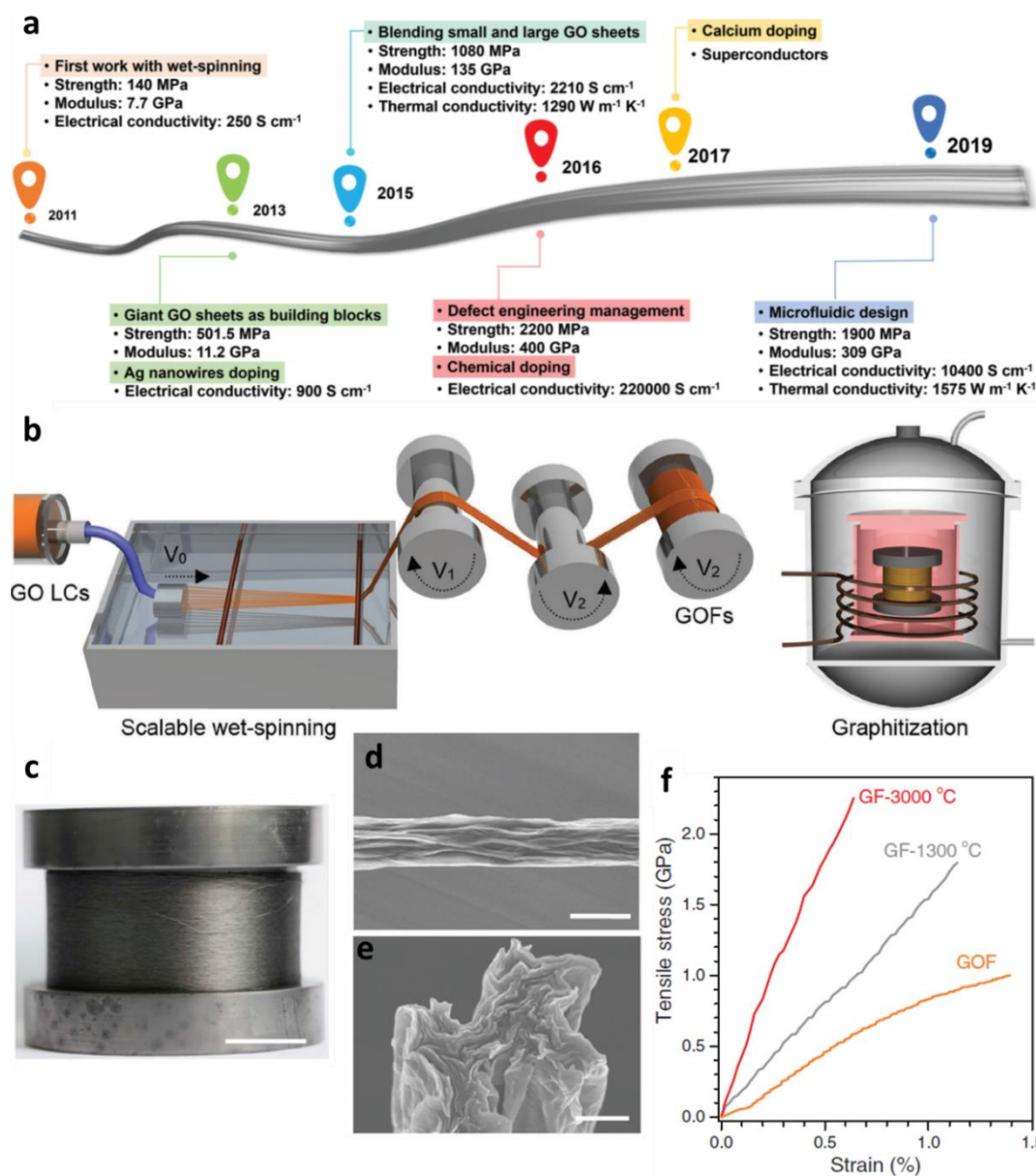


Figure 1.4. a, Key issues surrounding GFs since its discovery in 2011. (Reprinted with permission from ref.¹⁸. Copyright, 2019 WILEY-VCH.) b, Schematic illustration of wet-spinning of GOFs with continuous stretching in two stages, followed by graphitization up to 3000 °C to transform GOFs into GFs. V_0 is the extrusion velocity of GOFs liquid crystal dope. V_1 and V_2 are the linear velocities of the intermediate and terminal reel, respectively. $V_1 = 1.2V_0$, $V_2 = 1.1 V_1$. c, A roll of 500 m long 50-filament GFs with metallic luster. Scale bars is 2 cm. d and e, The surface (d) and cross-section (e) SEM images of multiscale structures of high-quality GFs. Scale bars are 2 μm (d) and 500 nm (e), respectively. f, Typical tensile stress curves of graphene single fibers. (Reprinted with permission from ref.⁴². Copyright, 2019 WILEY-VCH.)

1.1.3 Polymer-based high strength and toughness fiber materials

Polymer fibers of reduced size and dimensionality, typical polymer nanofibers, exhibit exceptional mechanical properties with a combination of high strength and toughness compared with traditional polymer microfibers. A significant improvement in the strength of carbon fibers as a decrease in diameter from 6.5–7.0 to 4.5–5.0 μm was proved in industry. Interestingly, the well-known size effects – the strength of fibers increases with the decrease of their diameter – showed no sign of saturation. However, conventional techniques in fiber production are generally unable to produce fibers of a diameter smaller than about 2 μm . Electrospinning is one of the most effective techniques to produce continuous nanofibers with diameters in the range from single nanometers to micrometers by jet-stretching polymer solutions thousands of times in high electric fields. To date, three typical testing methods have been developed to measure the mechanical properties of individual nanofibers, including the atomic force microscopy-based three-point bending test,^{52, 53} nano-indentation test^{54, 55} and micro-tension test.^{56, 57} Among these methods, the micro-tension test is a direct test method to measure the ultimate tensile strength and strain of individual nanofibers, in which the individual nanofiber is normally taken from the rectangle frame and then placed onto a paper frame by using electrically conductive adhesive tape and superglue (**Figure 1.5 a**). The strength value in the other two methods is acquired indirectly through calculation of the values of modulus and hardness.

Dzenis *et al.* used the micro-tension test method to analyze the relationship between the mechanical properties of electrospun PAN nanofibers (including the strength and toughness) and diameter of nanofibers (**Figure 1.5 b**).⁵⁸ They found that ultrafine as-spun PAN nanofibers exhibited extraordinary simultaneous strength, modulus and toughness. As the nanofiber diameter decreased from 2.8 to about 100 nm, a simultaneous increase in strength from 15 to 1750 MPa was observed. Meanwhile, toughness from 0.25 to 605 MPa with the largest increases was recorded for ultrafine nanofibers smaller than 250 nm. A similar size effect on the mechanical properties of ultra-high molecular weight polyethylene (UHMWPE) nanofibers was also reported by Rutledge *et al.* (**Figure 1.5 d and e**).⁵⁹ They fabricated the first example of stiff, strong and tough ultrafine polyethylene fibers (diameters less than one micron) by gel-electrospinning. The nanofibers obtained (diameter of 490 ± 50 nm) showed a

combination of high strength and toughness with a Young's modulus of 110 ± 16 GPa, ultimate tensile strength of 6.3 ± 0.9 GPa and toughness of 2.1 ± 0.3 GPa, which is unparalleled among polymer fibers to date. The high crystallinity and crystallite orientation, combined with fewer defects and an enhanced chain slip associated with small diameter and high specific surface area were considered to be a response to the correlation of stiffness, strength and toughness with fiber diameter.⁵⁹ The aromatic polyimides (PIs), with rigid heterocyclic imide rings and aromatic benzene rings in their macromolecular backbones, are one kind of high-performance polymer. Hou's group actively investigate high-performance PI nanofibers.⁵⁶ They firstly reported the mechanical properties of individual PI nanofibers from 3,3',4,4'-biphenyl-tetracarboxylic dianhydride and p-phenylenediamine, which exhibited high tensile strength, modulus and elongation at break with the respective values of 1.7 ± 0.12 GPa, 76 ± 12.6 GPa and 40 % (**Figure 1.5 c**).²³² Flexible 2,2'-bis[4-(4-aminophenoxy)phenyl]-hexafluoro-propane was used to synthesize PI to decrease the rigidity of its backbone and crystallinity.⁶⁰ A high toughness PI nanofiber was fabricated with a tensile strength, toughness and elongation to break of 308 ± 14 MPa, 365 ± 20 MPa and 202 ± 7 %, respectively. Many other PI nanofibers from different monomers were also reported by Hou's group; the nanofibers showed a range of tensile strength of 0.66–2 GPa and toughness of 17.5–300 J/g.⁵⁶ Kevlar is one kind of high strength (up to about 3.6 GPa) and high modulus (up to about 124 GPa) fiber but possesses a low toughness of about 33 J/g.^{3, 61} To increase the toughness of Kevlar fibers, Coleman *et al.* developed a new approach for the preparation of Kevlar/CNTs composite fibers by swelling commercially sourced Kevlar 129 yarns in CNT suspensions in NMP.⁵⁸ Compared to the Kevlar only fibers, the new Kevlar/CNTs composite fibers showed improved mechanical properties (maximum values only): Strength of 4.7–5.9 GPa and toughness of 63–99 J/g.

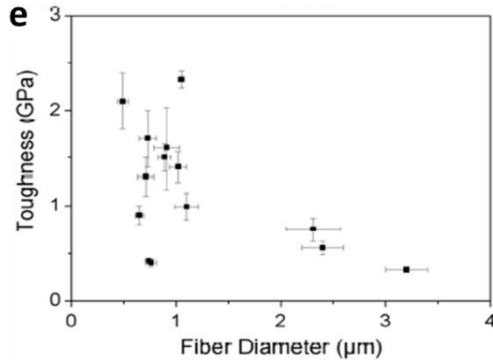
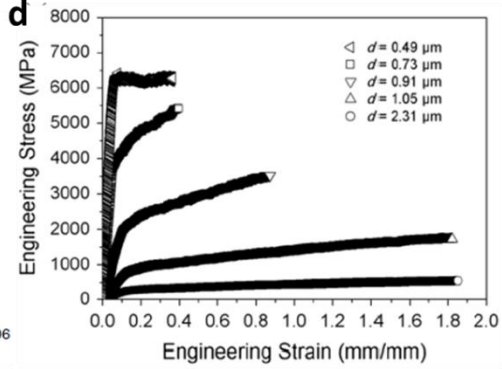
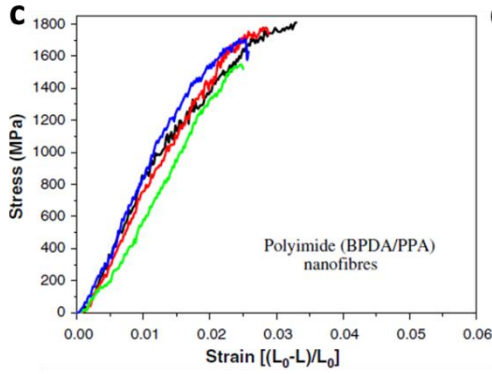
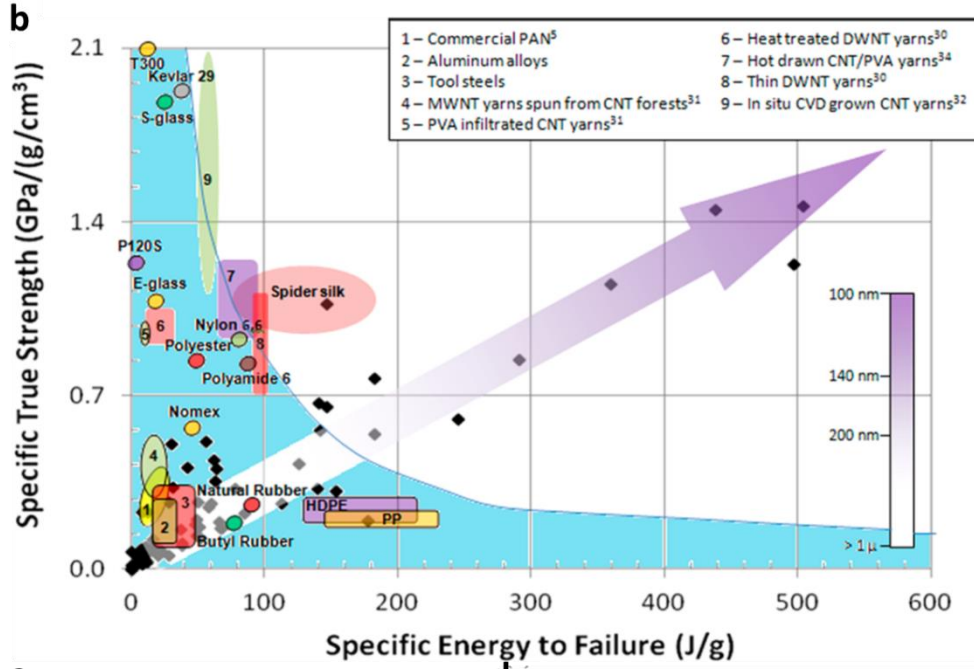
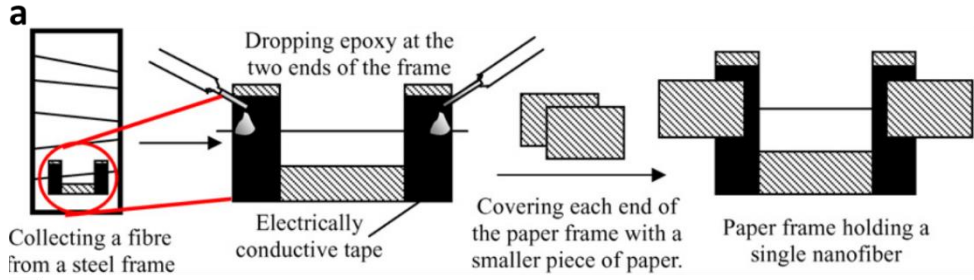


Figure 1.5. a, A schematic of carrying a single nanofiber on a paper frame for micro-tension test. (Reprinted with permission from ref.²³². Copyright, 2008 IOP Publishing Ltd.) b, Comparison of specific strength and specific energy to failure of as-spun PAN nanofibers (diamonds) with typical values for commercial and developmental fibers and materials. (the values of specific energy to failure is equal to the values of toughness used in this thesis) (Reprinted with permission from ref.⁵⁸. Copyright, 2013 American Chemical Society.) c, Typical stress-strain curves of single electrospun polyimide nanofibers. (Reprinted with permission from ref.²³². Copyright, 2008 IOP Publishing Ltd.) d and e, Tensile deformation behavior of gel-electrospun ultra-high molecular weight polyethylene (UHMWPE) fibres: d, Stress–strain curves for UHMWPE fibres having diameters of 0.49 (left pointing triangle), 0.73 (square), 0.91 (inverted triangle), 1.05 (triangle), and 2.31 μm (circle); e, Toughness versus nanofiber diameter of single UHMWPE fiber. (Reprinted with permission from ref.⁵⁹. Copyright, 2017 Springer Science Business Media, LLC.)

1.2 Electrospinning

Electrospinning is one of most versatile fiber-processing techniques, during which a charged jet of polymer solutions or polymer melts is created by an electric force, followed by stretching, elongation and solidification to form a fiber with a diameter which could be down to a few nanometers.^{56, 62-65} The thinnest electrospun nanofiber reported is about 1.6 nm in diameter.⁶⁶ Electrospun polymer fiber gained growing attention in the 1990s, which was partially initiated by the pioneer works of Reneker's group at the University of Akron.⁶⁷⁻⁷⁰ Since then, it has attracted tremendous attention from academia with the number of publications about electrospinning increasing exponentially every year (**Figure 1.6**). Industrial scale production of electrospun fiber assemblies for various applications are produced in numerous companies.^{56, 71, 72} The electrospun fibers show superb characteristics of nanofibers (diameters less than 100 nm), such as light weight, high mechanical strength and large surface area to volume ratio.⁷³ Due to the flexibility of the electrospinning process, the electrospun fibers could also be of varied morphology, from the most common single solid fibers⁷⁴ to, for example, porous fibers,^{75, 76} spring fibers,^{77, 78} beaded fibers,^{70, 79} side-by-side fibers,^{80,}

⁸¹ core-shell fibers,^{82, 83} hollow fibers^{84, 85} and ribbon-like fibers.^{86, 87} Due to the problem of handling single electrospun fiber, it is the electrospun fiber assemblies as a viable group of fibers gathered together that is widely used, for example, in textiles,^{88, 89} tissue engineering,^{90, 91} photonics,^{92, 93} catalysis,^{94, 95} drug delivery,^{96, 97} electronics,^{98, 99} energy storage,^{100, 101} sensors^{102, 103} and filtration.^{104, 105} Therefore, it is important for us to study various parameters and processes that could fabricate the electrospun fiber assemblies desired. Thus, in the following sections, a brief introduction of the electrospinning fundamentals, including the principles, materials and parameters of electrospinning, and the types and fabrication of electrospun fiber assemblies will be given.

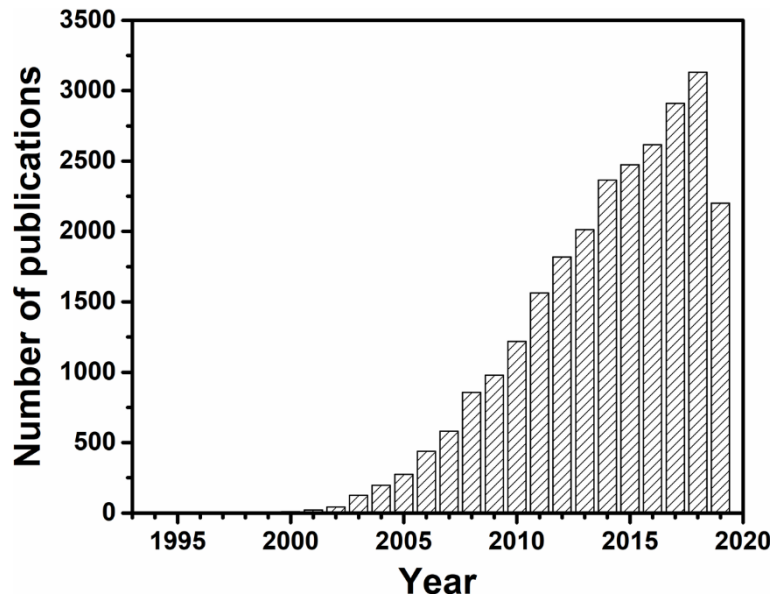


Figure 1.6. The numbers of publications with the keywords of “electrospinning” acquired from the Web of KnowledgeSM on Sep. 23, 2019.

1.2.1 Electrospinning principles

Electrospinning normally includes solution and melt electrospinning. Only a viscous solution of materials is required for the most common solution electrospinning. However, melt electrospinning requires that the material must have a melting point. Thus, melt electrospinning could only be applied for certain materials and it usually yields microfibers with a diameter in the micrometer range.¹⁰⁶ Electrospinning in this thesis refers to solution electrospinning. The typical electrospinning setup in the lab

includes four parts (**Figure 1.7**): A high voltage supply, a conductive spinneret (such as a syringe with a metal needle), a pump system and a grounded collector (dynamic or static). The electrospun process can generally be described in four sequential steps: 1) The charging of the solution droplet by the direct current high voltage and formation of a Taylor cone; 2) extension of the charged jet in a straight line; 3) thinning of the jet with solvent evaporation in the presence of an electric field and growth of electrical bending instability (also known as whipping instability); and 4) solidification and collection of the solid fiber on a grounded collector.⁶⁴ Furthermore, some researchers also utilized an alternate current high voltage supplier instead of the typical direct current high voltage supplier to charge the solution for electrospinning.¹⁰⁷⁻¹¹¹ Diverse fiber assemblies, such as 1D continuous yarns¹⁰⁷ and 2D partly aligned membranes,¹⁰⁸ were fabricated by alternate current electrospinning. Electrospinning without any spinnerets, such as ferromagnetic fluid,¹¹² metallic roller,¹¹³ gas bubbles,¹¹⁴ conical wire coil,¹¹⁵ metal plate,¹¹⁶ splashing spinneret,¹¹⁷ rotary cone,¹¹⁸ cylinder,¹¹⁹ ultrasonication¹²⁰ and bowel edge,¹²¹ have also been explored. In order to improve the productivity of fibers, gasblowing,¹²²⁻¹²⁴ multi-jets¹²⁵⁻¹²⁸ and multiple needles¹²⁹⁻¹³² were also developed by lots of researchers.

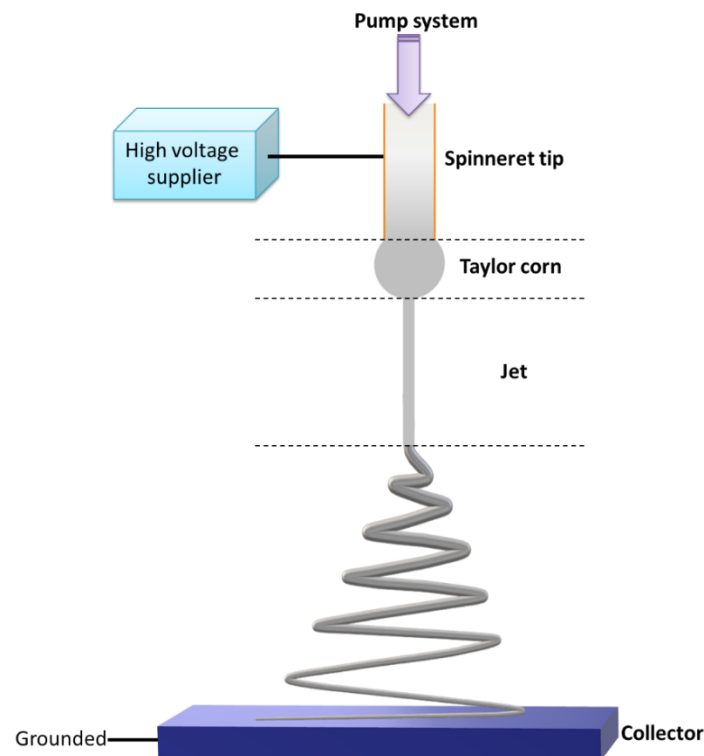


Figure 1.7. Schematic diagram showing fiber formation by electrospinning.

1.2.2 Electrospinning materials

The properties and function of electrospun fiber assemblies are mainly dependent on the characteristic properties of the materials used. Based on the materials, electrospinning can generate different kinds of fiber assemblies from natural or synthetic polymers to, for example, metals, inorganics and carbon-based materials. **Table 1.2** summarizes the typical materials, solvents and types of electrospun fiber assemblies. Among them, numbers of natural or commercial synthetic polymer fiber assemblies, such as chitosan, collagen, gelatin, silk, cellulose, poly(ethylene oxide) (PEO), poly(vinyl alcohol) (PVA), poly(vinylidene fluoride) (PVDF), poly(acrylonitrile) (PAN), poly(methyl methacrylate) (PMMA), polystyrene (PS) and poly(vinyl chloride) (PVC), could be electrospun directly from their water or organic solvent solutions and be further explored and applied to various applications. Lots of biocompatible and biodegradable natural or synthetic polymers fiber assemblies, such as alginate, collagen, chitosan, chitin, dextran, DNA, gelatin, silk, poly(caprolactone) (PCL), poly(lactic acid) (PLA) and poly(lactic-co-glycolic acid) (PLGA), have been prepared as scaffolds in biomedical or tissue engineering applications. A number of conductive electrospun fiber assemblies were achieved by directly electrospinning some conductive conjugated polymers, such as polyaniline (PANI) and polypyrrole (PPy), or some composites consisting of polymers with conductive metal particles/nanowire, CNTs, GR/GO oxide or conductive polymers. Light-emitting electrospun fiber assemblies can be obtained by blending emissive systems, such as quantum dots (QDs), dyes, light-emitting conjugated polymers and bio-chromophores, with optically inert polymers, or directly by using special light-emitting conjugated polymers.^{133, 134} In addition, inorganic materials, including metals, metal oxide/nitrides/carbides, ceramics and their precursors, can also be directly utilized for electrospinning to fabricate functional inorganic fiber assemblies.

Table 1.2. Summary of typical materials for electrospun fiber assemblies.

Materials	Solvent (supporting polymer)	Type of assembly	Ref.
<i>Natural polymers</i>			
Chitosan	Acetic acid	Membranes	135, 136
Collagen	HFIP, 40% acetic acid, phosphate buffered saline 20x buffer	Membranes	137, 138
Gelatin	Acetic acid, TFE, DMSO, ethylene glycol, formamide	Membranes	139, 140
Silk	HFIP, LiBr aqueous solution	Membranes	141, 142
Cellulose	LiCl, DMAc, N-methylmorpholine oxide, water	Membranes	143, 144
Hyaluronic acid	Dulbecco's modified eagle's medium, deionized water, formic acid and DMF	Membranes	145, 146
Natural rubber	Chloroform, 2-methyltetrahydrofuran	Aligned membranes	147, 148
DNA	Ethanol, chloroform, water based buffer	Membranes	149, 150
Protein	HFIP, formic acid	Membranes	151, 152
<i>Synthetic polymers</i>			
PVA	Water, ethanol, acetic acid, buffer	Membranes	153, 154
PEO	Distilled water, chloroform	Membranes	155, 156
PVP	Ethanol and water	Membranes	157, 158
Aliphatic polyamide (PA6, PA66, PA1010)	Formic acid and acetic acid	Membranes/yarns	159, 160

Aromatic nomex	LiCl, DMAc, DMF	Membranes	161, 162
PAN	DMF	Membranes/yarns/sponges	163, 164
PCL	Methylene chloride, DMF	Membranes/yarns	165, 166
PLA	Chloroform, DMF, HFIP	Membranes/yarns/sponges	167, 168
PVC	THF, DMF	Membranes	169, 170
PVDF	DMF, acetone	Membranes/yarns	171, 172
PS	THF, DMF	Membranes/yarns	173, 174
PI	DMF, DMAc	Membranes/yarns/sponges	56, 175
PU	DMF, DMAc	Membranes	176, 177
PC	Chloroform, THF, DMF	Membranes	178
PET	TFA, DCM	Membranes	179, 180
PMMA	DMF	Membranes	181, 182
Epoxy resin	Ethanol, acetone	Membranes	183
PDMS	THF, DMF	Membranes	184, 185
PP	Cyclohexane, acetone, DMF	Membranes	186, 187
PE	Cyclohexanone, p-xylene	Membranes	188, 189
PANi	Sulfuric acid solution, chloroform, DMF	Membranes	190, 191
PPy	Chloroform, DMF	Membranes	192, 193

Modified conjugated polymers	THF, chloroform, DMF, DMSO	Membranes	194, 195
P3HT	Chloroform	Membranes	196, 197
Poly(ionic liquid)	DMF, acetonitrile, water, methanol	Membranes	198, 199
Metals			
Cu	PVA/H ₂ O, PVB/isopropanol/H ₂ O	Membranes	200, 201
Ag	Ethylene glycol	Membranes	202
Fe	PVB/isopropanol/H ₂ O, PVA/H ₂ O	Membranes	203, 204
Co	PVB/isopropanol/H ₂ O, PVA/H ₂ O	Membranes	203, 204
Ni	PVA/H ₂ O	Membranes	204
Au	Poly(acrylic acid)/ethanol	Membranes	205
Pt	PVP/H ₂ O	Membranes	206
Metal oxides			
Al ₂ O ₃	PVP/ethanol	Membranes	207
CeO ₂	PVA/H ₂ O	Membranes	208
Co ₃ O ₄	PVP/DMF	Membranes	209
CuO	PVA/H ₂ O	Membranes	210
Fe ₂ O ₃	PVA/H ₂ O	Membranes	211
Mn ₃ O ₄	PMMA/chloroform/DMF	Membranes	212
SiO ₂	PVA/H ₂ O/H ₃ PO ₄	Membranes/sponges	213, 214
SnO ₂	PVA/H ₂ O/propanol/isopropanol	Membranes	215
TiO ₂	PVP/ethanol	Membranes	216
V ₂ O ₅	PMMA/chloroform/DMF	Membranes	217
WO ₃	PVA/propanol/DMF	Membranes	218
ZrO ₂	PVP/ethanol	Membranes	219
BaTiO ₃	PVP/ethanol/H ₂ O/acetic acid	Membranes	220
CoFe ₂ O ₄	PVA/DMF/THF	Membranes	221
LiCoO ₂	H ₂ O	Membranes	222
ZnCo ₂ O ₄	PVP/ethanol	Membranes	223

SrTi _{1-x} Fe _x O ₃	PVP/H ₂ O	Membranes	224
Carbon base and metal carbides			
Carbon base fibers	PAN/DMF	Membranes/yarns/sponges	225, 226
Mo ₂ C	PVA/H ₂ O	Membranes	227
SiC	PS/DMF	Membranes	228
TiC	PVP/DMF	Membranes	229
WC	PVP/H ₂ O	Membranes	230
ZrC	PVP/ethanol	Membranes	231
Metal nitrides			
Li ₃ N	PVA/H ₂ O	Membranes	232
NbN	PVP/ethanol	Membranes	233
TiN	PVP/ethanol	Membranes	233
VN	PVP/DMF	Membranes	234
Ti-V-N	PVP/ethanol	Membranes	233

1.2.3 Electrospinning parameters

A variation of process parameters in electrospinning (such as electrode separation and geometry, spinneret forms, collector shapes and states, temperature, humidity, electrical conductivity and feed rate) provide diverse possibilities for the targeted adjustment of the physical and chemical properties of electrospun fiber assemblies.^{63, 64} Meanwhile, the molecular parameters of polymers (such as polymer molecular weight and its distribution, solubility, glass-transition temperature, entanglement density, melting point, crystallization velocity and solvent vapor pressure) should also be taken into account.^{63, 64} Different dimensions and structures of electrospun fiber assemblies can be designed and tailored by changing the parameters above; this shows the charm of electrospinning. The electrospun fiber diameter, for example, can be reduced by adjusting several parameters, such as reducing the solution viscosity (concentration), enhancing the solution conductivity, increasing the spinneret tip-to-collector distance, reducing the solution feed rate or enlarging the voltage applied. Combining 3D printing and electrospinning to design ordered fiber assemblies has also been reported recently.²³⁵⁻²³⁹ Some researchers have put forward electrohydrodynamic (EHD) direct writing technology based on electrospinning and digital

direct writing, which enables the large-scale assembly of highly aligned fibers in diverse patterns by adjusting three key processing parameters: The substrate speed, the nozzle-to-substrate distance (500 μm – 5 cm) and the voltage applied.^{64, 240, 241} The EHD technology is able to deposit fibers accurately to create patterned fiber and complex porous structures, which are rather attractive in the fabrication of flexible electronics and tissue engineering scaffolds.²⁴⁰ Utilizing the changes of electrospun parameters, the development of electrospinning for different electrospun fiber assemblies could be divided into three stages: 1) The traditional electrospinning for the fabrication of nonwoven; 2) the field-induced electrospinning for the assembly of aligned fibers; and 3) the recent digital direct writing, consisting of near-field electrospinning,²⁴² mechano-electrospinning,²⁴³ and the helix EHD printing technique²⁴⁴ for orderly arranged microstructures.

1.3 Electrospun fiber assemblies

The electrospun fiber assemblies, as a group of single electrospun fibers, can be divided into three parts in terms of dimension: 1) One-dimensional yarns, 2) 2D membranes and 3) 3D assemblies. **Figure 1.8** shows the details of classification of electrospun fiber assemblies. Electrospun fiber assemblies are typically in a 2D membrane form and 1D yarn form. The 3D assemblies have been developed recently from the tube/conduit to flexible ultralight sponges and patterned fibers. The alignment of fibers as an important factor in the performance of the electrospun fiber assemblies is being studied by numerous researchers.

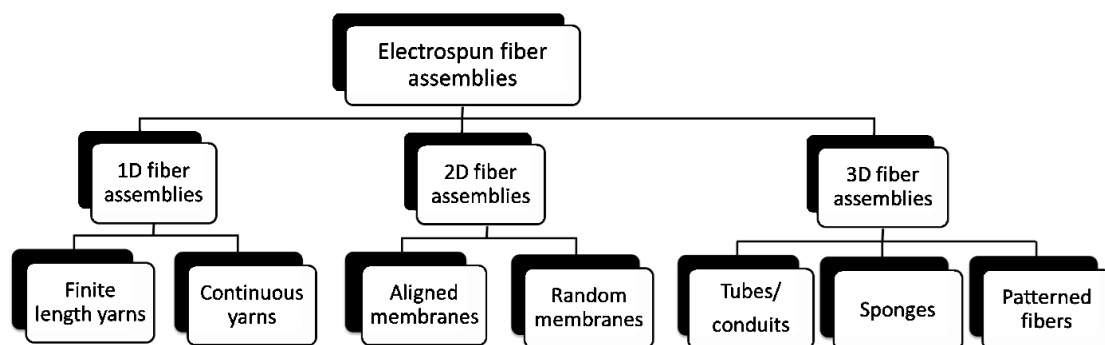


Figure 1.8. Classification of electrospun fiber assemblies.

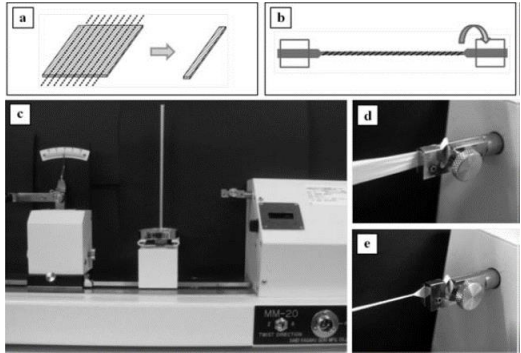
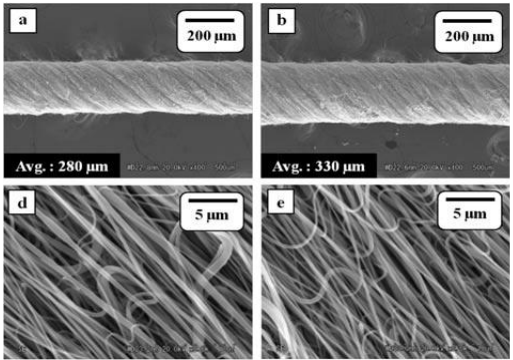
1.3.1 1D electrospun fiber assemblies

Though single 1D electrospun fibers exhibited extraordinary properties, typically the excellent mechanical properties with a combination of high strength and toughness.^{58, 59} However, according to process requirements, single electrospun fiber cannot be used directly in weaving, knitting and applications due partly to their submicron size and fragile nature. As a typical 1D electrospun fiber assemblies, electrospun fiber yarns (EFYs) can assemble numerous fibers in 1D with robust and visible form for the practice process. The EFYs show good opportunities for the development of electrospun fiber assemblies which are being used in textiles,^{245, 246} tissue scaffolds,²⁴⁷ flexible micro- and non-fluidic systems,²⁴⁸ artificial muscles,²⁴⁹ energy harvesting²⁵⁰ and biomedical fields.²⁵¹

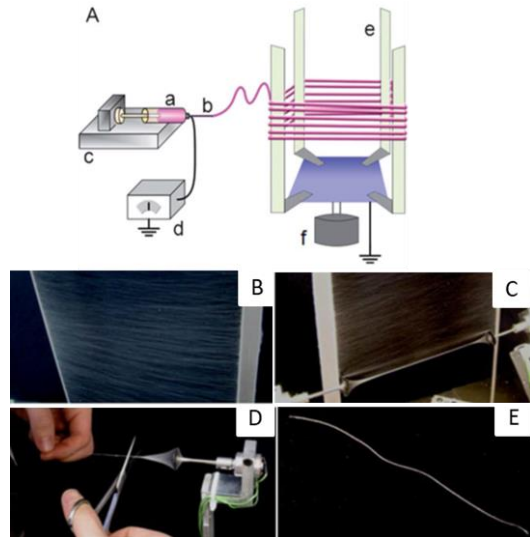
The EFYs can be achieved by using different mechanical collection devices and manipulation of the electric field, processing parameters, moving collector or spinneret systems. **Table 1.3** summarizes the typical fabrication methods and morphology of EFYs. Several approaches have been proposed to develop yarns with finite length directly by cutting and twisting 2D fiber membranes (**Table 1.3 a1 and a2**).^{159, 250, 252} Dalton *et al.*²⁵³ fabricated twisted yarn by suspending the electrospun fibers between dual collection rings and rotating one of the electrodes, which could twist the fibers into a yarn by the external force (**Table 1.3 a3**). Although the yarn had a uniform helix and the fibers were aligned in the direction of yarns, the finite length limited its end use. Lots of methods were developed to fabricate continuous electrospun yarns. Khil *et al.*²⁴⁷ and Ramakrishna *et al.*²⁵⁴ used a static or dynamic liquid bath for fabricating continuous EFYs (**Table 1.3 b1 and b2**). The yarns could be formed by the pulling the fibers into a line with continuous form. However, the fibers exhibited poor orientation and arrangement in the yarns, and the liquid media was hard to choose for the preparation of some polymer yarns. In addition, a lot of researchers were dedicated to fabricating continuous EFYs with the aid of air vortex tubes²⁵⁵, disks²⁵⁶ and different kinds of electrodes (**Table 1.3 b3-b6**).²⁵⁷⁻²⁶² However, the disadvantages of EFYs, such as fibers sticking to the setups, negative fiber alignment and difficulties controlling the fiber jet, were still unsolved. Moreover, continuous EFYs were produced by using two oppositely charged needles and a rotating collector. Under application of an electric field, the two oppositely charged

electrospun fibers could fly into each other and form a bundle with aggregated fibers. And the bundle could be collected by a rotating collector. The results are promising but the problem of entangled fibers needs to be settled. Furthermore, lots of modified methods were created by auxiliary metal plates,^{160, 263} cylinders,^{167, 264} rings^{265, 266} and funnels (Table 1.3 b7 and b8).^{174, 267-271} Aided by the rotating funnel, the two oppositely charged electrospun fibers could form a membrane at end of funnel, which could be pulled into a cone and twisted into a yarn at the tip of the cone. The twisted yarn was obtained with continuous form with the assist of collector. The results showed twisted yarns with improved mechanical strength compared with the aligned fiber bundles but further improvements are needed for effective fiber alignment in the yarn body architecture. Alternate current electrospinning is also being utilized for the fabrication of yarn (Table 1.3 b9).^{107, 110, 111} This method shows a very high production speed that could increase to 60 m/min. However, many entangled fibers in the EFYs were unavoidable.

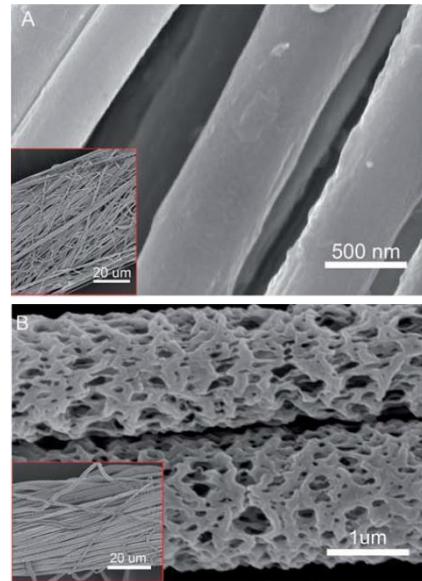
Table 1.3. Summary of the typical fabrication methods and morphology of EFYs.

Methods	Morphology of EFYs
<p>a Uncontinuous yarns</p> <p>a1) Cutting and twisting for PA6¹⁵⁹, PVDF^{250, 252} fiber membrane.</p> 	<p>PVDF yarn²⁵²</p> 

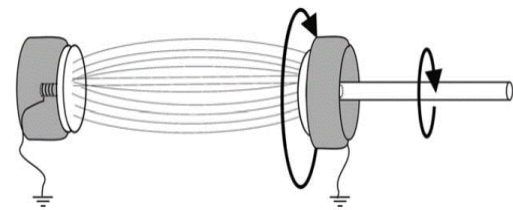
a2) Twisting from aligned PVDF/PEO fibers²⁷²



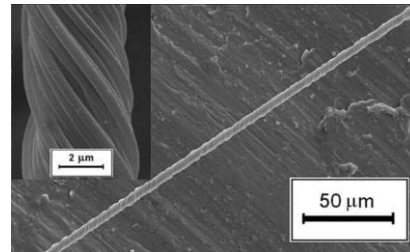
PVDF/PEO fibers²⁷²



a3) Dual electrodes for PCL yarn²⁵³

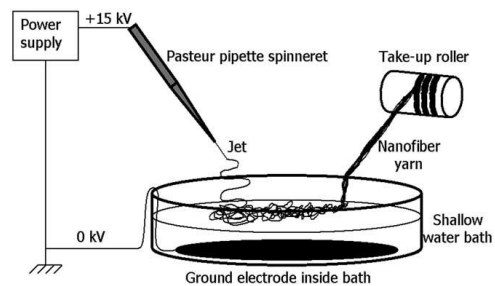


PCL yarn²⁵³

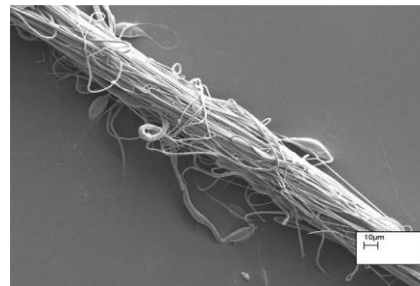


b Continuous yarns

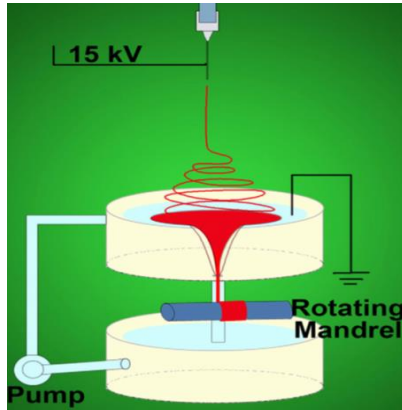
b1) Liquid bath for PCL²⁴⁷, PVAc²⁷³, PAN²⁷³, PVDF²⁷³ and PCL/silk/PANi²⁷⁴ yarns



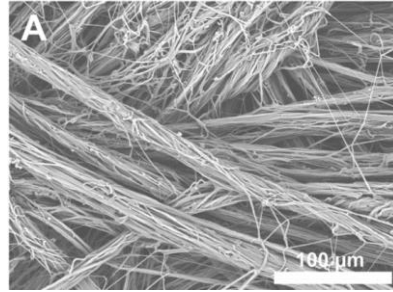
PCL yarns²⁴⁷



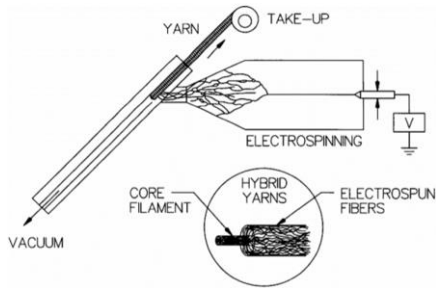
b2) Dynamic Liquid bath for Silk/P(LA-CL)²⁷⁵ and P(LA-CL)/collagen²⁷⁶ yarns



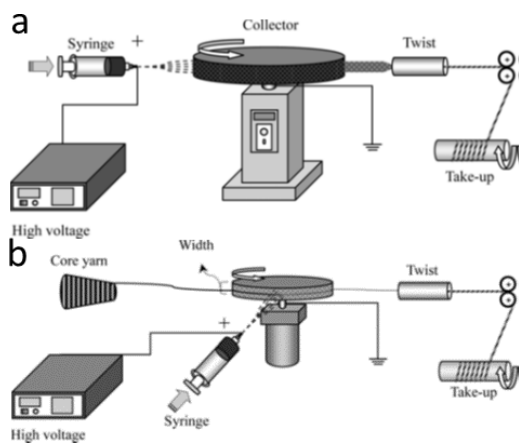
Silk/P(LA-CL)²⁷⁵



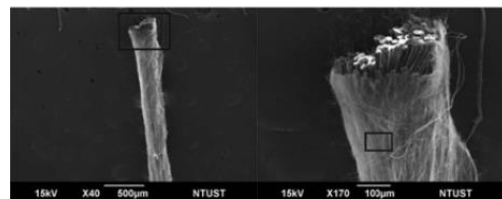
b3) Air vortex tube for P(LA-GA) yarn²⁵⁵



b4) Disk for PAN composite yarn²⁵⁶

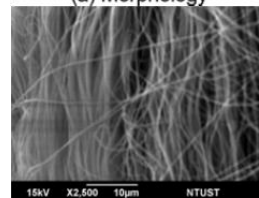


PAN composite yarn²⁵⁶



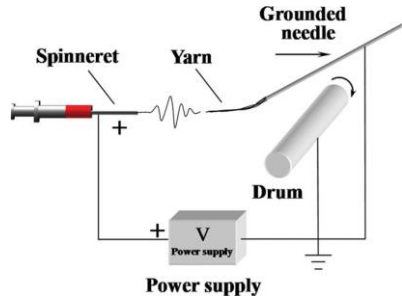
(a) Morphology

(b) Core and sheath

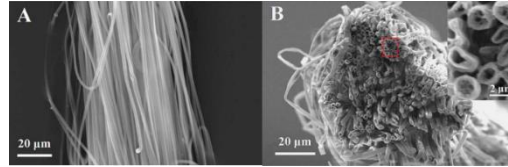


(c) Nanofibers of sheath

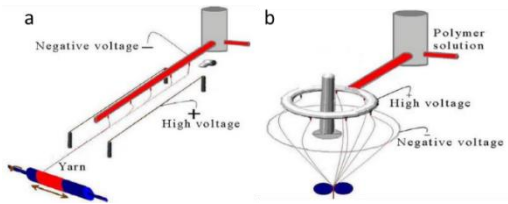
b5) Single electrodes for PLA²⁵⁷, PHBV²⁵⁸, PAN^{258, 259} and PMIA²⁵⁸



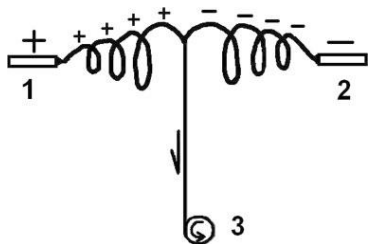
PLA yarn²⁵⁷



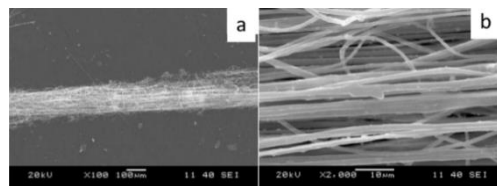
b6) Parallel or ring electrodes for artificial fibers²⁶⁰⁻²⁶²



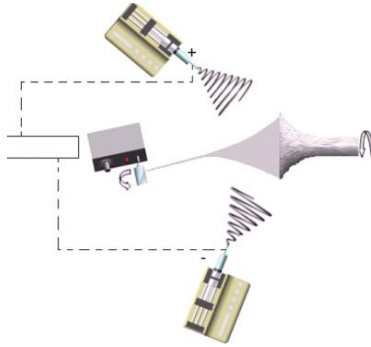
b7) Opposite charged needles for Zein²⁴⁵, zein/PLLA²⁴⁵ and PLLA yarn²⁵¹



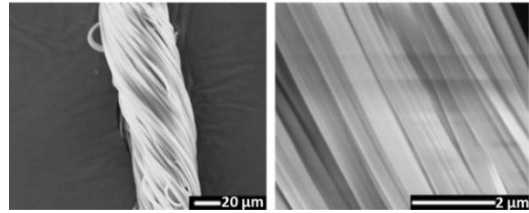
Zein/PLLA yarn²⁴⁵



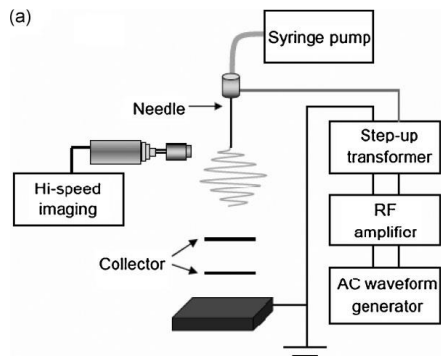
b8) Opposite charged needles with funnel for PVDF–HFP¹⁷⁴, PAN²⁶⁷⁻²⁷⁰, PCL²⁷¹ and PLA²⁷¹ yarn (or ring for PVDF–HFP^{265, 266} yarn, metal plate for PA66¹⁶⁰ and PLA²⁶³ yarn, and cylinder for PLA^{167, 264} yarn)



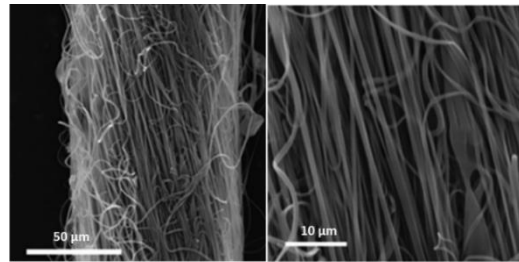
PVDF–HFP yarn¹⁷⁴



b9) AC electrospinning for PES¹⁰⁷, PA66¹⁰⁷, PVP¹¹⁰, PAN¹¹¹ and PVB¹¹¹ yarn



PES yarn¹⁰⁷



Although there have been various recent reports of preparing continuous yarns successfully, issues of controlling the twist level, yarn dimension, spinning stability and the general low mechanical properties of EFYs remain. It is still a challenge to develop highly aligned and continuous yarn with good mechanical properties.

1.3.2 2D electrospun fiber assemblies

Electrospun fiber assemblies are normally generated in a 2D membrane including a random and aligned form. Beside the characteristics of used materials, the alignment of fiber in the 2D assemblies is a key factor in pursuing high performance 2D fiber assemblies. Due to the random deposition of electrospun fibers, the random membranes are normally collected on the static collector (e.g. aluminum foil, stainless steel meshes or metal plate) and low speed drum collectors.⁶³ Moreover, some specially designed collectors, such as high-speed rotating discs and electric field-assisted conductive plates, have been used to increase the alignment of fibers. Kim *et al.*²⁷⁷ and Matthews *et al.*²⁷⁸ examined the effect of the linear velocity of the rotating mandrel on the alignment and mechanical properties of electrospun fiber membranes. An enhanced fiber alignment, tensile stress and modulus were observed by the increasing rotating speed. However, these properties tend to decrease above a linear velocity (at the surface of collector) of 30 m/min. Similar results were also observed by Zussman *et al.*²⁷⁹ Some researchers tried to reduce the chaotic path of the electrospun jet to achieve good fiber alignment by using field-controllable electrodes.^{132, 280} However, no matter what parameters were used, the presence of the disordered fibers collected on the collector was unavoidable. Thus, the posttreatments, including stretching in hot water or high temperature, were also used to further improve the alignment of fibers.^{163, 281} Youm *et al.*¹⁶³ stretched PAN fiber felts under optimal two-step drawing conditions (stretching using hot water of 90–95 °C and hot air of 160 °C); the stretched felts exhibited large improvements in both alignment and molecular chain orientation (**Figure 1.9**). The final stretched fiber membranes, with a draw ratio of 5, exhibited 5.3 times higher tensile strength (630 MPa) and 6.7 times higher tensile modulus (10.6 GPa) than those of the pristine one. However, this stretching process is not a continuous process and only produces a membrane with a finite length.

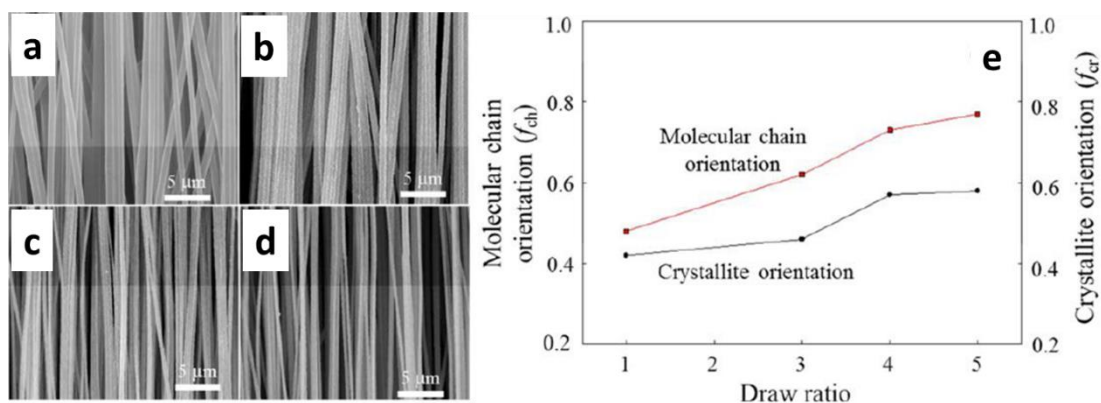


Figure 1.9. a-d, SEM images of aligned and drawn PAN-based nanofiber felts of draw ratio 1 (as-electrospun) (a), 3 (b), 4 (c), and 5 (d). e, Variation of molecular chain and crystallite orientation as the function of draw ratio. (Reprinted with permission from ref.¹⁶³. Copyright, 2016 Wiley Periodicals, Inc.)

1.3.3 3D electrospun fiber assemblies

Recently, 3D electrospun fiber assemblies possessing hierarchical structures have been attracting increasing attention in academia and industry for broad applications, for example, in tissue engineering,²⁸² infiltrations,²⁸³ electrodes,²⁸⁴ electronics^{175, 285} and oil adsorption.²⁸⁶ The evolution of 3D electrospun fiber assemblies experiences approximately three stages: The fibrous tubes/conduits deriving from 2D fibrous membranes, the shaped sponges from fibers and the patterned fiber assemblies derived by utilizing directly electrospun writing technology (**Figure 1.10 and 1.11**). The 3D fibrous tubes/conduits can be fabricated by depositing fibers over a rotating small rod (diameter normally less than 5 mm) or 3D interconnected tubular temple.²⁸⁷⁻²⁹² Lin *et al.*²⁸⁷ prepared fibrous conduits with aligned fibers on rotary mandrel and the fibrous conduits showed considerable improvement in nerve regeneration (**Figure 1.10 a**). Moreover, 3D fibrous tubes/conduits with different shapes and patterns were prepared by using this method, and the tubes are expected to be used in biomedical and industrial applications (**Figure 1.10 b**).²⁹⁰ Some researchers found that 3D fiber assemblies could be obtained directly from electrospinning with a static collector.^{293, 294} Due to the build-up of charged electrospun fibers, the electrostatic repulsion prevents incoming fibers from depositing directly on the collector and, therefore, forming a 3D structure. However, the fibers are only loosely packed during these 3D

assemblies, which result in assemblies without reversible manual compression.²⁹³ Based on the same principle, Cai *et al.* improved 3D electrospun fiber assemblies by adding some cross-linker into the fibers.²⁹⁴ These 3D assemblies show an improvement in cell proliferation compared with the 2D assemblies. However, it is difficult to control the structure of 3D assemblies only simply based on electrospinning. Our group recently developed an efficient method to fabricate ultralight 3D sponges based on freeze-drying a short electrospun fiber suspension (**Figure 1.10 d**).²⁹⁵ These kinds of electrospun fiber sponges show low density (less than 10 mg/cm³), high porosity (more than 99 %), superior compression properties and multifunctionality.²⁹⁶⁻²⁹⁹ Simultaneously, Ding's group obtained 3D composite fibrous assemblies with cellular structures, which exhibited an ultra-low density of 0.12 mg/cm³, rapid recovery from deformation, efficient energy absorption and high pressure-sensitivity, and showed broad applications in thermal insulation, sound absorption, emulsion separation, elasticity-responsive electric conduction, water/oil separation and sensors (**Figure 1.10 e**).^{214, 300, 301}

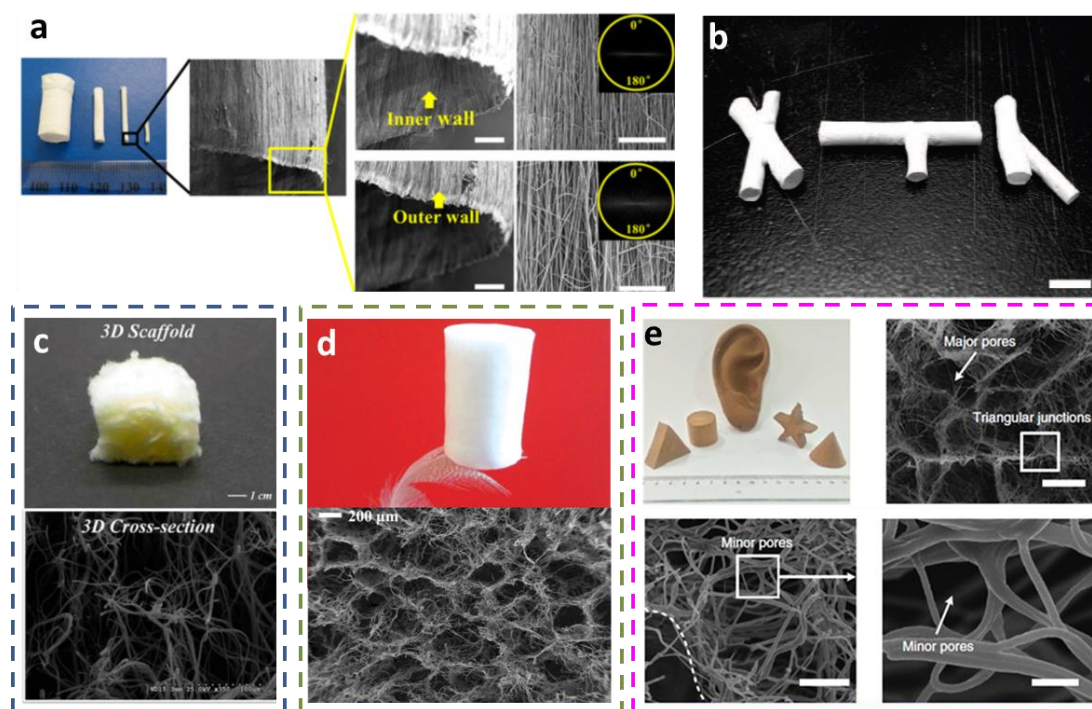


Figure 1.10. a, Digital photo and SEM images of cellulose acetate butyrate nanofibrous conduits (Scale bars = 100 μm), (Reprinted with permission from ref.²⁸⁷. Copyright, 2015 American Chemical Society.) b, Digital photos of polycaprolactone (PCL) nanofiber tubes with various interconnected tubular structures (scale bar = 5

mm) (Reprinted with permission from ref.²⁹⁰. Copyright, 2008 American Chemical Society.) c, Digital photo and SEM image of 3D zein electrospun scaffolds. (Reprinted with permission from ref.²⁹⁴. Copyright, 2013 American Chemical Society.) d, Optical photograph and SEM image of cross-linked electrospun fibrous sponges from short fibers. (Reprinted with permission from ref.²⁹⁵. Copyright, 2015, WILEY-VCH.) e, Optical photograph and SEM images of fiber sponges from short fibers. (Scale bars are 20 μm , 5 μm , 1 μm , successively), (Reprinted with permission from ref.²¹⁴. Copyright, 2014 Macmillan Publishers Limited.)

Furthermore, with the development of digital direct writing technology, such as 3D printing, some patterned fiber assemblies have been achieved by combining the advantages of conventional electrospinning and digital direct writing technology. These reported combining technologies consist mostly of near-field electrospinning,²⁴² mechano-electrospinning²⁴³ and the EHD printing technique²⁴⁴. This direct writing technology enables the direct depositing of electrospun fibers onto large-area substrates in an additive, non-contact and reproducible manner.³⁰² Yin *et al.* demonstrated smooth straight, serpentine, self-similar and bead-on-string structures on silicon/elastomer substrates with a resolution of 200 nm by optimizing the substrate speed, the nozzle-to-substrate distance and the voltage applied.²⁴¹ Li *et al.* produced microscale Mongolian yurts with a distinct hollow structure by layer-by-layer deposition of electrospun fibers. Conductive polymer composites were used for printing fibrous blocks with an average width of 120 μm and height of 630 μm , which were constructed into strain sensors.³⁰³ Hutmacher *et al.* designed and created complex 3D porous fibrous assemblies by accurately depositing melt electrospun PCL fibers on top of each other, as shown in **Figure 1.11**.²³⁶ These 3D patterned fiber assemblies show biomedical applications that allow cell and tissue invasiveness. However, in this case, the filament resolution (from single micrometer magnitudes to 50 μm) and fiber to fiber distances achievable are approaching submicrometer magnitudes. The thinnest melt-electrospun fiber diameter (from a blend of PEG-b-PCL and PCL) of 270 ± 100 nm was reported.³⁰⁴ Sun *et al.*³⁰⁵ fabricated a field-effect transistor by depositing ZnO thin fibers (from 500 to 1500 nm) precise utilizing an EHD printing technique.

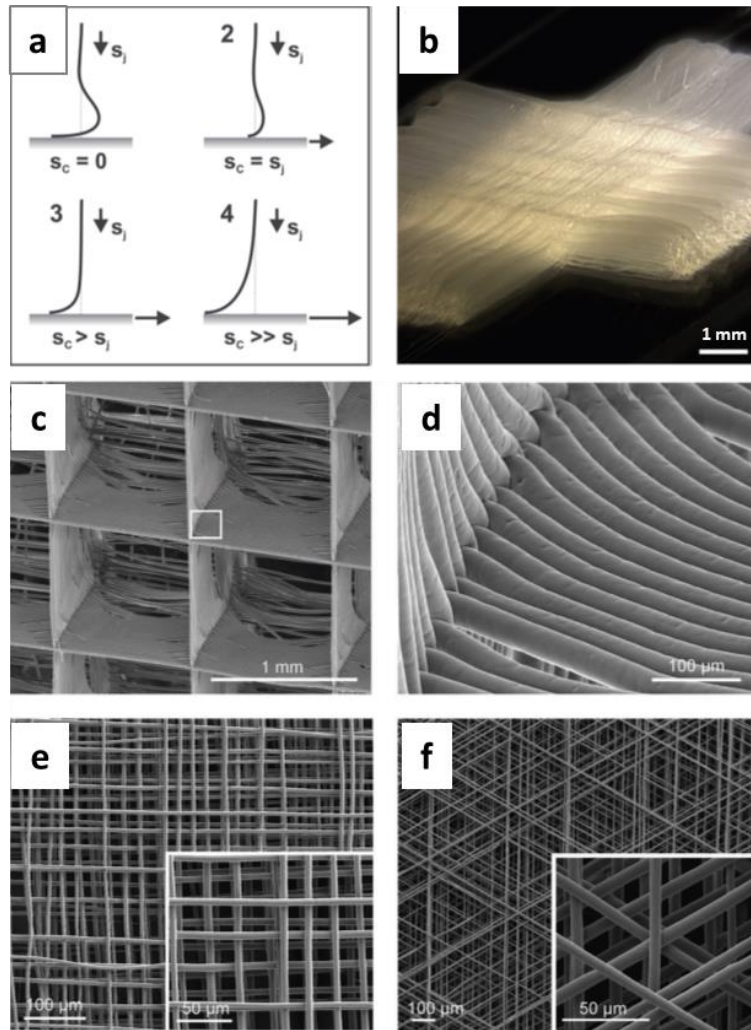


Figure 1.11. a, Correlation between the shape of the jet and the speed of the collector (s_c) relative to the speed of the jet (s_j) during melt electrospinning. b, Photograph of a scaffold created using a square wave pattern with alternating series of layers oriented at 90° . c and d, SEM images of the stacking (c) and interweaving (d) of fibers to form an array of $1\text{ mm} \times 1\text{ mm} \times 1\text{ mm}$ boxes. e and f, SEM images showing the assembly of PCL fibers into multilayered stacks with the orientation of fibers in adjacent layers rotated by 90° and 60° , respectively. (Reprinted with permission from ref.²³⁶. Copyright, 2011 Wiley-VCH.)

1.4 Electrospun light-emitting fiber materials

Light-emitting materials made from electrospun fibers are attracting increasing interest due to their potential applications in flexible light sources, waveguides, detectors and optical sensors.¹³³ Many experimental fabrications for electrospinning light-emitting composite fibers (e.g. doping QDs, nanowires, dyes or bio-chromophores in optically inert polymer matrices) and conjugated polymer fibers are presented.¹³⁴ The electrospinning process could tailor light-emitting fibers featuring evidently improved optical properties compared to the 2D film, such as enhanced photoluminescence quantum yield (PLQY), polarized emission and self-waveguiding.¹³³ These improved optical properties, combined with light weight, flexibility and high surface area to volume ratio, endow these light-emitting fibers with the ability to be a novel material in the light-emitting material field.

1.4.1 Processing of electrospun light-emitting fibers

Two main approaches are normally presented for obtaining electrospun light-emitting fibers (ELEF): i) Electrospinning composite light-emitting fiber from optical inert polymers (e.g. PMMA, PS, PEO, PVP) doped by luminescent systems (e.g. inorganic QDs or nanowires, dyes, organic chromophores or bio-chromophores); and ii) directly electrospinning intrinsically luminescent conjugated polymers.^{133, 134} The photoluminescent properties of the composite light-emitting fibers can be tailored by the luminescent systems which possess emissions in a broad spectral range (from visible to near infrared). Two principal approaches are presented for fabricating the inorganic QD or nanowires composite fibers: i) Blending synthesized QDs or nanowires with the polymer solution, as shown in **Figure 1.12 a and b**;³⁰⁶ and ii) embedding precursors in the polymer matrix, which enables the *in situ* synthesis of the QDs in electrospun fibers through posttreatments, such as gas reaction,¹⁵⁷ thermal treatment,³⁰⁷ and optical and electron beam exposures.³⁰⁸ Organic luminescent chromophores are also used embedded in polymer matrices for hunting electrospun light-emitting nanofibers. Due to fact that the optical properties of these organic chromophores are very sensitive to the solvents and to microenvironments, these composite fibers are used for optical sensing²³⁸ and in other photonic applications, such as light sources and microlasers.³⁰⁹ Hybrid luminescent systems in the composite

fibers were also developed by Botta *et al.*, who loaded inorganic zeolite L crystals with organic luminescent dyes (**Figure 1.12 c and d**).³¹⁰ The dye-loaded zeolites integrated into nanowires in the thin fibers with diameters down to 150 nm. The hybrid fibers obtained formed very bright nanometric light sources and possessed polarized light-emission at visible wavelengths.

Conjugated polymers are one kind of typical organic photoluminescent material.³¹¹ However, the electrospinning of conjugated polymers is a challenge, due to the low molar weight, significant chain rigidity and limited solubility.²³⁷ Moreover, these also stimulated the development of specific electrospun methodologies to obtain conjugated polymer light-emitting fibers. So far, three main methods can be identified to prepare uniform light-emitting fibers by electrospinning. The first and easiest method is mixing the conjugated polymers with an electrospun polymer matrix.³¹² With the assistance of high molar mass polymer matrices, the conjugated polymer can be encapsulated in fibers and exhibits the emission. Although blending is a very effective method to achieve conjugated polymer-based light-emitting fibers, it has a few criticalities: There is a limited choice of solvent that can dissolve both the conjugated polymer and the matrix properly and simultaneously, and phase separation effects between the two compounds can occur.^{134, 313} The second approach is based on core–shell electrospinning, consisting of an internal region (conjugated polymers) and a sheath (spinnable polymers). Xia *et al.* used a PVP solution in an ethanol/water mixture as outer spinnable polymers and a conjugated polymer dissolved in chloroform as the inner capillary. They finally overcame the problem of two incompatible solutions and electrospun conjugated polymers directly into uniform light-emitting fibers with controllable diameters and morphologies.³¹⁴ The third approach is conjugated polymer electrospun directly without any assistance from inert polymers by the modification of conjugated polymers with proper side-groups and a proper choice of the solution solvents. Pisignano *et al.* found that the conjugated polymer's side groups could increase the steric hindrance and the conformational plasticity of viscous solutions.¹⁹⁴ They also improved the processability of conjugated polymers by adding non-solvents with a high boiling point and dielectric constant, and they successfully electrospun single-component conjugated polymer fibers with uniform light emission (**Figure 1.12 e and f**).

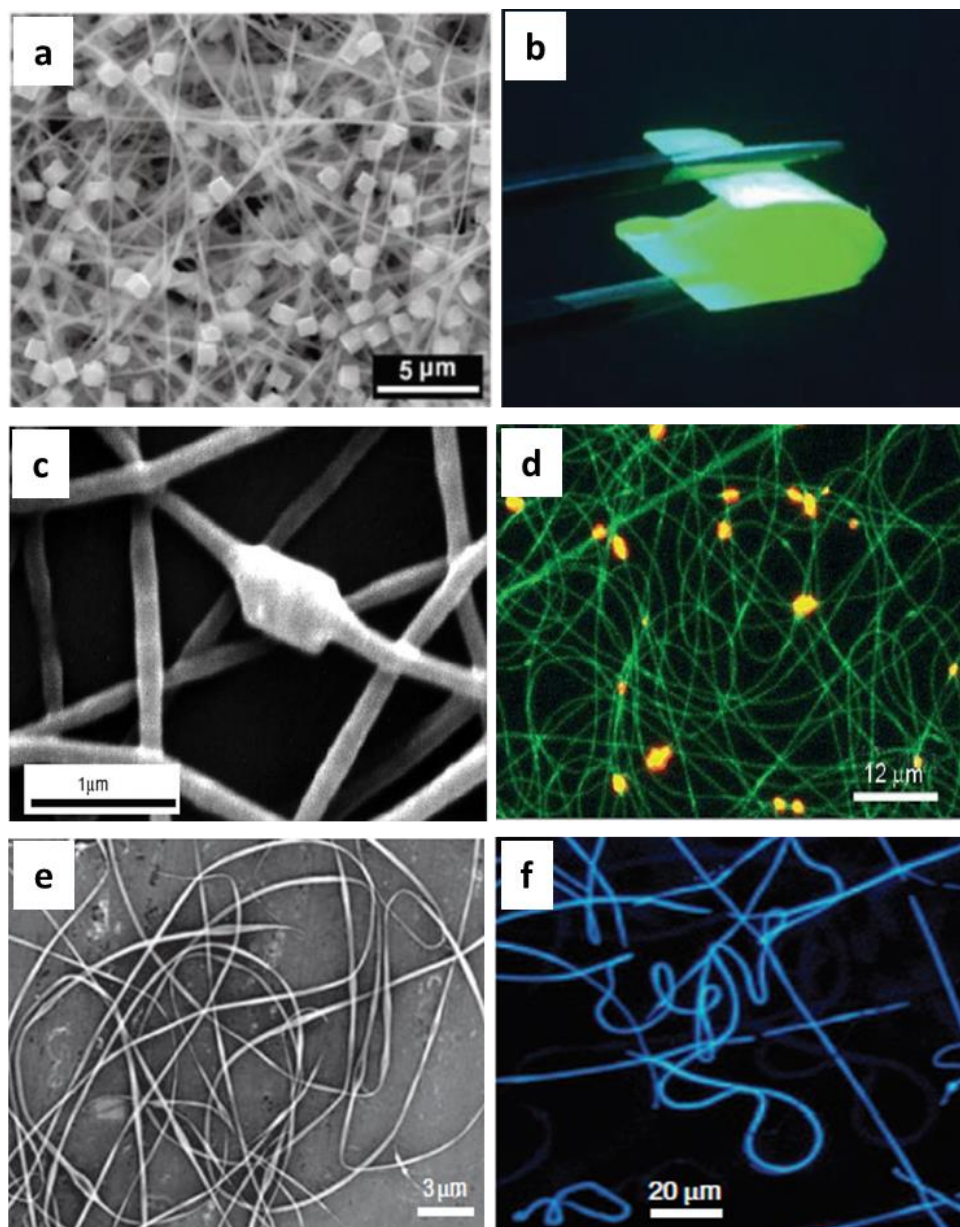


Figure 1.12. a SEM images of CsPbBr₃/Cs₄PbBr₆ perovskite crystals anchor onto Al₂O₃-La₂O₃ (CCAL) nanofibrous membranes. b, Images of CCAL nanofibrous membranes under UV-light (365 nm) excitation. (Reprinted with permission from ref.³⁰⁶. Copyright, 2018 WILEY-VCH.) c and d, SEM image (c) and confocal microscopy image (d) of luminescent nanofibers containing zeolites loaded with a red light-emitting system. (Reprinted with permission from ref.³¹⁰. Copyright, 2007 WILEY-VCH.) e and f, SEM image (e) and fluorescence micrograph (f) of conjugated polymer nanofibers. (Reprinted with permission from ref.¹⁹⁴. Copyright, 2008 Springer Nature.)

1.4.2 Properties of electrospun light-emitting fibers

The ELEFs display improved optical properties compared to the other solid-state systems, such as 2D thin films or bulk powders. The emission properties of ELEFs (e.g. changes of the emission wavelength, the emission efficiency and the radiative rates) are sensitive to local microenvironments and conformation of molecules.³¹⁵ Pisignano *et al.* found a blue-shift of the emission in the electrospun conjugated polymer fibers of 10 nm compared to the thin film (**Figure 1.13 a and b**).³¹⁶ Similar emission shifts in other conjugated polymers and chromophores, compared to the reference films, red-shift (toward lower energies) or blue-shift (toward lower energies), have also been reported.^{314, 316, 317} Some researchers have confirmed an enhanced PLQY in ELEFs compared to the other solid-state systems, such as thin films.^{312, 316, 318} Chen *et al.* have prepared some composite light-emitting fibers by blending PMMA with different conjugated polymers and found a higher photoluminescence efficiency for electrospun fibers compared to spin-coated films.³¹² Furthermore, Pisignano *et al.* also reported an enhancement of both the PLQY and the radiative rate (up to 22.5 %) of the electrospun fibers compared to spin-coated films.³¹⁶ Interestingly, polarized emission is evidently observed in the conjugated polymer or nanowire system fibers by electrospinning (**Figure 1.13 c**).^{310, 319-322} With the strong stretching forces in the ES process and the intermolecular interactions, the conjugated polymer chains or the crystal nanowires could align along the fiber axis and self-assemble into macroscopically alignment. As a result, an overall polarized light-emission can be produced. The individual fibers or aligned fiber assemblies were reported with polarized emission.^{319, 323} An easy and efficient method – post-processing – was proposed by Murata *et al.* to improve the polarization ratio of fibers.³²³ The mechanical stretching could further enhance chain orientation to obtain a higher polarization ratio compared to the as-spun aligned fibers (**Figure 1.13 d**).

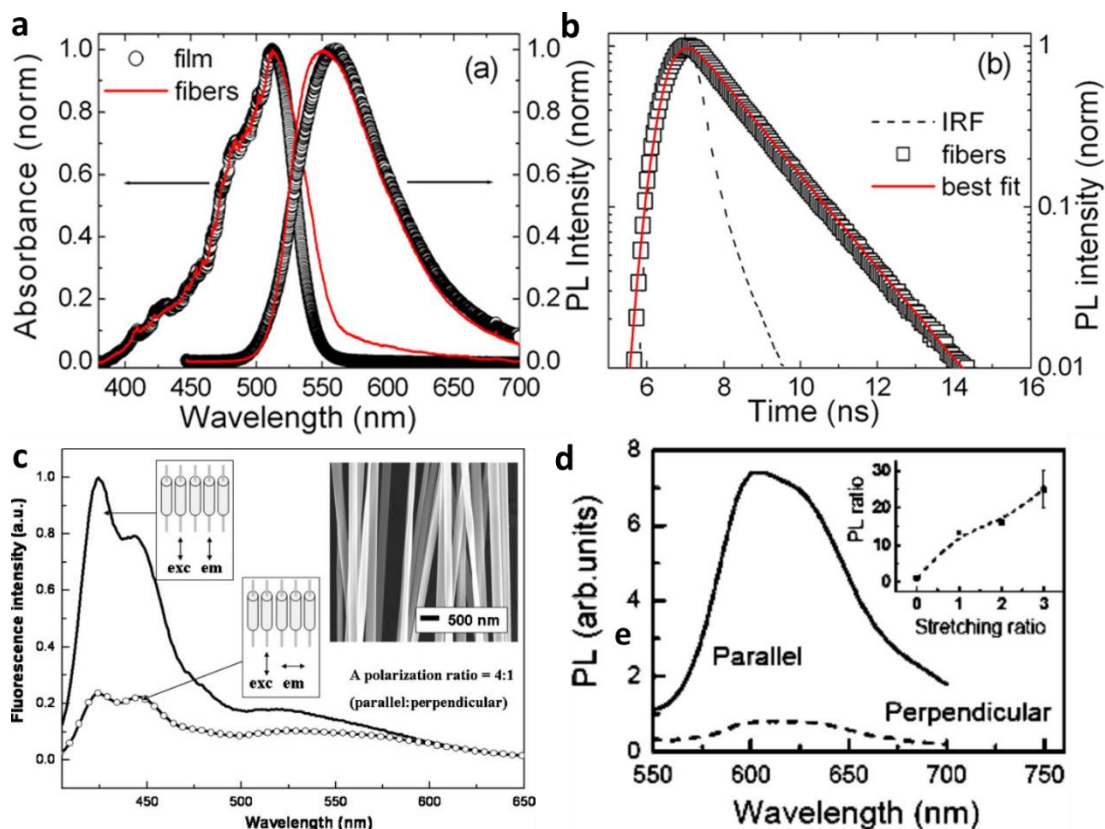


Figure 1.13. a, Comparison between the normalized absorbance (left vertical scale) and PL (right scale) spectra of poly[(9,9-dioctylfluorenyl-2,7-diyl)-co-(1,4-benzo-²³¹-thiadiazole)] (F8BT) fibers (red lines) and film (black symbols). b, PL temporal trace of F8BT fibers (symbols) and corresponding best fit (red continuous line) to an exponential function convoluted with the Instrumental Response Function (dashed line) on a semi-log scale. (Reprinted with permission from ref.³¹⁶. Copyright, 2013 AIP Publishing LLC.) c, Polarized photoluminescence spectra of uniaxially aligned fibers made by blending PMMA and the conjugated polymer salt. Inset: SEM image of uniaxially aligned PMMA/PF⁺ fibers. Scale bar: 500 nm. (Reprinted with permission from ref.³²⁰. Copyright, 2008 WILEY-VCH.) d, Polarized PL emission parallel (solid line) and perpendicular (dashed line) to the nanofiber axis for an aligned nonstretched MEH-PPV:PEO (1:2) sample. The inset shows the PL ratio as a function of stretching ratio, where 0 and 1 stand for a random mat and an aligned nonstretched sample, respectively. (Reprinted with permission from ref.³¹⁹. Copyright, 2008 American Institute of Physics.)

1.4.3 Applications of electrospun light-emitting fibers

The ELEFs, freestanding or coated on a substrate, possess enhanced emission properties compared to thin films and a high exposed surface, making them useful as optical sensors. Based on the analyte-induced quenching of the fluorescence, many optical sensing systems have been applied to metal ions,³²⁴ explosive molecules³²⁵ and bio-molecules,¹⁰³ with improved detection limits and time responses. Pavel *et al.* used reagents for the fabrication of fluorophore-polyamines (e.g. dansyl-polyamines) ELEFs that can be quenched by binding metal ions.³²⁴ The optical sensors exploited could detect a benchmark of ten metal ions (Al^{3+} , Fe^{3+} , Co^{2+} , Ni^{2+} , Cu^{2+} , Zn^{2+} , Hg^{2+} , Cd^{2+} , Ca^{2+} and Mg^{2+}), with a detection limit down to 2.0 ppm for Co^{2+} in water (pH 5). The nitroaromatic and its derivatives' explosive compounds, such as 2,4-dinitrotoluene³²⁶ and 2,4,6-trinitrotoluene,³²⁷ are electron-deficient systems which could induce the quenching of fluorescence of some polymers.³²⁵ Long *et al.* developed a reversible light-emitting fiber sensor based on PS composite electrospun fibers with a conjugated polymer that could be quenched by 2,4-dinitrotoluene and recovered after immersion in ammonia for 20 min. They found the sensor could have a loss of 25 % of the fluorescence intensity after five cycles of quenching/regeneration.³²⁶ Many biosensors made from electrospun fibers were developed to detect, for example, glucose,³²⁸ proteins³²⁹ or DNA.³²⁰ The optical detection in these ELEF biosensors exhibits lots of advantages, including enhanced and fast response, immunity of the signal to electrical or magnetic interference and a potential for higher information integration and processing.³³⁰

The ELEFs can be used as light sources which possess polarized spontaneous emission, color tenability or waveguiding.¹³⁴ Camposeo *et al.* tailored conjugated polymer blend ELEFs with full color tunability by changing the relative concentration of donor conjugated polymer (blue emitting) and acceptor conjugated polymer (red emitting).³³¹ The ELEFs could emit white light when an acceptor/donor molar concentration at about 10^{-2} . Additionally, if surrounded by air or by a medium with lower refractive index, ELEFs can guide light by total internal reflection, similar to the standard optical fibers.¹³⁴ Self-waveguided ELEFs are normally made by conjugated polymers or by inert polymers doped with light-emitting systems.¹⁹⁴ The emission can be partially waveguided along the ELEFs and emitted at the fiber tip or couple into

adjacent fibers.³⁰⁹ The ELEFs have recently been developed in an application in organic light-emitting diodes (OLEDs). Vohra *et al.* firstly reported electroluminescence from electrospun conjugated polymer nanofibers and used these ribbonlike ELEFs as active material in OLEDs. The OLEDs obtained possessed a brightness of 2300 cd/m² at 6 V.³³² Zheng *et al.* fabricated a QD LED using electrospun fibers. Compared to traditional QD polymer film, the thermal conductivities of the proposed QD polymer film increased by embedding electrospun nanofibers in it. It showed the luminous flux and efficiency of the LEDs increased by up to 51.8 % and 42.9 %, respectively, under a current of 800 mA.³³³ Some researchers found the ELEFs are a good candidate with high potential used in nanofiber lasers and organic field-effect transistors (OFETs). Camposeo *et al.* presented flexible lasers by embedding Rhodamine 6G in PMMA electrospun fibers, which showed laser emission with a small linewidth of 0.3 nm, a threshold of a few tens of mJ cm⁻² and well-behaved input–output characteristics.³⁰⁹ The charge-carrier mobility of 1D conjugated nanostructures and fibers is one to three orders of magnitude larger than films,³³⁴ which endow individual fibers the potential used in OFET active channels with reduced device cost and size. Liu *et al.* reported OFET devices developed from P3HT nanofibers, which exhibited performance comparable to thin film.³³⁵ High field-effect mobility (about 2 cm² V⁻¹ s⁻¹) and an on/off ratio in the order of 10⁵ were also reported in P3HT fiber OFETs.³³⁶

1.5 Polyacrylonitrile

Polyacrylonitrile (PAN) is a synthetic semicrystalline non-conjugated polymer from acrylonitrile (**Fig. 1.14**). A high dipole moment of 3.9 Debye was reported for the substituent cyano group.^{337, 338} This can induce strong attraction or repulsion between adjacent macromolecular chains, which results in the dominant characteristic of PAN.³³⁷ Due to the interactions among the cyano groups, distinct AIE characteristics were found in the concentrated PAN solutions, solid powders and films.³³⁹ The PAN solid powder also exhibited triplet emissions of delayed fluorescence and room temperature phosphorescence. The PAN is a versatile polymer utilized to fabricate a large variety of products, such as ultrafiltration membranes,³⁴⁰ sensors,³⁴¹ separators for Li-ion batteries,³⁴² artificial muscle,³⁴³ oxidized PAN fibers³⁴⁴ and carbon fibers.³⁴⁵ The most products containing acrylonitrile are copolymers. With the aid of other monomers, the properties of products could be improved: the adding of vinyl acetate

and methyl acrylate (**Fig. 1.14 c and d**) could increase the solubility of copolymers in polar organic solvents, such as DMF, DMSO and DMAc, which could be used for the spinning of fibers; halogen-containing monomers, such as vinyl chloride (**Fig. 1.14 e**), endow the copolymers with flame retardancy. Normally, PAN has a high melting point of above 300 °C.³⁴⁶ However, it is oxidized before melting. Thus, it is difficult to do a melt process for fabricating products from PAN. Therefore, PAN is used mainly to produce synthetic fibers by solution spinning. The PAN fiber is in an extremely important position in the development and application of synthetic fibers. Unique properties of PAN fiber are characterized by, for example, excellent weather resistance, high strength, low density (1.17–1.20 kg·m⁻³), low cost, low thermal conductivity values (1.113±0.117 W·m⁻¹·K⁻¹, lower than wool), and fluffiness and softness.³⁴⁷ To date, most practical applications of PAN fibers in industry have been based on the microfibers with diameters above 10 μm.

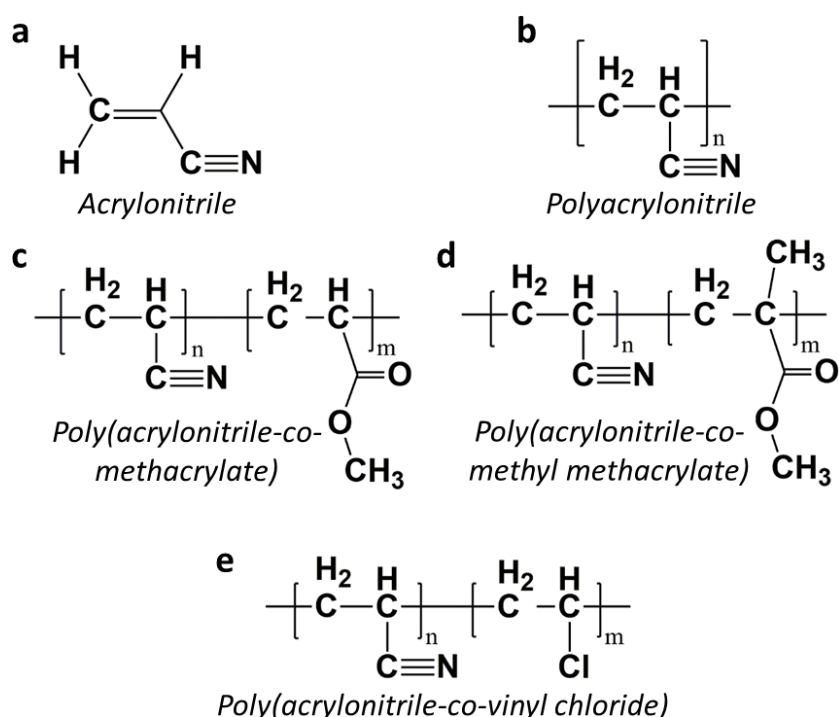


Figure 1.14. Molecular formula of acrylonitrile (a), Poly(acrylonitrile) (b), Poly(acrylonitrile-co-methacrylate) (c), Poly(acrylonitrile-co-methyl methacrylate) (d) and Poly(acrylonitrile-co-vinyl chloride) (e).

Compared to the PAN microfiber with its large size, PAN nanofiber with enhanced properties was confirmed in the lab, such as an ultralight weight, larger aspect ratio,

higher specific surface area, and size effect on high tensile strength, Young's modulus and toughness.³⁴⁶ Single PAN electrospun nanofibers with a diameter about 100 nm possessing simultaneously high strength and toughness were studied by pioneer work.⁵⁸ However, handling of such single nanofibers has prevented these from finding real-world technological processes in a viable and robust form. The normal robust 2D electrospun PAN fibrous membranes show mediocre mechanical properties, which cannot even be compared with PAN microfibers.^{348, 349} Therefore, fabricating mechanically strong, tough and multifunctional products with a viable and robust form from electrospun PAN fibers and exploring the applications of these products has become an interesting and important topic that is drawing increasing attention. Studies regarding the preparation and exploration of electrospun PAN fibers with simultaneous high tensile strength and toughness and multifunctional properties in different dimensional productions are highlighted in this thesis.

1.6 Thesis Objectives

The aim of this thesis is to prepare and study the electrospun fiber assemblies in different dimensions. Firstly, we designed a straightforward concept for combining high strength with high toughness through the preparation of 1D polymeric fibers by yarn electrospinning, which created fibers consisting of thousands of aligned nanofibrils in combination with a specified amount of linker molecule. During the experiments, the PAN doped with a small amount of PEG-BA as an interconnecting molecule were used for electrospinning into yarns. The yarns obtained were then stretched at above the T_g followed by an annealing process for crosslinking. Stretching at above T_g can not only align the fibrils efficiently but also increase the crystallinity and crystal orientation of the polymer in the fibrils. These rigid and oriented crystalline areas can endow the fibers with high strength and modulus. Moreover, the aligned molecules between adjacent nanofibrils should be interconnected by a conical covalent bond. Therefore, a reaction between nitrile groups in PAN and bisazide group in the PEG-BA was induced which could favorably lead to bridging between the fibrils in the yarns. When the resulting fibers were exposed to the force, these interconnected structures could enhance the lateral interaction between fibrils and transfer the load between chains under lateral loading. As a result, the fracture of fibers could occur at large deformation (high toughness) and large loads (high strength).

Next step, a concise and efficient fabrication approach to achieve polarized emission from commercial non-conjugated PAN fibers by mesoscopic order were presented. Three important molecular design rules were induced to achieve polarized emission in non-conjugated polymeric fibers: i) Electrospinning the non-conjugated polymer into nanofibers, ii) aligned crystal arrangement by sufficient heat-stretching at high temperatures above T_g , and iii) using functional groups that show AIE when interactions between adjacent groups lead to the formation of a more extended π -conjugated system. Non-conjugated PAN electrospun fibers satisfy these design requirements by forming a highly ordered, macroscopically aligned structure upon stretching at temperatures above T_g . Interactions between adjacent cyano side groups result in the formation of an extended π -system and the occurrence of aggregate-induced polarized deep blue emission. Due to the contribution of $n-\pi^*$ transitions

resulting from the nitrogen atoms in the cyano groups, intersystem crossing occurs that leads to the formation of highly mobile triplet states with a high lifetime. These triplets give rise to delayed fluorescence via triplet-triplet annihilation and to phosphorescence.

Meanwhile, we aim to evaluate the impact of short fiber length distribution on the microstructure and mechanical properties of 3D electrospun fiber sponges by preparing short electrospun fiber dispersions with controlled fiber length and using them for the preparation of the 3D electrospun fiber sponges. The short individual PAN fibers of well controlled length could be designed by cryo-microcutting of multifibrillar highly oriented electrospun PAN yarns. Fiber dispersions of different fiber length CV were obtained by mixing short fibers of different length, which were used for the preparation of sponges following the established method. Thus, the role of the fiber length distribution on the morphology and compression strength of sponges could be quantified.

1.7 References

- 1 R. O. Ritchie, *Nature Materials*, 2011, **10**, 817-822.
- 2 S. Keten, Z. Xu, B. Ihle and M. J. Buehler, *Nature Materials*, 2010, **9**, 359-367.
- 3 F. Vollrath and D. P. Knight, *Nature*, 2001, **410**, 541-548.
- 4 Z. Shao and F. Vollrath, *Nature*, 2002, **418**, 741.
- 5 U. G. Wegst, H. Bai, E. Saiz, A. P. Tomsia, and R. O. Ritchie, *Nature materials*, 2015, **14**, 23–36.
- 6 B. L. Thiel, K. B. Guess and C. Viney, *Biopolymers: Original Research on Biomolecules*, 1997, **41**, 703-719.
- 7 J. D. van Beek, S. Hess, F. Vollrath and B. H. Meier, *Proceedings of the National Academy of Sciences*, 2002, **99**, 10266-10271.
- 8 T. Lefèvre, M. E. Rousseau and M. Pézolet, *Biophysical Journal*, 2007, **92**, 2885-2895.
- 9 M. J. Buehler and Y. C. Yung, *Nature Materials*, 2009, **8**, 175-188.
- 10 C. Y. Hayashi, N. H. Shipley and R. V. Lewis, *International journal of biological macromolecules*, 1999, **24**, 271-275.
- 11 A. Heidebrecht and T. Scheibel, in *Advances in applied microbiology*, Elsevier, 2013, vol. 82, pp. 115-153.
- 12 F. Vollrath, B. Madsen and Z. Shao, *Proceedings of the Royal Society of London. Series B: Biological Sciences*, 2001, **268**, 2339-2346.
- 13 B. Madsen, Z. Z. Shao and F. Vollrath, *International journal of biological macromolecules*, 1999, **24**, 301-306.
- 14 Q. Wang, C. Wang, M. Zhang, M. Jian and Y. Zhang, *Nano Letters*, 2016, **16**, 6695-6700.
- 15 J. T. Wang, L. L. Li, M. Y. Zhang, S. L. Liu, L. H. Jiang and Q. Shen, *Mater Sci Eng C Mater Biol Appl*, 2014, **34**, 417-421.
- 16 S. M. Lee, E. Pippel, U. Gösele, C. Dresbach, Y. Qin, C. V. Chandran, T. Bräuniger, G. Hause and M. Knez, *Science*, 2009, **324**, 488-492.
- 17 X. Zhang, W. Lu, G. Zhou and Q. Li, *Advanced Materials*, 2020, **32**, 1902028.
- 18 B. Fang, D. Chang, Z. Xu and C. Gao, *Advanced Materials*, 2020, **32**, 1902664.
- 19 Z. Xu, Z. Liu, H. Sun and C. Gao, *Advanced Materials*, 2013, **25**, 3249-3253.
- 20 W. Guo, C. Liu, F. Zhao, X. Sun, Z. Yang, T. Chen, X. Chen, L. Qiu, X. Hu and H. Peng, *Advanced Materials*, 2012, **24**, 5379-5384.
- 21 M. D. Lima, M. W. Hussain, G. M. Spinks, S. Naficy, D. Hagenasr, J. S. Bykova, D. Tolly and R. H. Baughman, *Small*, 2015, **11**, 3113-3118.
- 22 T. Chen, S. Wang, Z. Yang, Q. Feng, X. Sun, L. Li, Z. S. Wang and H. Peng, *Angew Chem Int Ed Engl*, 2011, **50**, 1815-1819.
- 23 X. Li, T. Zhao, Q. Chen, P. Li, K. Wang, M. Zhong, J. Wei, D. Wu, B. Wei and H. Zhu, *Phys Chem Chem Phys*, 2013, **15**, 17752-17757.
- 24 W. G. Chong, J. Q. Huang, Z. L. Xu, X. Qin, X. Wang and J. K. Kim, *Advanced Functional Materials*, 2017, **27**, 1604815.
- 25 K. S. Novoselov, V. I. Fal'ko, L. Colombo, P. R. Gellert, M. G. Schwab and K. Kim, *Nature*, 2012, **490**, 192-200.

- 26 Y. Jang, S. M. Kim, G. M. Spinks and S. J. Kim, *Advanced Materials*, 2020, **32**, 1902670.
- 27 B. Peng, M. Locascio, P. Zapol, S. Li, S. L. Mielke, G. C. Schatz and H. D. Espinosa, *Nature Nanotechnology*, 2008, **3**, 626-631.
- 28 R. Zhang, Y. Zhang and F. Wei, *Accounts of Chemical Research*, 2017, **50**, 179-189.
- 29 F. Liu, P. Ming and J. Li, *Physical Review B*, 2007, **76**, 064120.
- 30 C. Lee, X. Wei, J. W. Kysar and J. Hone, *science*, 2008, **321**, 385-388.
- 31 K. Jiang, Q. Li and S. Fan, *Nature*, 2002, **419**, 801.
- 32 A. B. Dalton, S. Collins, E. Munoz, J. M. Razal, V. H. Ebron, J. P. Ferraris, J. N. Coleman, B. G. Kim and R. H. Baughman, *Nature*, 2003, **423**, 703.
- 33 E. Munoz, A. B. Dalton, S. Collins, M. Kozlov, J. Razal, J. N. Coleman, B. G. Kim, V. H. Ebron, M. Selvidge and J. P. Ferraris, *Advanced Engineering Materials*, 2004, **6**, 801-804.
- 34 N. Behabtu, C. C. Young, D. E. Tsentelovich, O. Kleinerman, X. Wang, A. W. Ma, E. A. Bengio, R. F. ter Waarbeek, J. J. de Jong and R. E. Hoogerwerf, *science*, 2013, **339**, 182-186.
- 35 M. Zhang, K. R. Atkinson and R. H. Baughman, *Science*, 2004, **306**, 1358-1361.
- 36 F. Meng, X. Zhang, R. Li, J. Zhao, X. Xuan, X. Wang, J. Zou and Q. Li, *Advanced Materials*, 2014, **26**, 2480-2485.
- 37 Y. Bai, R. Zhang, X. Ye, Z. Zhu, H. Xie, B. Shen, D. Cai, B. Liu, C. Zhang and Z. Jia, *Nature nanotechnology*, 2018, **13**, 589.
- 38 W. Xu, Y. Chen, H. Zhan and J. N. Wang, *Nano Letters*, 2016, **16**, 946-952.
- 39 J. N. Wang, X. G. Luo, T. Wu and Y. Chen, *Nature Communications*, 2014, **5**, 3848.
- 40 X. Li, T. Zhao, K. Wang, Y. Yang, J. Wei, F. Kang, D. Wu and H. Zhu, *Langmuir*, 2011, **27**, 12164-12171.
- 41 Z. Xu and C. Gao, *Nature Communications*, 2011, **2**, 571.
- 42 Z. Xu, Y. Liu, X. Zhao, L. Peng, H. Sun, Y. Xu, X. Ren, C. Jin, P. Xu, M. Wang and C. Gao, *Advanced Materials*, 2016, **28**, 6449-6456.
- 43 X. Hu, Z. Xu and C. Gao, *Scientific Reports*, 2012, **2**, 767.
- 44 X. Zhao, Z. Xu, B. Zheng and C. Gao, *Scientific Reports*, 2013, **3**, 3164.
- 45 Z. Liu, Z. Xu, X. Hu and C. Gao, *Macromolecules*, 2013, **46**, 6931-6941.
- 46 L. Kou and C. Gao, *Nanoscale*, 2013, **5**, 4370.
- 47 Y. Zhang, Y. Li, P. Ming, Q. Zhang, T. Liu, L. Jiang and Q. Cheng, *Advanced Materials*, 2016, **28**, 2834-2839.
- 48 X. Hu, S. Rajendran, Y. Yao, Z. Liu, K. Gopalsamy, L. Peng and C. Gao, *Nano Research*, 2016, **9**, 735-744.
- 49 R. Wang, J. Sun, L. Gao, C. Xu and J. Zhang, *Chemical Communications*, 2011, **47**, 8650.
- 50 M. K. Shin, B. Lee, S. H. Kim, J. A. Lee, G. M. Spinks, S. Gambhir, G. G. Wallace, M. E. Kozlov, R. H. Baughman and S. J. Kim, *Nature Communications*, 2012, **3**, 650.
- 51 H. Kim, Y. Jang, D. Y. Lee, J. H. Moon, J. G. Choi, G. M. Spinks, S. Gambhir, D. L. Officer, G. G. Wallace and S. J. Kim, *ACS Applied Materials & Interfaces*, 2019, **11**, 31162-31168.
- 52 E. Tan and C. Lim, *Composites science and technology*, 2006, **66**, 1102-1111.
- 53 S. Y. Gu, Q. L. Wu, J. Ren and G. J. Vancso, *Macromolecular Rapid Communications*, 2005, **26**, 716-720.
- 54 X. Li, H. Gao, C. J. Murphy and K. Caswell, *Nano letters*, 2003, **3**, 1495-1498.

- 55 E. P. S. Tan and C. T. Lim, *Applied Physics Letters*, 2005, **87**, 123106.
- 56 Y. Ding, H. Hou, Y. Zhao, Z. Zhu and H. Fong, *Progress in Polymer Science*, 2016, **61**, 67-103.
- 57 F. Chen, X. Peng, T. Li, S. Chen, X. F. Wu, D. H. Reneker and H. Hou, *Journal of Physics D: Applied Physics*, 2008, **41**, 025308.
- 58 D. Papkov, Y. Zou, M. N. Andalib, A. Goponenko, S. Z. Cheng and Y. A. Dzenis, *ACS nano*, 2013, **7**, 3324-3331.
- 59 J. H. Park and G. C. Rutledge, *Journal of materials science*, 2018, **53**, 3049-3063.
- 60 C. Cheng, J. Chen, F. Chen, P. Hu, X. F. Wu, D. H. Reneker and H. Hou, *Journal of Applied Polymer Science*, 2010, **116**, 1581-1586.
- 61 D. Zhu, X. Zhang, Y. Ou and M. Huang, *Journal of Composite Materials*, 2016, **51**, 2449-2465.
- 62 D. H. Reneker and A. L. Yarin, *Polymer*, 2008, **49**, 2387-2425.
- 63 A. Greiner and J. H. Wendorff, *Angew Chem Int Ed Engl*, 2007, **46**, 5670-5703.
- 64 J. Xue, T. Wu, Y. Dai and Y. Xia, *Chemical Review*, 2019, **119**, 5298-5415.
- 65 D. Li and Y. Xia, *Advanced materials*, 2004, **16**, 1151-1170.
- 66 C. Huang, S. Chen, C. Lai, D. H. Reneker, H. Qiu, Y. Ye and H. Hou, *Nanotechnology*, 2006, **17**, 1558-1563.
- 67 A. F. Spivak, Y. Dzenis and D. H. Reneker, *Mechanical Materials Engineering*, 2000, **27**, 37-42.
- 68 J. Doshi and D. H. Reneker, *Journal of electrostatics*, 1995, **35**, 151-160.
- 69 D. H. Reneker and I. Chun, *Nanotechnology*, 1996, **7**, 216.
- 70 H. Fong, I. Chun and D. H. Reneker, *Polymer*, 1999, **40**, 4585-4592.
- 71 L. Persano, A. Camposeo, C. Tekmen and D. Pisignano, *Macromolecular Materials and Engineering*, 2013, **298**, 504-520.
- 72 Y. Huang, J. Song, C. Yang, Y. Long and H. Wu, *Materials Today*, 2019, **28**, 98-113.
- 73 Z. M. Huang, Y. Z. Zhang, M. Kotaki and S. Ramakrishna, *Composites science and technology*, 2003, **63**, 2223-2253.
- 74 Z. Zhou, C. Lai, L. Zhang, Y. Qian, H. Hou, D. H. Reneker and H. Fong, *Polymer*, 2009, **50**, 2999-3006.
- 75 J. Lin, B. Ding and J. Yu, *ACS Appl Mater Interfaces*, 2010, **2**, 521-528.
- 76 M. Bognitzki, W. Czado, T. Frese, A. Schaper, M. Hellwig, M. Steinhart, A. Greiner and J. H. Wendorff, *Advanced materials*, 2001, **13**, 70-72.
- 77 S. Chen, H. Hou, P. Hu, J. H. Wendorff, A. Greiner and S. Agarwal, *Macromolecular Materials and Engineering*, 2009, **294**, 781-786.
- 78 S. Fleischer, R. Feiner, A. Shapira, J. Ji, X. Sui, H. Daniel Wagner and T. Dvir, *Biomaterials*, 2013, **34**, 8599-8606.
- 79 J. E. Díaz, A. Barrero, M. Márquez and I. G. Loscertales, *Advanced Functional Materials*, 2006, **16**, 2110-2116.
- 80 P. Gupta and G. L. Wilkes, *Polymer*, 2003, **44**, 6353-6359.
- 81 L. Peng, S. Jiang, M. Seuß, A. Fery, G. Lang, T. Scheibel and S. Agarwal, *Macromolecular Materials and Engineering*, 2016, **301**, 48-55.
- 82 Z. Sun, E. Zussman, A. L. Yarin, J. H. Wendorff and A. Greiner, *Advanced materials*, 2003, **15**, 1929-1932.
- 83 H. Chen, N. Wang, J. Di, Y. Zhao, Y. Song and L. Jiang, *Langmuir*, 2010, **26**, 11291-11296.

- 84 D. Li and Y. Xia, *Nano letters*, 2004, **4**, 933-938.
- 85 J. Di, H. Chen, X. Wang, Y. Zhao, L. Jiang, J. Yu and R. Xu, *Chemistry of Materials*, 2008, **20**, 3543-3545.
- 86 J. Tao and S. Shivkumar, *Materials Letters*, 2007, **61**, 2325-2328.
- 87 S. Koombhongse, W. Liu and D. H. Reneker, *Journal of Polymer Science Part B: Polymer Physics*, 2001, **39**, 2598-2606.
- 88 X. J. Han, Z. M. Huang, C. L. He, L. Liu and Q. S. Wu, *Polymer Composites*, 2006, **27**, 381-387.
- 89 M. Mirjalili and S. Zohoori, *Journal of Nanostructure in Chemistry*, 2016, **6**, 207-213.
- 90 S. Agarwal, J. H. Wendorff and A. Greiner, *Advanced Materials*, 2009, **21**, 3343-3351.
- 91 U. Boudriot, R. Dersch, A. Greiner and J. H. Wendorff, *Artificial organs*, 2006, **30**, 785-792.
- 92 H. Cho, S. Y. Min and T. W. Lee, *Macromolecular Materials and Engineering*, 2013, **298**, 475-486.
- 93 N. Tomczak, N. F. van Hulst and G. J. Vancso, *Macromolecules*, 2005, **38**, 7863-7866.
- 94 M. Stasiak, A. Studer, A. Greiner and J. H. Wendorff, *Chemistry*, 2007, **13**, 6150-6156.
- 95 E. Formo, E. Lee, D. Campbell and Y. Xia, *Nano Letters*, 2008, **8**, 668-672.
- 96 T. J. Sill and H. A. von Recum, *Biomaterials*, 2008, **29**, 1989-2006.
- 97 X. Hu, S. Liu, G. Zhou, Y. Huang, Z. Xie and X. Jing, *Journal of controlled release*, 2014, **185**, 12-21.
- 98 A. Luzio, E. V. Canesi, C. Bertarelli and M. Caironi, *Materials (Basel)*, 2014, **7**, 906-947.
- 99 S. Reich, M. Burgard, M. Langner, S. Jiang, X. Wang, S. Agarwal, B. Ding, J. Yu and A. Greiner, *npj Flexible Electronics*, 2018, **2**, 5.
- 100 B. Zhang, F. Kang, J. M. Tarascon and J.-K. Kim, *Progress in Materials Science*, 2016, **76**, 319-380.
- 101 S. Peng, L. Li, Y. Hu, M. Srinivasan, F. Cheng, J. Chen and S. Ramakrishna, *Acs Nano*, 2015, **9**, 1945-1954.
- 102 K. Maity and D. Mandal, *ACS Appl Mater Interfaces*, 2018, **10**, 18257-18269.
- 103 B. Ding, M. Wang, X. Wang, J. Yu and G. Sun, *Materials Today*, 2010, **13**, 16-27.
- 104 J. Xu, C. Liu, P. C. Hsu, K. Liu, R. Zhang, Y. Liu and Y. Cui, *Nano Letters*, 2016, **16**, 1270-1275.
- 105 M. Langner and A. Greiner, *Macromol Rapid Commun*, 2016, **37**, 351-355.
- 106 J. Lyons, C. Li and F. Ko, *Polymer*, 2004, **45**, 7597-7603.
- 107 J. Valtera, T. Kalous, P. Pokorný, O. Batka, M. Bilek, J. Chvojka, P. Mikes, E. K. Kostakova, P. Zabka and J. Ornstova, *Scientific reports*, 2019, **9**, 1801.
- 108 R. Kessick, J. Fenn and G. Tepper, *Polymer*, 2004, **45**, 2981-2984.
- 109 S. Sarkar, S. Deevi and G. Tepper, *Macromolecular Rapid Communications*, 2007, **28**, 1034-1039.
- 110 S. Maheshwari and H. C. Chang, *Advanced Materials*, 2009, **21**, 349-354.
- 111 P. Pokorný, E. Kostakova, F. Sanetrník, P. Mikes, J. Chvojka, T. Kalous, M. Bilek, K. Pejchar, J. Valtera and D. Lukas, *Phys Chem Chem Phys*, 2014, **16**, 26816-26822.
- 112 A. L. Yarin and E. Zussman, *Polymer*, 2004, **45**, 2977-2980.
- 113 O. Jirsak, P. Sysel, F. Sanetrník, J. Hruza and J. Chaloupek, *Journal of Nanomaterials*, 2010, **2010**, 1-6.
- 114 Y. Liu and J. H. He, *International Journal of Nonlinear Sciences and Numerical Simulation*, 2007, **8**, 393-396.
- 115 X. Wang, H. Niu, T. Lin and X. Wang, *Polymer Engineering & Science*, 2009, **49**, 1582-1586.
- 116 N. M. Thoppey, J. R. Bochinski, L. I. Clarke and R. E. Gorga, *Polymer*, 2010, **51**, 4928-4936.

- 117 S. Tang, Y. Zeng and X. Wang, *Polymer Engineering & Science*, 2010, **50**, 2252-2257.
- 118 B. Lu, Y. Wang, Y. Liu, H. Duan, J. Zhou, Z. Zhang, Y. Wang, X. Li, W. Wang, W. Lan and E. Xie, *Small*, 2010, **6**, 1612-1616.
- 119 D. Wu, X. Huang, X. Lai, D. Sun and L. Lin, *J Nanosci Nanotechnol*, 2010, **10**, 4221-4226.
- 120 H. J. Nieminen, I. Laidmäe, A. Salmi, T. Rauhala, T. Paulin, J. Heinämäki and E. Hægström, *Scientific reports*, 2018, **8**, 4437.
- 121 N. M. Thoppey, J. R. Bochinski, L. I. Clarke and R. E. Gorga, *Nanotechnology*, 2011, **22**, 345301.
- 122 W. Zhou, Z. Li, Q. Zhang, Y. Liu, F. Wei and G. Luo, *J Nanosci Nanotechnol*, 2007, **7**, 2667-2673.
- 123 Y. Lin, Y. Yao, X. Yang, N. Wei, X. Li, P. Gong, R. Li and D. Wu, *Journal of Applied Polymer Science*, 2008, **107**, 909-917.
- 124 B. Chu, B. S. Hsiao, D. Fang and A. Okamoto, *Electro-blowing technology for fabrication of fibrous articles and its applications of hyaluronan*, patent, 2005-4-14.
- 125 A. Vaseashta, *Applied Physics Letters*, 2007, **90**, 093115.
- 126 C. S. Kong, S. G. Lee, S. H. Lee, K. H. Lee, H. W. Noh, W. S. Yoo and H. S. Kim, *Journal of Macromolecular Science, Part B*, 2011, **50**, 528-539.
- 127 S. Paruchuri and M. P. Brenner, *Physical Review Letters*, 2007, **98**, 134502.
- 128 M. H. Duby, W. Deng, K. Kim, T. Gomez and A. Gomez, *Journal of Aerosol Science*, 2006, **37**, 306-322.
- 129 A. Varesano, R. A. Carletto and G. Mazzuchetti, *Journal of Materials Processing Technology*, 2009, **209**, 5178-5185.
- 130 Y. Liu and L. Guo, *J Nanosci Nanotechnol*, 2013, **13**, 843-847.
- 131 S. A. Theron, A. L. Yarin, E. Zussman and E. Kroll, *Polymer*, 2005, **46**, 2889-2899.
- 132 G. Kim, Y. S. Cho and W. D. Kim, *European Polymer Journal*, 2006, **42**, 2031-2038.
- 133 A. Macagnano, E. Zampetti and E. Kny, *Electrospinning for high performance sensors*, Springer, 2015.
- 134 A. Camposeo, L. Persano and D. Pisignano, *Macromolecular Materials and Engineering*, 2013, **298**, 487-503.
- 135 N. Bhattarai, D. Edmondson, O. Veiseh, F. A. Matsen and M. Zhang, *Biomaterials*, 2005, **26**, 6176-6184.
- 136 X. Geng, O. H. Kwon and J. Jang, *Biomaterials*, 2005, **26**, 5427-5432.
- 137 T. Liu, W. K. Teng, B. P. Chan and S. Y. Chew, *Journal of Biomedical Materials Research Part A*, 2010, **95**, 276-282.
- 138 L. Meng, O. Arnoult, M. Smith and G. E. Wnek, *Journal of Materials Chemistry*, 2012, **22**, 19412.
- 139 N. Choktaweasap, K. Arayanarakul, D. Aht-Ong, C. Meechaisue and P. Supaphol, *Polymer journal*, 2007, **39**, 622.
- 140 S. Panzavolta, M. Gioffre, M. L. Focarete, C. Gualandi, L. Foroni and A. Bigi, *Acta Biomaterialia*, 2011, **7**, 1702-1709.
- 141 S. Zarkoob, R. K. Eby, D. H. Reneker, S. D. Hudson, D. Ertley and W. W. Adams, *Polymer*, 2004, **45**, 3973-3977.
- 142 C. R. Wittmer, T. Claudepierre, M. Reber, P. Wiedemann, J. A. Garlick, D. Kaplan and C. Egles, *Advanced Functional Materials*, 2011, **21**, 4232-4242.

- 143 C. W. Kim, M. W. Frey, M. Marquez and Y. L. Joo, *Journal of Polymer Science Part B: Polymer Physics*, 2005, **43**, 1673-1683.
- 144 C. W. Kim, D. S. Kim, S. Y. Kang, M. Marquez and Y. L. Joo, *Polymer*, 2006, **47**, 5097-5107.
- 145 Y. Ji, K. Ghosh, X. Z. Shu, B. Li, J. C. Sokolov, G. D. Prestwich, R. A. Clark and M. H. Rafailovich, *Biomaterials*, 2006, **27**, 3782-3792.
- 146 Y. Liu, G. Ma, D. Fang, J. Xu, H. Zhang and J. Nie, *Carbohydrate Polymers*, 2011, **83**, 1011-1015.
- 147 I. Cacciotti, J. N. House, C. Mazzuca, M. Valentini, F. Madau, A. Palleschi, P. Straffi and F. Nanni, *Materials & Design*, 2015, **88**, 1109-1118.
- 148 J. R. Kim and A. N. Netravali, *ACS Sustainable Chemistry & Engineering*, 2017, **5**, 4957-4968.
- 149 Y. Ner, J. G. Grote, J. A. Stuart and G. A. Sotzing, *Angewandte Chemie International Edition*, 2009, **48**, 5134-5138.
- 150 K. Maleckis and Y. Dzenis, *Macromolecular Materials and Engineering*, 2018, **303**, 1800302.
- 151 M. Li, M. J. Mondrinos, M. R. Gandhi, F. K. Ko, A. S. Weiss and P. I. Lelkes, *Biomaterials*, 2005, **26**, 5999-6008.
- 152 J. E. Martín-Alfonso, A. A. Cuadri and J. M. Franco, *Fibers and Polymers*, 2019, **20**, 1586-1593.
- 153 L. Wu, X. Yuan and J. Sheng, *Journal of Membrane Science*, 2005, **250**, 167-173.
- 154 C. Zhang, X. Yuan, L. Wu, Y. Han and J. Sheng, *European Polymer Journal*, 2005, **41**, 423-432.
- 155 R. Jaeger, M. M. Bergshoef, C. M. I. Batlle, H. Schönherr and G. Julius Vancso, 1998.
- 156 J. M. Deitzel, J. Kleinmeyer, J. Hirvonen and N. B. Tan, *Polymer*, 2001, **42**, 8163-8170.
- 157 X. Lu, Y. Zhao and C. Wang, *Advanced Materials*, 2005, **17**, 2485-2488.
- 158 M. Chen, H. Qu, J. Zhu, Z. Luo, A. Khasanov, A. S. Kucknoor, N. Haldolaarachchige, D. P. Young, S. Wei and Z. Guo, *Polymer*, 2012, **53**, 4501-4511.
- 159 Y. J. Yun, W. G. Hong, W. J. Kim, Y. Jun and B. H. Kim, *Advanced Materials*, 2013, **25**, 5701-5705.
- 160 R. H. Sanatgar, S. Borhani, S. A. H. Ravandi and A. A. Gharehaghaji, *Journal of Applied Polymer Science*, 2012, **126**, 1112-1120.
- 161 W. Liu, M. Graham, E. A. Evans and D. H. Reneker, *Journal of Materials Research*, 2002, **17**, 3206-3212.
- 162 S. Chen, H. Hou, P. Hu, J. H. Wendorff, A. Greiner and S. Agarwal, *Macromolecular Materials and Engineering*, 2009, **294**, 265-271.
- 163 J. S. Youm, J. H. Kim, C. H. Kim, J. C. Kim, Y. A. Kim and K. S. Yang, *Journal of Applied Polymer Science*, 2016, **133**, 37.
- 164 Y. Bin, Y. Hao, M. Zhu and H. Wang, *Journal of Nanoscience and Nanotechnology*, 2016, **16**, 5633-5638.
- 165 K. Lee, H. Kim, M. Khil, Y. Ra and D. Lee, *Polymer*, 2003, **44**, 1287-1294.
- 166 A. Cipitria, A. Skelton, T. R. Dargaville, P. D. Dalton and D. W. Huttmacher, *Journal of Materials Chemistry*, 2011, **21**, 9419.
- 167 H. Maleki, A. A. Gharehaghaji, L. Moroni and P. J. Dijkstra, *Biofabrication*, 2013, **5**, 035014.
- 168 W. Chen, J. Ma, L. Zhu, Y. Morsi, H. Ei-Hamshary, S. S. Al-Deyab and X. Mo, *Colloids Surf B Biointerfaces*, 2016, **142**, 165-172.
- 169 K. H. Lee, H. Y. Kim, Y. M. La, D. R. Lee and N. H. Sung, *Journal of Polymer Science Part B: Polymer Physics*, 2002, **40**, 2259-2268.

- 170 K. H. Lee, H. Y. Kim, Y. J. Ryu, K. W. Kim and S. W. Choi, *Journal of Polymer Science Part B: Polymer Physics*, 2003, **41**, 1256-1262.
- 171 U. Ali, H. Niu, A. Abbas, H. Shao and T. Lin, *RSC Advances*, 2016, **6**, 30564-30569.
- 172 Z. Zhou and X. F. Wu, *Materials Letters*, 2015, **160**, 423-427.
- 173 M. Kang, R. Jung, H.-S. Kim and H.-J. Jin, *Colloids and Surfaces A: Physicochemical and Engineering Aspects*, 2008, **313**, 411-414.
- 174 U. Ali, Y. Zhou, X. Wang and T. Lin, *Journal of the Textile Institute*, 2012, **103**, 80-88.
- 175 S. Jiang, S. Reich, B. Uch, P. Hu, S. Agarwal and A. Greiner, *ACS Appl Mater Interfaces*, 2017, **9**, 34286-34293.
- 176 R. Sen, B. Zhao, D. Perea, M. E. Itkis, H. Hu, J. Love, E. Bekyarova and R. C. Haddon, *Nano letters*, 2004, **4**, 459-464.
- 177 L. D. Tijing, C. H. Park, W. L. Choi, M. T. G. Ruelo, A. Amarjargal, H. R. Pant, I.-T. Im and C. S. Kim, *Composites Part B: Engineering*, 2013, **44**, 613-619.
- 178 Q. Li, Y. Xu, H. Wei and X. Wang, *RSC Advances*, 2016, **6**, 65275-65281.
- 179 I. N. Strain, Q. Wu, A. M. Pourrahimi, M. S. Hedenqvist, R. T. Olsson and R. L. Andersson, *Journal of Materials Chemistry A*, 2015, **3**, 1632-1640.
- 180 J. Hao, G. Lei, Z. Li, L. Wu, Q. Xiao and L. Wang, *Journal of Membrane Science*, 2013, **428**, 11-16.
- 181 H. M. Khanlou, B. C. Ang, S. Talebian, M. M. Barzani, M. Silakhori and H. Fauzi, *Measurement*, 2015, **65**, 193-206.
- 182 T. Uyar, A. Balan, L. Toppare and F. Besenbacher, *Polymer*, 2009, **50**, 475-480.
- 183 X. Wang, W. J. Zhang, D. G. Yu, X. Y. Li and H. Yang, *Macromolecular Materials and Engineering*, 2013, **298**, 664-669.
- 184 D. Yang, X. Liu, Y. Jin, Y. Zhu, D. Zeng, X. Jiang and H. Ma, *Biomacromolecules*, 2009, **10**, 3335-3340.
- 185 A. K. An, J. Guo, E. J. Lee, S. Jeong, Y. Zhao, Z. Wang and T. Leiknes, *Journal of Membrane Science*, 2017, **525**, 57-67.
- 186 S. U. Patel and G. G. Chase, *Separation and Purification Technology*, 2014, **126**, 62-68.
- 187 K. H. Lee, O. Ohsawa, K. Watanabe, I. S. Kim, S. R. Givens, B. Chase and J. F. Rabolt, *Macromolecules*, 2009, **42**, 5215-5218.
- 188 T. Yoshioka, R. Dersch, M. Tsuji and A. K. Schaper, *Polymer*, 2010, **51**, 2383-2389.
- 189 J. Ma, Q. Zhang, A. Mayo, Z. Ni, H. Yi, Y. Chen, R. Mu, L. M. Bellan and D. Li, *Nanoscale*, 2015, **7**, 16899-16908.
- 190 Q. Z. Yu, M. M. Shi, M. Deng, M. Wang and H. Z. Chen, *Materials Science and Engineering: B*, 2008, **150**, 70-76.
- 191 Y. Zhang and G. C. Rutledge, *Macromolecules*, 2012, **45**, 4238-4246.
- 192 I. S. Chronakis, S. Grapenson and A. Jakob, *Polymer*, 2006, **47**, 1597-1603.
- 193 T. S. Kang, S. W. Lee, J. Joo and J. Y. Lee, *Synthetic Metals*, 2005, **153**, 61-64.
- 194 F. Di Benedetto, A. Camposeo, S. Pagliara, E. Mele, L. Persano, R. Stabile, R. Cingolani and D. Pisignano, *Nature Nanotechnology*, 2008, **3**, 614-619.
- 195 W. Zhao, B. Yalcin and M. Cakmak, *Synthetic Metals*, 2015, **203**, 107-116.
- 196 S. Lee, G. D. Moon and U. Jeong, *Journal of Materials Chemistry*, 2009, **19**, 743-748.
- 197 K. H. K. Chan, T. Yamao, M. Kotaki and S. Hotta, *Synthetic Metals*, 2010, **160**, 2587-2595.

- 198 H. Chen and Y. A. Elabd, *Macromolecules*, 2009, **42**, 3368-3373.
- 199 M. G. McKee, M. T. Hunley, J. M. Layman and T. E. Long, *Macromolecules*, 2006, **39**, 575-583.
- 200 H. Wu, L. Hu, M. W. Rowell, D. Kong, J. J. Cha, J. R. McDonough, J. Zhu, Y. Yang, M. D. McGehee and Y. Cui, *Nano Letters*, 2010, **10**, 4242-4248.
- 201 M. Bognitzki, M. Becker, M. Graeser, W. Massa, J. H. Wendorff, A. Schaper, D. Weber, A. Beyer, A. Götzhäuser and A. Greiner, *Advanced Materials*, 2006, **18**, 2384-2386.
- 202 J. Jang, B. G. Hyun, S. Ji, E. Cho, B. W. An, W. H. Cheong and J. U. Park, *NPG Asia Materials*, 2017, **9**, e432.
- 203 M. Graeser, M. Bognitzki, W. Massa, C. Pietzonka, A. Greiner and J. H. Wendorff, *Advanced Materials*, 2007, **19**, 4244-4247.
- 204 H. Wu, R. Zhang, X. Liu, D. Lin and W. Pan, *Chemistry of materials*, 2007, **19**, 3506-3511.
- 205 V. G. Pol, E. Koren and A. Zaban, *Chemistry of Materials*, 2008, **20**, 3055-3062.
- 206 J. M. Kim, H.-I. Joh, S. M. Jo, D. J. Ahn, H. Y. Ha, S.-A. Hong and S.-K. Kim, *Electrochimica Acta*, 2010, **55**, 4827-4835.
- 207 A. M. Azad, *Materials Science and Engineering: A*, 2006, **435-436**, 468-473.
- 208 X. Yang, C. Shao, Y. Liu, R. Mu and H. Guan, *Thin Solid Films*, 2005, **478**, 228-231.
- 209 Z. Cui, S. Wang, Y. Zhang and M. Cao, *Electrochimica Acta*, 2015, **182**, 507-515.
- 210 R. Sahay, P. Suresh Kumar, V. Aravindan, J. Sundaramurthy, W. Chui Ling, S. G. Mhaisalkar, S. Ramakrishna and S. Madhavi, *The Journal of Physical Chemistry C*, 2012, **116**, 18087-18092.
- 211 W. Zheng, Z. Li, H. Zhang, W. Wang, Y. Wang and C. Wang, *Materials Research Bulletin*, 2009, **44**, 1432-1436.
- 212 Q. Fan and M. S. Whittingham, *Electrochemical and Solid-State Letters*, 2007, **10**, A48.
- 213 S. S. Choi, S. G. Lee, S. S. Im, S. H. Kim and Y. L. Joo, *Journal of Materials Science Letters*, 2003, **22**, 891-893.
- 214 Y. Si, J. Yu, X. Tang, J. Ge and B. Ding, *Nature Communications*, 2014, **5**, 5802.
- 215 Y. Zhang, J. Li, G. An and X. He, *Sensors and Actuators B: Chemical*, 2010, **144**, 43-48.
- 216 D. Li and Y. Xia, *Nano letters*, 2003, **3**, 555-560.
- 217 C. Ban, N. A. Chernova and M. S. Whittingham, *Electrochemistry Communications*, 2009, **11**, 522-525.
- 218 G. Wang, Y. Ji, X. Huang, X. Yang, P. I. Gouma and M. Dudley, *The Journal of Physical Chemistry B*, 2006, **110**, 23777-23782.
- 219 E. Formo, P. H. C. Camargo, B. Lim, M. Jiang and Y. Xia, *Chemical Physics Letters*, 2009, **476**, 56-61.
- 220 J. Yan, Y. Han, S. Xia, X. Wang, Y. Zhang, J. Yu and B. Ding, *Advanced Functional Materials*, 2019, **29**, 1907919.
- 221 Y. W. Ju, J. H. Park, H. R. Jung, S. J. Cho and W. J. Lee, *Materials Science and Engineering: B*, 2008, **147**, 7-12.
- 222 C. Shao, N. Yu, Y. Liu and R. Mu, *Journal of Physics and Chemistry of Solids*, 2006, **67**, 1423-1426.
- 223 W. Luo, X. Hu, Y. Sun and Y. Huang, *Journal of Materials Chemistry*, 2012, **22**, 8916.
- 224 K. Sahner, P. Gouma and R. Moos, *Sensors*, 2007, **7**, 1871-1886.
- 225 G. Wang, Q. Dong, T. Wu, F. Zhan, M. Zhou and J. Qiu, *Carbon*, 2016, **103**, 311-317.
- 226 S. Moon and R. J. Farris, *Carbon*, 2009, **47**, 2829-2839.

- 227 M. Shi, L. Zhao, X. Song, J. Liu, P. Zhang and L. Gao, *ACS Appl Mater Interfaces*, 2016, **8**, 32460-32467.
- 228 B. M. Eick and J. P. Youngblood, *Journal of Materials Science*, 2009, **44**, 160-165.
- 229 L. Zhang, J. Hu, A. A. Voevodin and H. Fong, *Nanoscale*, 2010, **2**, 1670-1673.
- 230 X. Zhou, Y. Qiu, J. Yu, J. Yin and S. Gao, *International Journal of Hydrogen Energy*, 2011, **36**, 7398-7404.
- 231 X. Tao, S. Zhou, J. Ma, Z. Xiang, R. Hou, J. Wang and X. Li, *Ceramics International*, 2017, **43**, 3910-3914.
- 232 G. Xia, D. Li, X. Chen, Y. Tan, Z. Tang, Z. Guo, H. Liu, Z. Liu and X. Yu, *Advanced Materials*, 2013, **25**, 6238-6244.
- 233 W. Li, C. Y. Cao, C. Q. Chen, Y. Zhao, W. G. Song and L. Jiang, *Chemical Communications*, 2011, **47**, 3619-3621.
- 234 Y. Xu, J. Wang, L. Shen, H. Dou and X. Zhang, *Electrochimica Acta*, 2015, **173**, 680-686.
- 235 G. Kim, J. Son, S. Park and W. Kim, *Macromolecular Rapid Communications*, 2008, **29**, 1577-1581.
- 236 T. D. Brown, P. D. Dalton and D. W. Hutmacher, *Advanced Materials*, 2011, **23**, 5651-5657.
- 237 Y. Yu, S. Hua, M. Yang, Z. Fu, S. Teng, K. Niu, Q. Zhao and C. Yi, *RSC Advances*, 2016, **6**, 110557-110565.
- 238 S. J. Lee, M. Nowicki, B. Harris and L. G. Zhang, *Tissue Engineering Part A*, 2017, **23**, 491-502.
- 239 S. Naghie, E. Foroozmehr, M. Badrossamay and M. Kharaziha, *Materials & Design*, 2017, **133**, 128-135.
- 240 D. Ye, Y. Ding, Y. Duan, J. Su, Z. Yin and Y. A. Huang, *Small*, 2018, **14**, e1703521.
- 241 Y. Huang, Y. Duan, Y. Ding, N. Bu, Y. Pan, N. Lu and Z. Yin, *Scientific Reports*, 2014, **4**, 5949.
- 242 D. Sun, C. Chang, S. Li and L. Lin, *Nano letters*, 2006, **6**, 839-842.
- 243 N. Bu, Y. Huang, X. Wang and Z. Yin, *Materials and Manufacturing Processes*, 2012, **27**, 1318-1323.
- 244 Y. Huang, Y. Ding, J. Bian, Y. Su, J. Zhou, Y. Duan and Z. Yin, *Nano Energy*, 2017, **40**, 432-439.
- 245 C. Yao, X. Li and T. Song, *Journal of Applied Polymer Science*, 2009, **114**, 2079-2086.
- 246 U. Ali, X. Wang and T. Lin, *AATCC review*, 2013, **13**.
- 247 M. S. Khil, S. R. Bhattarai, H. Y. Kim, S. Z. Kim and K. H. Lee, *Journal of Biomedical Materials Research*, 2005, **72B**, 117-124.
- 248 C. C. Tsai and K. G. Kornev, *Langmuir*, 2013, **29**, 10596-10602.
- 249 S. M. Mirvakili, A. Pazukha, W. Sikkema, C. W. Sinclair, G. M. Spinks, R. H. Baughman and J. D. W. Madden, *Advanced Functional Materials*, 2013, **23**, 4311-4316.
- 250 M. Baniasadi, J. Huang, Z. Xu, S. Moreno, X. Yang, J. Chang, M. A. Quevedo-Lopez, M. Naraghi and M. Minary-Jolandan, *ACS Applied Materials & Interfaces*, 2015, **7**, 5358-5366.
- 251 X. Li, C. Yao, F. Sun, T. Song, Y. Li and Y. Pu, *Journal of Applied Polymer Science*, 2008, **107**, 3756-3764.
- 252 R. Nakashima, K. Watanabe, Y. Lee, B. S. Kim and I. S. Kim, *Advances in Polymer Technology*, 2013, **32**, E44-E52.
- 253 P. D. Dalton, D. Klee and M. Möller, *Polymer*, 2005, **46**, 611-614.
- 254 W. E. Teo, R. Gopal, R. Ramaseshan, K. Fujihara and S. Ramakrishna, *Polymer*, 2007, **48**, 3400-3405.

- 255 F. L. Scardino and R. J. Balonis, *U.S. Patent*, 6,106,913, 2000-8-22.
- 256 C. I. Su, T. C. Lai, C. H. Lu, Y. S. Liu and S. P. Wu, *Fibers and Polymers*, 2013, **14**, 542-549.
- 257 K. Zhang, X. Wang, Y. Yang, L. Wang, M. Zhu, B. S. Hsiao and B. Chu, *Journal of Polymer Science Part B: Polymer Physics*, 2010, **48**, 1118-1125.
- 258 X. Wang, K. Zhang, M. Zhu, H. Yu, Z. Zhou, Y. Chen and B. S. Hsiao, *Polymer*, 2008, **49**, 2755-2761.
- 259 X. Wang, K. Zhang, M. Zhu, B. S. Hsiao and B. Chu, *Macromolecular Rapid Communications*, 2008, **29**, 826-831.
- 260 F. Anton, Artificial thread and method of producing same: *U.S. Patent*, 2,187,306, 1940-1-16.
- 261 F. Anton, Production of artificial fibers from fiber forming liquids: *U.S. Patent*, 2,323,025, 1943-6-29.
- 262 F. Anton, Method and apparatus for spinning: *U.S. Patent*, 2,349,950, 1944-5-30.
- 263 F. Dabirian, S. A. H. Ravandi, J. P. Hinstroza and R. A. Abuzade, *Polymer Engineering & Science*, 2012, **52**, 1724-1732.
- 264 H. Maleki, A. A. Gharehaghaji, G. Criscenti, L. Moroni and P. J. Dijkstra, *Journal of Applied Polymer Science*, 2015, **132**, 41388.
- 265 M. N. Shuakat and T. Lin, *The Journal of The Textile Institute*, 2015, **107**, 791-799.
- 266 M. N. Shuakat, X. Wang and T. Lin, *Stress (MPa)*, 2013, **10**, 30.
- 267 D. H. Kim, S. J. Kim, H. Shin, W. T. Koo, J. S. Jang, J. Y. Kang, Y. J. Jeong and I. D. Kim, *ACS Nano*, 2019, **13**, 6071-6082.
- 268 J. X. He, K. Qi, Y. M. Zhou and S. Z. Cui, *Polymer International*, 2014, **63**, 1288-1294.
- 269 J. He, K. Qi, Y. Zhou and S. Cui, *Journal of Applied Polymer Science*, 2014, **131**.
- 270 Z. Xie, H. Niu and T. Lin, *RSC Advances*, 2015, **5**, 15147-15153.
- 271 D. Li, X. Pan, B. Sun, T. Wu, W. Chen, C. Huang, Q. Ke, H. A. Ei-Hamshary, S. S. Al-Deyab and X. Mo, *Journal of Materials Chemistry B*, 2015, **3**, 8823-8831.
- 272 C. C. Tsai, P. Mikes, T. Andruk, E. White, D. Monaenkova, O. Burtovyy, R. Burtovyy, B. Rubin, D. Lukas, I. Luzinov, J. R. Owens and K. G. Kornev, *Nanoscale*, 2011, **3**, 4685.
- 273 E. Smit, U. Büttner and R. D. Sanderson, *Polymer*, 2005, **46**, 2419-2423.
- 274 L. Wang, Y. Wu, B. Guo and P. X. Ma, *ACS nano*, 2015, **9**, 9167-9179.
- 275 J. Wu, S. Liu, L. He, H. Wang, C. He, C. Fan and X. Mo, *Materials Letters*, 2012, **89**, 146-149.
- 276 S. Liu, J. Wu, X. Liu, D. Chen, G. L. Bowlin, L. Cao, J. Lu, F. Li, X. Mo and C. Fan, *Journal of Biomedical Materials Research Part A*, 2015, **103**, 581-592.
- 277 K. W. Kim, K. H. Lee, M. S. Khil, Y. S. Ho and H. Y. Kim, *Fibers and Polymers*, 2004, **5**, 122-127.
- 278 J. A. Matthews, G. E. Wnek, D. G. Simpson and G. L. Bowlin, *Biomacromolecules*, 2002, **3**, 232-238.
- 279 E. Zussman, D. Rittel and A. L. Yarin, *Applied Physics Letters*, 2003, **82**, 3958-3960.
- 280 G. H. Kim, *Journal of Polymer Science Part B: Polymer Physics*, 2006, **44**, 1426-1433.
- 281 Z. Song, X. Hou, L. Zhang and S. Wu, *Materials (Basel)*, 2011, **4**, 621-632.
- 282 J. M. Holzwarth and P. X. Ma, *Journal of Materials Chemistry*, 2011, **21**, 10243-10251.
- 283 S. Zhong, Y. Zhang and C. T. Lim, *Tissue Engineering Part B: Reviews*, 2011, **18**, 77-87.
- 284 S. Chen, H. Hou, F. Harnisch, S. A. Patil, A. A. Carmona-Martinez, S. Agarwal, Y. Zhang, S. Sinha-Ray, A. L. Yarin and A. Greiner, *Energy Environmental Science*, 2011, **4**, 1417-1421.
- 285 T. Xu, Y. Ding, Z. Wang, Y. Zhao, W. Wu, H. Fong and Z. Zhu, *Journal of Materials Chemistry C*, 2017,

- 5, 10288-10294.
- 286 J. Wu, N. Wang, L. Wang, H. Dong, Y. Zhao and L. Jiang, *ACS Applied Materials Interfaces*, 2012, **4**, 3207-3212.
- 287 C. Huang, Y. Ouyang, H. Niu, N. He, Q. Ke, X. Jin, D. Li, J. Fang, W. Liu, C. Fan and T. Lin, *ACS Appl Mater Interfaces*, 2015, **7**, 7189-7196.
- 288 W. Yu, W. Zhao, C. Zhu, X. Zhang, D. Ye, W. Zhang, Y. Zhou, X. Jiang and Z. Zhang, *BMC neuroscience*, 2011, **12**, 68.
- 289 T. M. Dinis, R. Elia, G. Vidal, Q. Dermigny, C. Denoëud, D. L. Kaplan, C. Egles and F. Marin, *J Mech Behav Biomed Mater*, 2015, **41**, 43-55.
- 290 D. Zhang and J. Chang, *Nano letters*, 2008, **8**, 3283-3287.
- 291 H. Ahn, Y. M. Ju, H. Takahashi, D. F. Williams, J. J. Yoo, S. J. Lee, T. Okano and A. Atala, *Acta Biomater*, 2015, **16**, 14-22.
- 292 J. Han, R. W. Cao, B. Chen, L. Ye, A. Y. Zhang, J. Zhang and Z. G. Feng, *Journal of Biomedical Materials Research Part A*, 2011, **96A**, 705-714.
- 293 W. E. Teo and S. Ramakrishna, *Nanotechnology*, 2006, **17**, R89-R106.
- 294 S. Cai, H. Xu, Q. Jiang and Y. Yang, *Langmuir*, 2013, **29**, 2311-2318.
- 295 H. L. Gao, Y. B. Zhu, L. B. Mao, F. C. Wang, X. S. Luo, Y. Y. Liu, Y. Lu, Z. Pan, J. Ge, W. Shen, Y. R. Zheng, L. Xu, L. J. Wang, W. H. Xu, H. A. Wu and S. H. Yu, *Nature Communications*, 2016, **7**, 12920.
- 296 S. Jiang, S. Agarwal and A. Greiner, *Angewandte Chemie International Edition*, 2017, **56**, 15520-15538.
- 297 S. Jiang, V. Gruen, S. Rosenfeldt, A. S. Schenk, S. Agarwal, Z.K. Xu and A. Greiner, *Research*, 2019, **2019**, 1-10.
- 298 G. Duan, A. R. Bagheri, S. Jiang, J. Golenser, S. Agarwal and A. Greiner, *Biomacromolecules*, 2017, **18**, 3215-3221.
- 299 S. Jiang, G. Duan, U. Kuhn, M. Mörl, V. Altstädt, A. L. Yarin and A. Greiner, *Angewandte Chemie International Edition*, 2017, **56**, 3285-3288.
- 300 Y. Si, Q. Fu, X. Wang, J. Zhu, J. Yu, G. Sun and B. Ding, *ACS nano*, 2015, **9**, 3791-3799.
- 301 Y. Si, X. Wang, C. Yan, L. Yang, J. Yu and B. Ding, *Advanced Materials*, 2016, **28**, 9512-9518.
- 302 Y. Huang, N. Bu, Y. Duan, Y. Pan, H. Liu, Z. Yin and Y. Xiong, *Nanoscale*, 2013, **5**, 12007-12017.
- 303 Q. Liu, Q. Wu, S. Xie, L. Zhao, Z. Chen, Z. Ding and X. Li, *Nanotechnology*, 2019, **30**, 375301.
- 304 P. D. Dalton, D. Grafahrend, K. Klinkhammer, D. Klee and M. Möller, *Polymer*, 2007, **48**, 6823-6833.
- 305 X. Wang, G. Zheng, G. He, J. Wei, H. Liu, Y. Lin, J. Zheng and D. Sun, *Materials Letters*, 2013, **109**, 58-61.
- 306 W. Han, F. Cui, Y. Si, X. Mao, B. Ding and H. Kim, *Small*, 2018, **14**, 1801963.
- 307 F. Di Benedetto, A. Camposeo, L. Persano, A. M. Laera, E. Piscopiello, R. Cingolani, L. Tapfer and D. Pisignano, *Nanoscale*, 2011, **3**, 4234-4239.
- 308 L. Persano, A. Camposeo, F. Di Benedetto, R. Stabile, A. M. Laera, E. Piscopiello, L. Tapfer and D. Pisignano, *Advanced Materials*, 2012, **24**, 5320-5326.
- 309 A. Camposeo, F. D. Benedetto, R. Stabile, A. A. Neves, R. Cingolani and D. Pisignano, *Small*, 2009, **5**, 562-566.
- 310 I. Cucchi, F. Spano, U. Giovanella, M. Catellani, A. Varesano, G. Calzaferri and C. Botta, *Small*, 2007,

- 3, 305-309.
- 311 A. Köhler, J. S. Wilson and R. H. Friend, *Advanced Materials*, 2002, **14**, 701-707.
- 312 C. C. Kuo, C. H. Lin and W. C. Chen, *Macromolecules*, 2007, **40**, 6959-6966.
- 313 L. A. García, E. Arias, I. Moggio, J. Romero, A. Ledezma, A. Ponce and O. Perez, *Polymer*, 2011, **52**, 5326-5334.
- 314 D. Li, A. Babel, S. A. Jenekhe and Y. Xia, *Advanced Materials*, 2004, **16**, 2062-2066.
- 315 J. C. Bolinger, M. C. Traub, J. Brazard, T. Adachi, P. F. Barbara and D. A. Vanden Bout, *Accounts of chemical research*, 2012, **45**, 1992-2001.
- 316 G. Morello, A. Polini, S. Girardo, A. Camposeo and D. Pisignano, *Applied Physics Letters*, 2013, **102**, 211911.
- 317 S. Pagliara, A. Camposeo, R. Cingolani and D. Pisignano, *Applied Physics Letters*, 2009, **95**, 263301.
- 318 C. C. Lee, S. Y. Lai, W. B. Su, H. L. Chen, C. L. Chung and J. H. Chen, *The Journal of Physical Chemistry C*, 2013, **117**, 20387-20396.
- 319 M. Campoy-Quiles, Y. Ishii, H. Sakai and H. Murata, *Applied Physics Letters*, 2008, **92**, 213305.
- 320 C. C. Kuo, C. T. Wang and W. C. Chen, *Macromolecular Materials and Engineering*, 2008, **293**, 999-1008.
- 321 S. Pagliara, A. Camposeo, A. Polini, R. Cingolani and D. Pisignano, *Lab Chip*, 2009, **9**, 2851-2856.
- 322 T. Güner, G. Topçu, U. Savacı, A. Genç, S. Turan, E. Sari and M. M. Demir, *Nanotechnology*, 2018, **29**, 135202.
- 323 C. R. Jeukens, P. Jonkheijm, F. J. Wijnen, J. C. Gielen, P. C. Christianen, A. P. Schenning, E. Meijer and J. C. Maan, *Journal of the American Chemical Society*, 2005, **127**, 8280-8281.
- 324 P. Anzenbacher, F. Li and M. A. Palacios, *Angewandte Chemie International Edition*, 2012, **51**, 2345-2348.
- 325 B. Zu, Y. Guo and X. Dou, *Nanoscale*, 2013, **5**, 10693-10701.
- 326 Y. Long, H. Chen, Y. Yang, H. Wang, Y. Yang, N. Li, K. Li, J. Pei and F. Liu, *Macromolecules*, 2009, **42**, 6501-6509.
- 327 J. S. Yang and T. M. Swager, *Journal of the American Chemical Society*, 1998, **120**, 5321-5322.
- 328 C. Zhou, Y. Shi, X. Ding, M. Li, J. Luo, Z. Lu and D. Xiao, *Analytical Chemistry*, 2013, **85**, 1171-1176.
- 329 B. W. Davis, N. Niamnont, C. D. Hare, M. Sukwattanasinitt and Q. Cheng, *ACS Appl Mater Interfaces*, 2010, **2**, 1798-1803.
- 330 M. N. Velasco-Garcia, *Seminars in Cell Developmental Biology*, 2009, **20**, 27-33.
- 331 A. Camposeo, F. Di Benedetto, R. Cingolani and D. Pisignano, *Applied Physics Letters*, 2009, **94**, 043109.
- 332 V. Vohra, U. Giovanella, R. Tubino, H. Murata and C. Botta, *ACS nano*, 2011, **5**, 5572-5578.
- 333 H. Zheng, X. Lei, T. Cheng, S. Liu, X. Zeng and R. Sun, *Nanotechnology*, 2017, **28**, 265204.
- 334 F. S. Kim, G. Ren and S. A. Jenekhe, *Chemistry of Materials*, 2011, **23**, 682-732.
- 335 H. Liu, C. H. Reccius and H. G. Craighead, *Applied Physics Letters*, 2005, **87**, 253106.
- 336 S. W. Lee, H. J. Lee, J. H. Choi, W. G. Koh, J. M. Myoung, J. H. Hur, J. J. Park, J. H. Cho and U. Jeong, *Nano Letters*, 2010, **10**, 347-351.
- 337 G. Henrici-Olivé and S. Olivé, in *Chemistry*, Springer, 1979, pp. 123-152.
- 338 D. R. Lide, *CRC handbook of chemistry and physics*, CRC press, 2004.

- 339 Q. Zhou, B. Cao, C. Zhu, S. Xu, Y. Gong, W. Z. Yuan and Y. Zhang, *Small*, 2016, **12**, 6586-6592.
- 340 M. Makaremi, R. T. De Silva and P. Pasbakhsh, *The Journal of Physical Chemistry C*, 2015, **119**, 7949-7958.
- 341 H. Zheng, H. Xue, Y. Zhang and Z. Shen, *Biosensors and Bioelectronics*, 2002, **17**, 541-545.
- 342 Y. Shuai, D. Wang, K. Chen, Z. Zhang, Y. Wang and J. Lou, *Chemical Communications*, 2019, **55**, 11271-11274.
- 343 R. Samatham, I. S. Park, K. J. Kim, J. D. Nam, N. Whisman and J. Adams, *Smart Materials and Structures*, 2006, **15**, N152-N156.
- 344 K. Perepelkin, *Fibre Chemistry*, 2003, **35**, 409-416.
- 345 H. Khayyam, R. N. Jazar, S. Nunna, G. Golkarnarenji, K. Badii, S. M. Fakhrhoseini, S. Kumar and M. Naebe, *Progress in Materials Science*, 2020, **107**, 100575.
- 346 S. K. Nataraj, K. S. Yang and T. M. Aminabhavi, *Progress in Polymer Science*, 2012, **37**, 487-513.
- 347 B. Geller, *Fibre Chemistry*, 2002, **34**, 151-161.
- 348 J. J. Ge, H. Hou, Q. Li, M. J. Graham, A. Greiner, D. H. Reneker, F. W. Harris and S. Z. Cheng, *Journal of the American Chemical Society*, 2004, **126**, 15754-15761.
- 349 H. Hou, J. J. Ge, J. Zeng, Q. Li, D. H. Reneker, A. Greiner and S. Z. Cheng, *Chemistry of Materials*, 2005, **17**, 967-973.

2 Overview of the Thesis

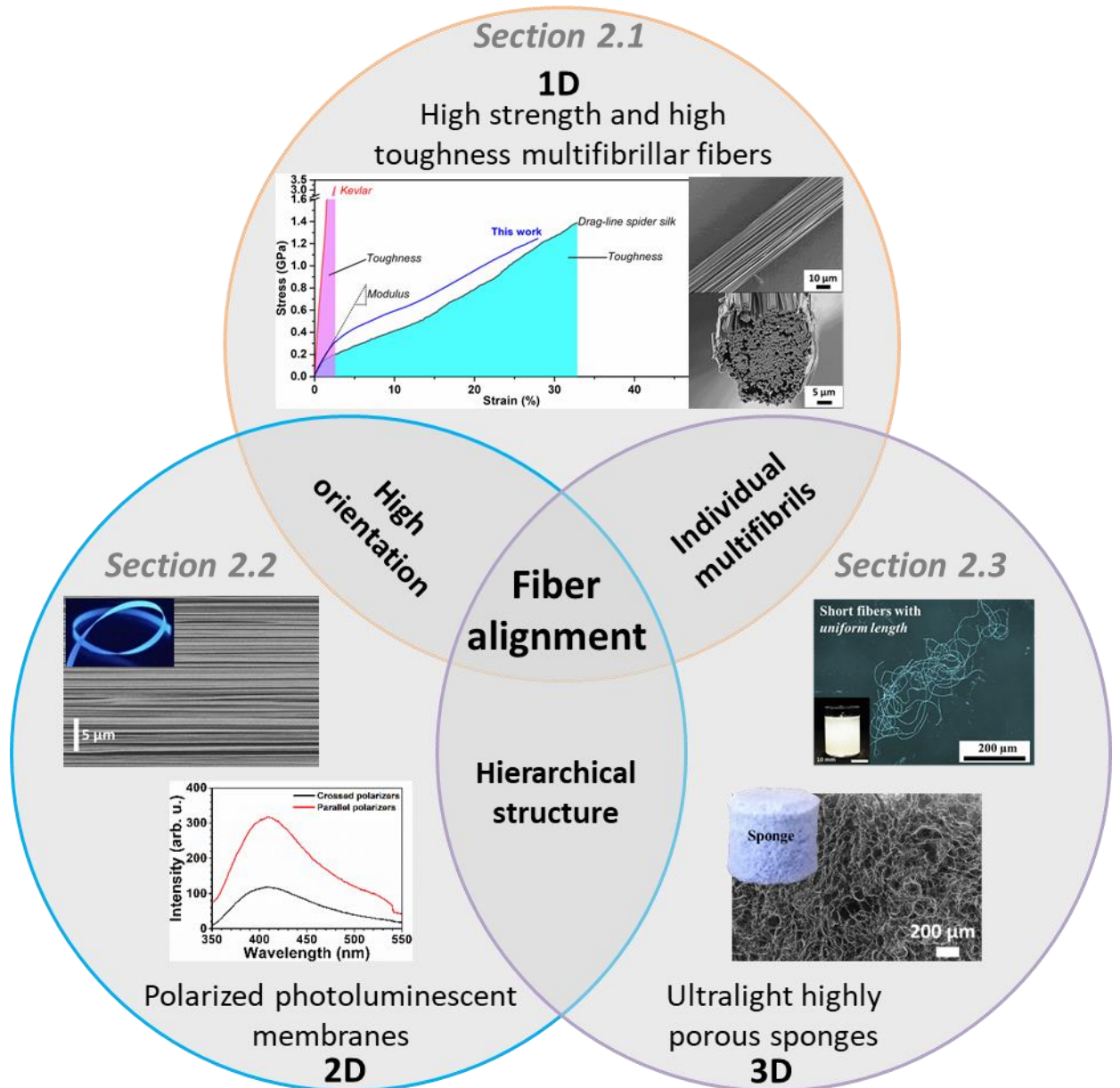


Figure 2.1. Context of this thesis combining three subjects: (i) high strength and toughness multifibrillar fibers, (ii) polarized photoluminescent membranes made from non-conjugated polyacrylonitrile, (iii) the impact of short fiber length distribution on the ultralight sponges.

This thesis contains two publications and one manuscript in **Section 2.1** to **2.3**. The context of this thesis is creating fiber assemblies with tailored properties through the organization of fiber alignment, hierarchical structures and interactions of fibers,

which are summarized in the above **Fig. 2.1** and in the following sections. The main contents involve the preparation, properties and investigations of electrospun fiber assemblies with tailored properties in different dimensions. In **Section 2.1**, preparation and investigation of 1D electrospun multifibrillar fibers with the combination of high strength and high toughness was performed. **Section 2.2** firstly exhibited the polarized blue photoluminescence of mesoscopically ordered 2D electrospun non-conjugated polyacrylonitrile fibrous membranes. The last section (**Section 2.3**) aims to address the covered impact of short fiber length distribution on the compressibility of the 3D sponges made from electrospun multifibrillar fibers. The details of experimental parts, results and discussions of each work will be presented in **Chapter 3**.

2.1 High strength in combination with high toughness in robust and sustainable polymeric materials

Xiaojian Liao, Martin Dulle, Juliana Martins de Souza e Silva, Ralf B. Wehrspohn, Seema Agarwal, Stephan Förster, Haoqing Hou, Paul Smith, Andreas Greiner*. *Science*, **2019**, 366(6471): 1376-1379.

Specific contributions by the authors:

Prof. A. Greiner and Prof. S. Agarwal conceived and supervised the project. X. Liao prepared the yarns; measured WAXS, TGA, NMR, and IR; and performed stress-strain tests. X. Liao, Prof. A. Greiner and Prof. S. Agarwal wrote the manuscript. M. Dulle measured the crystal data and evaluated and discussed with Prof. S. Förster. X-ray computed tomography was performed by J. M. d. S. e. Silva and was evaluated and discussed by J. M. d. S. e. Silva and Prof. R. B. Wehrspohn. Prof. P. Smith and Prof. H. Hou evaluated and discussed the mechanical data of the yarns with X. Liao and Prof. A. Greiner. All authors contributed to the analysis and discussion of the data. The manuscript writing was led by Prof. A. Greiner with contributions from all other authors.

1D single electrospun polymer nanofibers with a small diameter possess a combination of high strength and high toughness. However, the handling difficulty of these single nanofibers has prevented them from using in real-world applications. This work present an innovative design principle to develop 1D electrospun yarns robust enough for use, through a combination of thousands of fibrils with high alignment and

interfibrillar reactions between the matrix PAN molecules and interconnecting poly(ethylene glycol) bisazide (PEG-BA) molecules. The obtained yarns have a tensile strength of 1236 ± 40 MPa in combination with a toughness of 137 ± 21 J/g, which is similar to the properties of dragline spider silk.

The high strength and high toughness polymer yarns were fabricated in three steps. First, continuous yarns were prepared by yarn electrospinning from polyacrylonitrile and small amounts of PEG-BA. Second, the as-spun yarns were then stretched at 160 °C. Third, the stretched yarns were adjacently annealed at 130 °C under tension for several hours. The as-spun yarns had an average diameter of 130 ± 12 μm and consisted of about 3000 nonoriented individual fibrils with 1.17 ± 0.12 μm diameter. (**Fig. 2.2 A-C**) Naturally, a reduction of diameters were induced by stretching process, the diameter of yarn down to 36 ± 1.3 μm and the diameters of the fibrils to 0.37 ± 0.07 μm [at stretch ratio of 9 (SR 9) at 160 °C], respectively. (**Fig. 2.2 D-F**) Meanwhile, the alignment factor of fibrils in the yarns increased from about 46.0% (as-spun) to 99.6% (SR 9) and the orientation of the PAN macromolecules along the yarn's main axis increase from 66.1% (as-spun) to 83.3% (SR 9) as well. Heat stretching also resulted in a marked increase in the crystallinity from about 56.9% (as-spun) to about 92.4% (SR 9), which were confirmed by WAXS experiments. Simultaneously, the crystallinity orientation increased, but no significant increase was observed upon annealing. Interesting, heat stretching also reduced the linear densities of the yarns, which changed from 3.74 ± 0.14 tex (as-spun) to 0.39 ± 0.04 tex (SR 9). The interaction between cyano groups and azide groups in the annealing process was confirmed by $^1\text{H-NMR}$, $^{13}\text{C-NMR}$ and ATR-FTIR spectra.

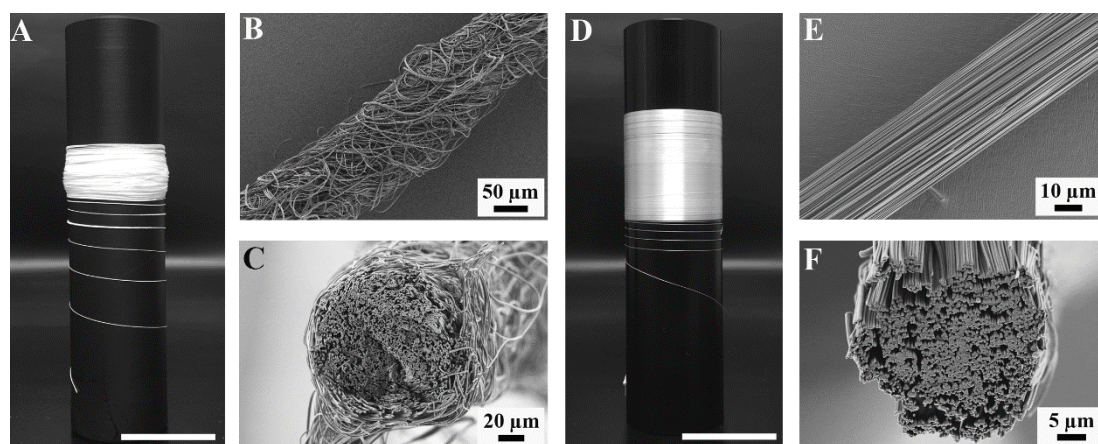


Figure 2.2. Photographs and SEM images of the yarns. (A) Photograph of continuous as-spun yarns. (B) SEM image of the long axis of the as-spun yarns. (C) SEM image of a cross-section of the as-spun yarns. (D) Photograph of stretched yarns. (E) SEM image of the long axis of stretched (at SR 8 at 160 °C) and annealed (130°C for 4 hours) yarns (EASY). (F) SEM image of a cross-section of the stretched (at SR 8 at 160 °C) and annealed (130 °C for 4 hours) yarns (EASY). The scale bars in the photographs of the as-spun yarns (A) and stretched yarns (D) are 20 mm.

To understand the mechanical properties of yarns, we also presented a possible model. In this mode, a reduction in the fractional-free volume after strain-induced crystallization and shrinking is pronounced. Thus, PEG-BA macromolecules in the PAN matrix probably diffuse to the fibril-free surface, which is the optimal position for efficient interfibrils reaction. Starting from pristine yarns, the PAN fibrils in the yarns start to disentangle, resulting in a yield point. Beyond the yield point, the PEG-BA moieties bridging the PAN fibrils are responsible for stress transfer, impeding their ability to slide over each other. At a critical stress, the PEG-BA bridges might rupture, causing the yarns to break at high strain position with high strength.

In conclusion, 1D high strength and high toughness electrospun yarns in robust form were fabricated from commercial polymer. Based on the results, we postulate that the nearly perfect uniaxial orientation of the fibrils, annealing under tension in the presence of linking molecules in combination with high crystallinity is essential for the mechanical properties of yarns. This underlying principle is not restricted to the present system, which can be used to develop strong and tough fibers from other polymers.

2.2 Polarized blue photoluminescence of mesoscopically ordered electrospun non-conjugated polyacrylonitrile nanofibers

Xiaojian Liao, Frank-Julian Kahle, Bin Liu, Heinz Bässler, Xinghong Zhang, Anna Köhler*, Andreas Greiner*. **2020**, 7(6), 1605-1612.

Specific contributions by authors:

Prof. A. Greiner and Prof. A. Köhler devised the study. X. Liao, Prof. A. Köhler and Prof. A. Greiner wrote the manuscript with input from B. Liu, F. Kahle, Prof. X. Zhang and Prof. H. Bässler. Prof. A. Greiner and X. Liao designed the samples that were performed by X. Liao. X. Liao performed and analysed SEM measurements, WAXS measurements and tensile tests with input from Prof. A. Greiner. X. Liao, B. Liu and F. Kahle performed and analysed the fluorescence measurements, which were also analysed by Prof. A. Köhler and Prof. A. Greiner with input from Prof. H. Bässler, and Prof. X. Zhang. F. Kahle performed and analysed the phosphorescence measurements with input from X. Liao, Prof. H. Bässler, Prof. A. Köhler and Prof. A. Greiner. The authors contributed to the scientific discussion and edited the manuscript.

In this work, we demonstrated the fabrication of 2D electrospun PAN fibrous membranes with polarized light-emitting from the non-conjugated polymer that can be aligned by a simple heat-stretching process. Upon excitation at 340 nm these electrospun membranes show polarized deep blue luminescence with an anisotropy of 0.37 and a quantum yield of about 31%. Furthermore, they exhibit room temperature green phosphorescences with a lifetime of about 200 ms as well as a delayed deep blue fluorescence resulting from triplet-triplet annihilation (non-coherent photon upconversion) (TTA).

The cyano groups in PAN are known to interact such as to show AIE with fluorescence as well as room temperature phosphorescence. We present a concise and efficient fabrication approach to achieve polarized emission in PAN electrospun nanofiber ribbons (ENRs) by mesoscopic order. To achieve polarized emission in non-conjugated polymers, three important molecular rules are designed: i) electrospinning the non-conjugated polymer into nanofibers, ii) aligned crystal arrangement by sufficient heat-stretching at high temperatures above T_g , and iii) using functional groups that show

AIE when interactions between adjacent groups lead to the formation of a more extended π -system.

We were able to obtain highly aligned chains using two sequential steps. As-spun ENRs from pure PAN solution were prepared by electrospinning using a high-speed rotating disc (1,200 rpm). These as-spun ENRs consist of individual nanofibers with a diameter of 710 ± 160 nm. And the nanofibers in the as-spun ENRs have an alignment factor of 92.6 ± 25.7 %. After heat stretching these as-spun ribbons at a stretching ratio of 6, not only the nanofiber diameter was also reduced down to 236 ± 62 nm, a nearly perfect uniaxial orientation of the nanofibers along the axis of ENRs could be achieved with an alignment factor of 99.97 ± 0.06 %.

The orientation of molecular chains and packing patterns were investigated by wide-angle/small-angle X-ray scattering (WAXS/SAXS). The crystallinity increases drastically from 51% in the as-spun ribbon to 89% in the heat-stretched SR6 ENRs. For the as-spun samples, we observed a ring in the 2D SAXS image, implying a near-isotropic orientation of the crystallites, whereas the SR6 ENRs show two sharp (200)-reflections, implying alignment accompanied by a high orientational order. The calculated orientational order parameters are $S = 0.58$ for the as-spun ENRs and $S = 0.96$ for the SR6 ENRs. Thus, the process of heat-stretching leads to the formation of aligned, highly crystalline PAN ENRs.

The photoluminescent properties of samples were investigated as shown in the **Fig. 2.3**. We found that solid state samples of ENRs showed bright blue emission under irradiation with UV-light (**Fig. 2.3 a**). After turning off the excitation, we observed a green afterglow that lasted for several seconds at 77K (**Fig. 2.3 b**). While the films and the as-spun ENRs feature similar spectra with a maximum at around 394-388 nm, SR6 ENRs features a red shifted, broadened emission maximum at around 410 nm (**Fig. 2.3 c**). The quantum yields of emission are similar for both ribbons and in the range of 30-32%, thus exceeding the value of 22% that we measure in a DMF solution at 80 mg/mL. When excited with linearly polarized light, the stretched ribbons feature a considerable anisotropy of 0.37 and a degree of polarization of 0.47 for the emission, whereas as-spun ENRs do not show a dependence of the emission intensity on the position of the analyser (**Fig. 2.3 e**). For the as-spun ENRs, both anisotropy and

polarization are basically zero (**Fig. 2.3 d**). Evidently, the polarization is induced by the heat-stretching process. We observed a delayed blue fluorescence as well as green phosphorescence at room temperature in addition to the prompt fluorescence. The delayed fluorescence (DF) results from TTA, also referred to as triplet upconversion (UC). The observation of TTA implies that triplet excitons are remarkably mobile in these non-conjugated materials. This opens up a new perspective for electrospun fibers from non-conjugated polymers.

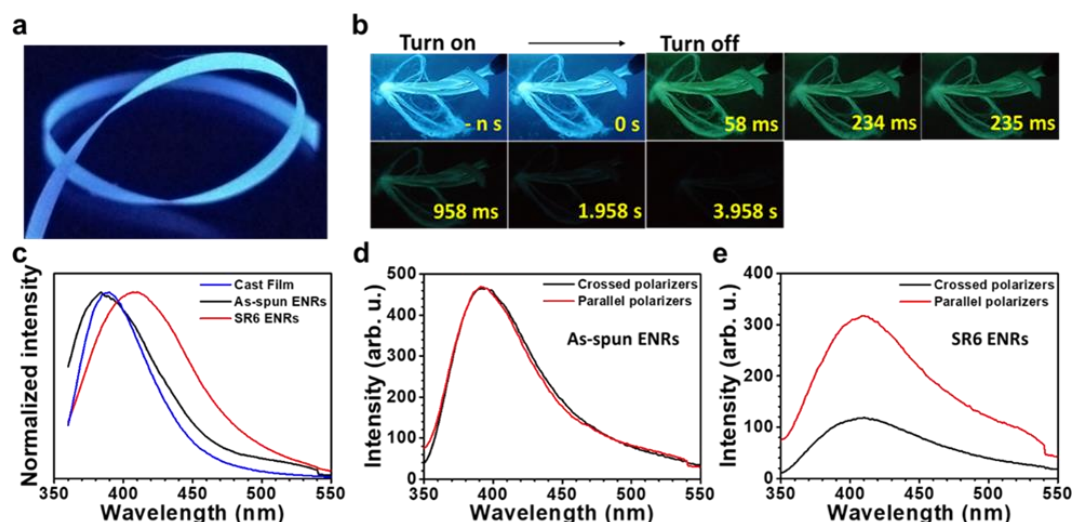


Figure 2.3. Photoluminescence properties of ENRs. (a) Photograph of SR6 ENRs under UV light irradiation (365 nm). (b) Luminescence photographs of ENRs taken at 77 K under 365 nm UV irradiation and at different times after turning off the UV lamp. (c) Comparison of the PL spectra of film, as-spun ENRs and SR6 ENRs excited at 340 nm. (d and e) Polarization dependent emission spectra of as-spun ENRs (d) and SR6 ENRs (e) excited at 337 nm. The excitation light was linearly polarized parallel to the long axis of the ENRs.

In conclusion, PAN ENRs satisfy the designed rules by forming a highly ordered macroscopically aligned structure upon heat stretching. Interactions between adjacent cyano side groups result in the formation of an extended π -system and the occurrence of aggregate induced polarized deep blue emission. They exhibit a photoluminescence quantum yield of 30-32%, which is remarkable for a simple non-conjugated polymer. Due to the contribution of $n-\pi^*$ transitions resulting from the nitrogen atoms in the cyano groups, intersystem crossing occurs that leads to the formation of highly mobile

triplet states. These triplets give rise to delayed fluorescence via TTA and to phosphorescence. The combination of efficient polarized deep blue luminescence, room temperature phosphorescence, TTA, mechanical robustness and flexibility of these fibers opens up new avenues for applications of non-conjugated polymers.

2.3 Impact of the Fiber Length Distribution on Porous Sponges Originating from Short Electrospun Fibers Made from Polymer Yarn

Xiaojian Liao, Pin Hu, Seema Agarwal, and Andreas Greiner*. *Macromolecular Materials and Engineering*, 2020, 1900629

Specific contributions by authors:

X. Liao performed and designed the experimental work, co-analyzed, co-wrote the manuscript. P. Hu synthesized Polyurethane (PU). Prof. S. Agarwal co-analyzed the sample, co-wrote the manuscript. Prof. A. Greiner designed the topic and concept, guided the research, co-analyzed the samples, co-wrote the manuscript.

In this work, highly aligned pure PAN yarns prepared in the previous section were used for the preparation of the ultralight and high porous 3D sponges with controlled fiber length distribution, and the role of the fiber length distribution in the compressibility of the sponges is analyzed quantitatively.

We prepared short fibers of two different lengths (416 ± 83 and 1034 ± 156 μm) by cryo-microcutting of the stretched pure PAN yarns in liquid nitrogen with designed homemade cutters and followed by ultrasonification in dioxane as shown in the **Fig. 2.4**. The obtained short fibers possess tunable aspect ratios and narrow fiber length distribution, represented by the low CV values of 15.1% and 20.0%, respectively. Furthermore, short fibers with uncontrollable length (average length of 145 ± 129 μm) and broad length distribution with high CV of 89.0% were investigated in control experiment of making short fibers by normal mixer cutting.

Short nanofibers (lengths 416 ± 83 and 1034 ± 156 μm) dispersions in a dioxane solution of PU were used for the preparation of the sponges. Dispersion of short fibers with well-controlled fiber length distribution was obtained by mixing of short fibers of different lengths in dispersion. The PU was used here as glue, assembled on the surface of fibers, which could induce further physical gluing and reinforce the mechanical properties of sponges. The sponges (density of ≈ 7.0 mg cm^{-3}) showed dual pore-structure with small (pores between the fibers) and big pores (pore size of about 112 ± 18.3 μm formed by sublimation of ice during freeze-drying).

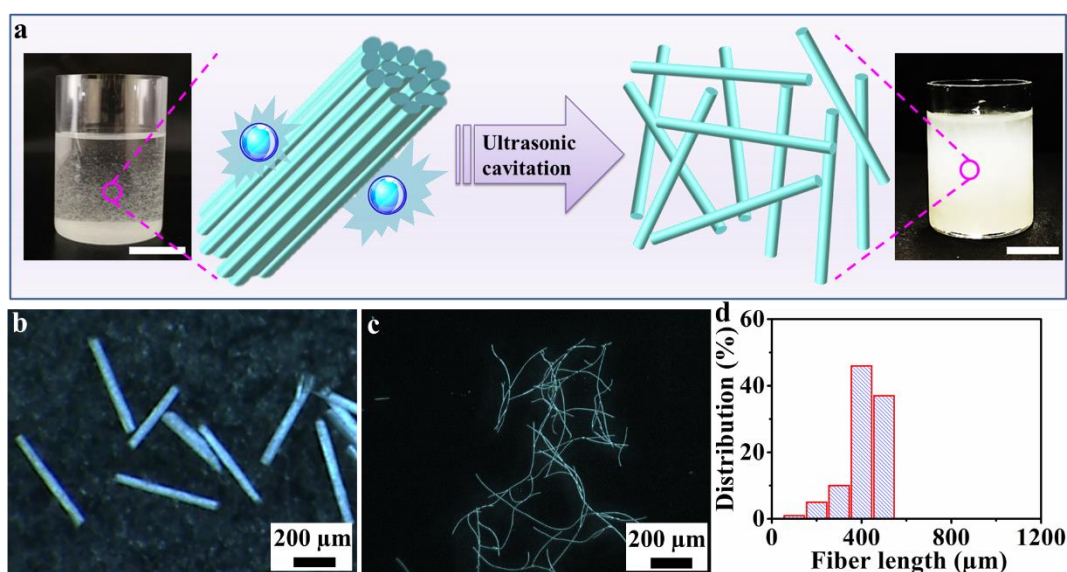


Figure 2.4. (a) Schematic representation of the ultrasonic cavitation process to produce individual fibers from short yarns. The inset digital pictures are dispersion of short yarns with 0.4 mm length (left) and corresponding dispersion of short fibers (right) in dioxane. The inset scale bar in the picture is 15 mm. Microscope pictures of: (b) short yarns and (c) fibers at 0.4 mm length. (d) Fiber length distribution of short fibers made from cutter 0.4 mm.

For understanding the role of the fiber length and its CV in the pore size, we investigated pore morphology, and compression strength of the sponges. The sponges with different content of 1 mm length fibers showed similar average visual pore sizes (range of 112–118 μm). Compression test were used to investigate the compressibility of sponges. It showed that sponges with low CV exhibited enhancement in stress by 32% and in modulus by 45% compared to sponges with high CV. Moreover, the longer fibers (1.0 mm length) could endow the sponge with higher modulus than the shorter fibers (0.4 mm length) (**Fig. 2.5**).

In conclusion, cryo-microcutting of multifibrillar electrospun fibrillar yarns results in short fibers of well-controlled length. Sponges obtained from the short fiber of controlled length distribution showed similar pore size and pore size distribution, but significantly higher compression strength and modulus for sponges with low CV. From this, we postulate that the mechanical properties of sponges could be tailored over a wide range by adjustment of fiber length.

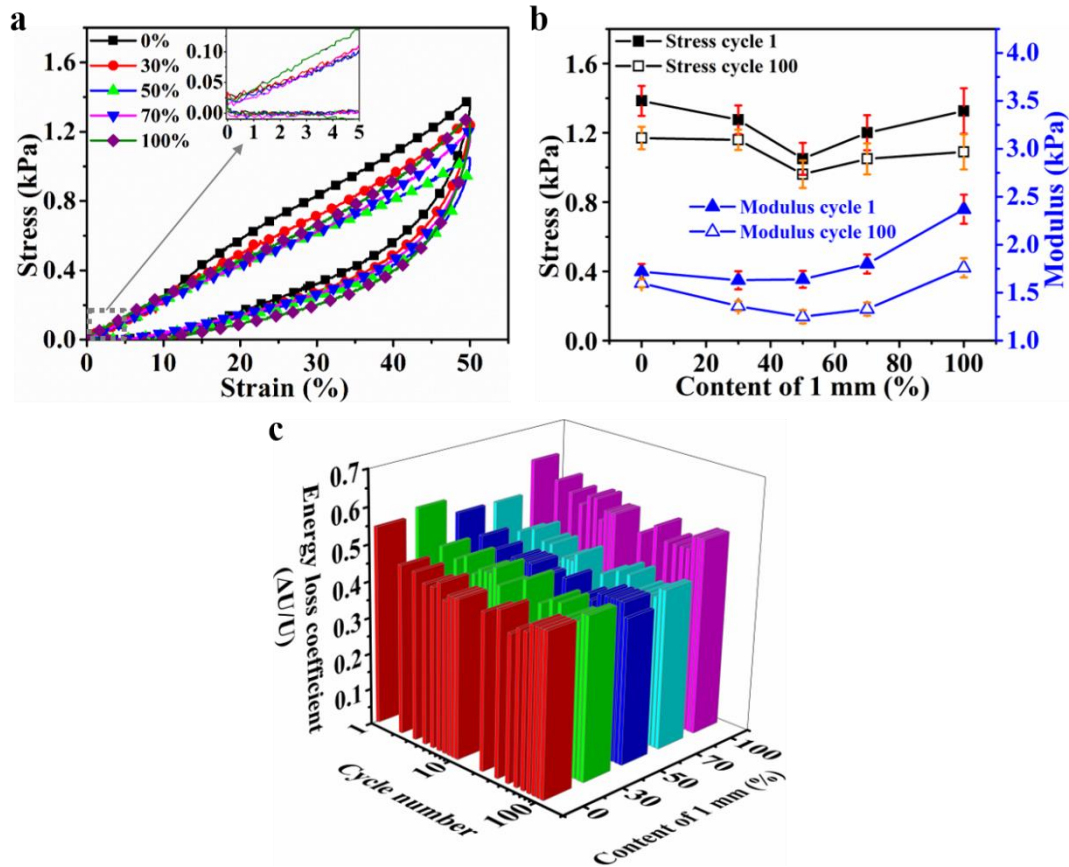


Figure 2.5. Microstructure and mechanical properties of sponges. (a) Compression stress versus strain curves in compression test of sponges with different contents of 0.4 and 1.0 mm length short fibers. (b) Changes of stress and modulus of sponges with different contents of 0.4 and 1 mm length short fibers during first and 100th cycle loading–unloading compression test. (c) Changes of energy loss coefficient of the sponges with different contents of 0.4 and 1 mm length short fibers during 100 cycles compression test.

3 Publications

3.1 High strength in combination with high toughness in robust and sustainable polymeric materials

Xiaojian Liao, Martin Dulle, Juliana Martins de Souza e Silva, Ralf B. Wehrspohn, Seema Agarwal, Stephan Förster, Haoqing Hou, Paul Smith, Andreas Greiner. High strength in combination with high toughness in robust and sustainable polymeric materials. *Science*, **2019**, 366(6471), 1376-1379.

RESEARCH

POLYMERS

High strength in combination with high toughness in robust and sustainable polymeric materials

Xiaojian Liao¹, Martin Dulle², Juliana Martins de Souza e Silva³, Ralf B. Wehrspohn^{3,4}, Seema Agarwal¹, Stephan Förster^{2,5}, Haoqing Hou⁶, Paul Smith⁷, Andreas Greiner^{1*}

In materials science, there is an intrinsic conflict between high strength and high toughness, which can be resolved for different materials only through the use of innovative design principles. Advanced materials must be highly resistant to both deformation and fracture. We overcome this conflict in man-made polymer fibers and show multifibrillar polyacrylonitrile yarn with a toughness of 137 ± 21 joules per gram in combination with a tensile strength of 1236 ± 40 megapascals. The nearly perfect uniaxial orientation of the fibrils, annealing under tension in the presence of linking molecules, is essential for the yarn's notable mechanical properties. This underlying principle can be used to create similar strong and tough fibers from other commodity polymers in the future and can be used in a variety of applications in areas such as biomedicine, satellite technology, textiles, aircrafts, and automobiles.

Synthetic materials with a combination of high strength and high toughness are rare and represent an important technological challenge (1). Engineered metal alloys (2), metallic glass composites (3), nanocellulose paper (4), glass (5), and carbon-based materials (6–9) are some examples of materials with this property combination. High resistance to both deformation (high strength) and fracture (high toughness) is achieved in man-made single-polymer nanofibers of very small diameter by electrospinning (10–14). However, these single nanofibers are not robust enough for handling for real-world applications. Natural fibers, like dragline spider silks (15, 16) and recombinant spider silks (17), achieve the

combination of high strength and high toughness as well, but their applicability is restricted by either low availability or high prices for various applications.

We discovered a straightforward concept for combination of high strength and high toughness through the preparation of polymeric fibers by yarn electrospinning, which creates fibers consisting of thousands of aligned nanofibrils in combination with a specified amount of a linker molecule. Simple alignment of the nanofibrils in electrospun yarns in combination with a high degree of crystallization does not result in high toughness in conjunction with high strength. Rather, this combination is achievable through the addition of a small

amount of an interconnecting molecule during yarn electrospinning and annealing after the heat stretching of the nanofibrils.

We fabricated the high-strength and high-toughness polymer yarns in three steps (fig. S1). First, continuous yarns were obtained by yarn electrospinning a solution of commercial polyacrylonitrile (PAN) {Dolan, copolymer with 4.18 mole % [6.35 weight % (wt %)] methyl acrylate according to our ¹H-NMR (proton nuclear magnetic resonance) analysis, number average molar mass (M_n) = 120,000; molar mass dispersity (D) = 2.79} and different amounts of the bifunctional poly(ethylene glycol) bisazide (PEG-BA) as an interconnecting molecule. Azides were applied in “click” reactions (18). These yarns were then stretched at 160°C in air. The stretched yarns were further annealed at 120°, 130°, and 140°C under tension for several hours, which finally resulted in high-strength and high-toughness yarns, depending on the applied conditions and the composition of PAN and PEG-BA (we tested amounts ranging from 0 to 6 wt % of

¹Macromolecular Chemistry and Bavarian Polymer Institute, University of Bayreuth, 95440 Bayreuth, Germany. ²JCNS-1/ICS-1, Forschungszentrum Jülich, 52425 Jülich, Germany. ³Institute of Physics, Martin Luther University Halle-Wittenberg, Heinrich-Damerow-Straße 4, 06120 Halle (Saale), Germany. ⁴Fraunhofer Institute for Microstructure of Materials and Systems (IMWS), Walter-Hülse-Straße 1, 06120 Halle (Saale), Germany. ⁵Physical Chemistry, Rheinisch-Westfälische Technische Hochschule Aachen University, 52074 Aachen, Germany. ⁶College of Chemistry and Chemical Engineering, Jiangxi Normal University, Nanchang, Jiangxi 330022, People's Republic of China. ⁷ETH Zürich, HCP F41.2, 8093 Zürich, Switzerland. *Corresponding author. Email: greiner@uni-bayreuth.de

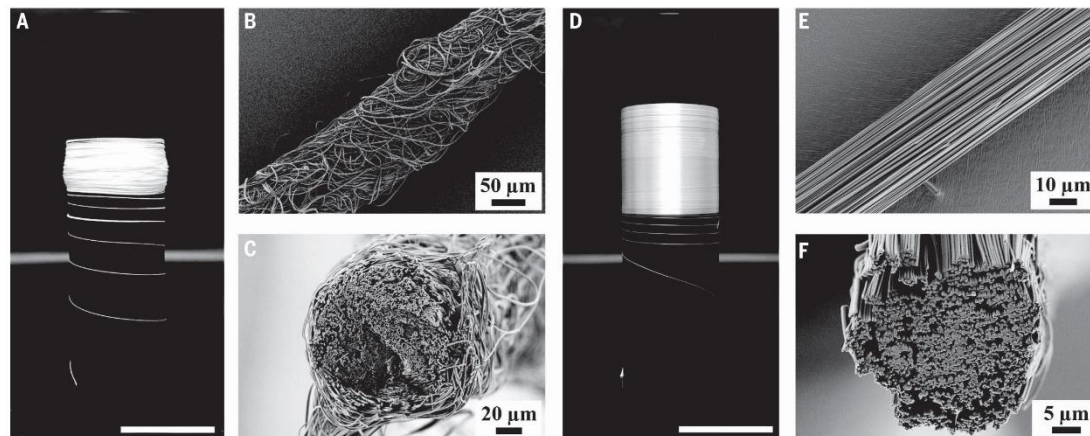


Fig. 1. Photographs and scanning electron microscopy (SEM) images of the yarns. (A) Photograph of continuous as-spun yarns. (B) SEM image of the long axis of the as-spun yarns. (C) SEM image of a cross-section of the as-spun yarns. (D) Photograph of stretched yarns. (E) SEM image of the long axis of stretched (at SR 8 at 160°C) and annealed (130°C for 4 hours) yarns (EASY). (F) SEM image of a cross-section of the stretched (at SR 8 at 160°C) and annealed (130°C for 4 hours) yarns (EASY). The scale bars in the photographs of the as-spun yarns (A) and stretched yarns (D) are 20 mm.

RESEARCH | REPORT

PEG-BA relative to PAN). The electrospun, stretched, and annealed yarns are hereafter abbreviated as EASYS; the yarns processed with PEG-BA are abbreviated as i-EASYS.

In a model study for the systematic understanding of the effect of stretching with commercial PAN without PEG-BA, we found that as-spun yarns had an average diameter of $130 \pm 12 \mu\text{m}$ and consisted of ~ 3000 nonoriented individual fibrils with $1.17 \pm 0.12 \mu\text{m}$ diameter (Fig. 1, A to C, and fig. S2, A and B). Heat stretching of the yarns for several minutes resulted in their manifold elongation accompanied by a change in the macroscopic appearance (Fig. 1D) and the alignment of the fibrils in the yarns (Fig. 1E). Stretching needed to be conducted above the glass transition temperature (T_g) of PAN ($T_g = 103^\circ\text{C}$ according to our differential scanning calorimetry measurement) but below the onset of oxidation at 180°C (19). We investigated yarns with different stretch ratios (SRs) ranging from 1 to 9 (where SR is the length of stretched yarn divided by the length of as-spun yarn, and a SR of 1 is unstretched) at stretch temperatures of 130°C and 160°C and determined the alignment factor. The alignment factor [orientation of the fibrils of the yarn, with values ranging from 0 for an isotropic orientation to 100% for a perfect alignment (20)] increased from $\sim 46.0\%$ (at SR 1) to 99.6% at SR 9 and stretch temperature 160°C (fig. S3A). The orientation of the fibrils can also be seen in the three-dimensional (3D) x-ray images of the yarn samples (fig. S4 and movies S1 and S2). The tortuosity estimation, calculated using the 3D images, is equal to 1.00 for stretched yarns (at SR 8 at 160°C) and agrees well with the uniform orientation of the fibrils. The stretching of yarns naturally caused a reduction of their diameter, from $130 \pm 12 \mu\text{m}$ (unstretched yarns) to $50 \pm 3.3 \mu\text{m}$ (at SR 5 at 130°C) and $36 \pm 1.3 \mu\text{m}$ (at SR 9 at 160°C) (fig. S2, C and D). Simultaneously, the diameters of the fibrils reduced from $1.17 \pm 0.12 \mu\text{m}$ to $0.57 \pm 0.01 \mu\text{m}$ and to $0.37 \pm 0.07 \mu\text{m}$ at 130°C and 160°C , respectively (Fig. 1F and fig. S3B). The reduction in diameter of the yarns after stretching can be explained by the untwisting and alignment of the fibrils. Stretching also reduced the linear densities of the yarns, which changed from $3.74 \pm 0.14 \text{ tex}$ [mass of fiber (g)/1000 m] in the as-spun yarns to $0.39 \pm 0.04 \text{ tex}$ at SR 9 at 160°C (fig. S3C). After heat stretching, annealing under tension (about 15 to 20 cN) was applied to achieve high toughness and high strength of the yarns. This annealing step (130°C for 4 hours in air) did not result in any further changes in the diameters of the yarns (EASY) or of the fibrils (fig. S3D).

The results of the model studies were transferred to yarns composed of PAN and the interconnecting molecule PEG-BA. Bisazides were reported to undergo the [2+3] click azide cyclo-

addition reaction (18) with the acrylonitrile groups of PAN, which could either favorably lead to bridging between the fibrils in the yarns or cause reaction with PAN in the bulk of the yarns. PEG-BA contents in yarns in the range from 0 to 4 wt % had no significant effect on the diameter of stretched and annealed yarns (fig. S3D). To analyze the effect of PEG-BA on the mechanical properties of the yarns, the toughness and the specific strength were analyzed for stretched yarns with different contents of PEG-BA relative to PAN. The maximum stress (fig. S5A) and modulus (fig. S5B) increased with the SR, whereas the toughness did not linearly increase with the SR (fig. S5C). The increase of PEG-BA content decreased the maximum stress and modulus slightly (fig. S5, D and E). In contrast, the toughness increased slightly (fig. S5F). However, the subsequent annealing step had a significant effect on the toughness of the yarns when PEG-BA was present. An annealing time of 4 hours was found to be optimal for the maximum strength, modulus, and toughness at an annealing temperature of 130°C (fig. S5, G to I). Optimum values were obtained with 4 wt % PEG-BA, at SR 8 at 160°C , with subsequent annealing at 130°C for 4 hours (Fig. 2 and Fig. 3, A and C). These yarns (i-EASY) have a tensile strength of $1236 \pm 40 \text{ MPa}$, a modulus of $13.5 \pm 1.1 \text{ GPa}$, and a toughness of $137 \pm 21 \text{ J/g}$, which are similar properties to those of dragline spider silk (15, 16). They also have a value for the tensile modulus of 13.5 GPa , which is close to the theoretical limit calculated for atactic crystalline PAN fibers (21). For comparison, the strength of an aligned, electrospun PAN nonwoven is $110 \pm$

12 MPa and its toughness is $57 \pm 3.0 \text{ J/g}$. Untreated as-electrospun PAN yarn has a strength of $72 \pm 3.0 \text{ MP}$ and its toughness is $76 \pm 10 \text{ J/g}$. The linear density of i-EASY was only $0.4 \pm 0.06 \text{ tex}$ and it had an alignment factor of the fibrils of 99.4%. This yarn, weighing 0.008 mg , could lift a total mass of up to 30 g repeatedly without breaking (movie S3) and could even be used to sew a button to a shirt (movie S4). After repeatedly lifting 30-g weights, the yarn elongated slightly, most likely because of the elongation at the yielding point (strain of $\sim 2.5\%$). Even after 5000 cycles of loading and unloading at a maximum tensile strength of 400 MPa , only a negligible change in the final tensile strength ($\sim 5.3\%$) and plastic deformation ($\sim 4.2\%$) was observed (fig. S6, A and B). The plastic deformation occurred mainly in the first 10 cycles. Owing to minor structural changes after 10 cycles, the energy loss coefficient with cycling showed a slight decrease, with values in the range of 0.23 to 0.15 (fig. S6C).

On the basis of our findings, we postulate that only the combination of high-fibril orientation, caused by stretching and annealing in the presence of a certain amount of PEG-BA as an interlinking molecule, yielded high strength and high toughness in combination with high crystallinity (Fig. 3, A to C). Clearly, the crystallinity of the PAN in the yarns is insufficient on its own for the achievement of high strength in combination with high toughness. Polarized Raman spectroscopy confirmed that the heat stretching procedure caused the orientation of the PAN macromolecules along the yarn's main axis (fig. S7A), with the percentage of aligned yarns increasing from 66.1% at no-stretch to

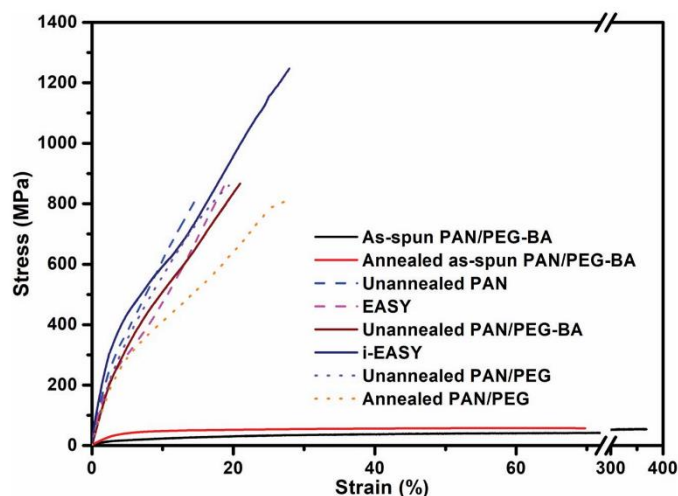


Fig. 2. Comparison of different yarns. Stress-versus-strain curves of unannealed and annealed (130°C for 4 hours) yarns (at SR 8) with 0 wt % PEG-BA, 4 wt % PEG-BA, and 4 wt % PEG.

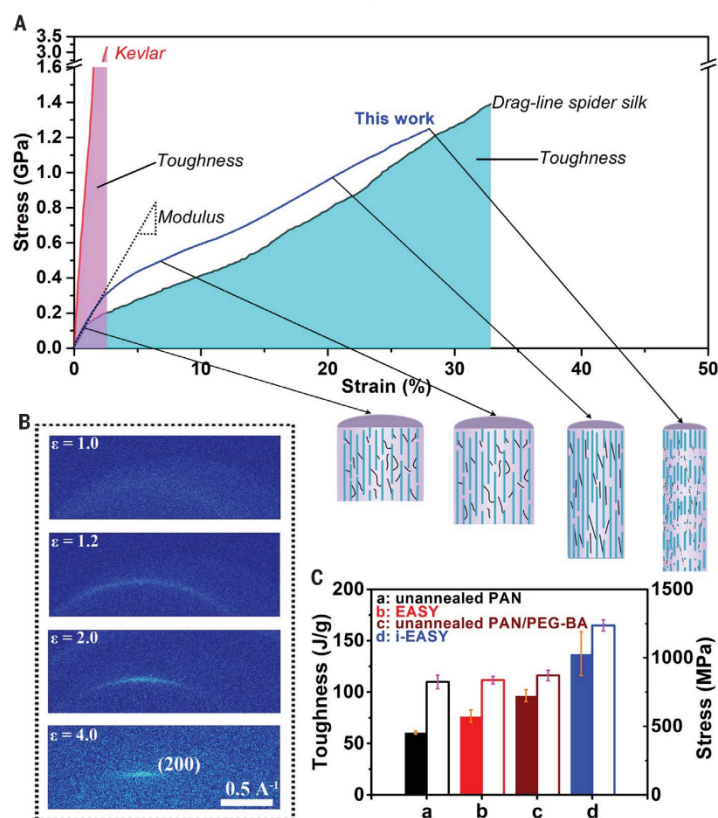


Fig. 3. Comparison of tensile strength and toughness of stretched and annealed yarns and their crystallization during heat stretching. (A) Comparison of stress-strain behavior and toughness of yarns (at SR 8 at 160°C, annealed at 130°C for 4 hours) with dragline spider silk and Kevlar [silk and Kevlar data are taken from the literature (16, 25)]. A model for the stress/strain behavior of yarns is presented beneath the graph. The blue lines represent PAN fibrils, and the black lines denote PEG-BA moieties. (B) In situ 2D-WAXS patterns recorded during the stretching process of a single yarn at 160°C. With increasing extension, we observe the development of a sharp Debye-Scherrer ring, subsequently followed by the development of a sharp (200) reflection, indicating crystal formation and alignment with high-orientation orders. (C) Comparison of the toughness (filled columns) and strength at break (open columns) of unannealed and annealed yarns with a SR 8 at 160°C. Error bars indicate the standard deviation of toughness and strength.

83.3% at SR 8 (stretched at 160°C). Wide-angle x-ray scattering experiments demonstrated that heat stretching resulted in a marked increase in the crystallinity from ~56.9% (at no stretch) to ~92.4% (at SR 9; fig. S7B), whereas annealing alone did not significantly increase crystallinity (fig. S7C). The size of the crystallites increased during stretching, from ~3.4 nm (as-spun) to ~12.9 nm and accompanied the increase in the degree of crystallinity (at SR 9; fig. S7D). Tensional forces during annealing are necessary to preserve the high degree of crystalline orientation. This is also supported by in situ x-ray

diffraction measurements of the crystalline orientation during stretching at 160°C (Fig. 3B). The crystallinity orientational order parameter (22) increased from 0.37 to 0.96 by heat stretching, but no significant increase was observed upon annealing (Fig. 3B and fig. S7, E to I). If no tension force was applied, the orientation parameters dropped from 0.96 to 0.82 during annealing because of thermal motion, which caused macromolecular relaxation and a reduction in the mechanical properties.

We analyzed the development of the specific strength and toughness throughout different

steps of preparation, which are: as-spun (green star in fig. S8), stretched (purple star in fig. S8), and finally annealed (blue oval in fig. S8). The strength primarily increased because of the stretching, whereas the toughness increased because of the annealing after stretching, which caused alignment of the fibrils and crystallization of PAN.

Too much PEG-BA can have an adverse impact on fibril resilience. Yarns with 5 wt % and 6 wt % PEG-BA featured lower strength and toughness than those with 4 wt % PEG-BA (fig. S5, E and F). Simultaneously, control experiments were performed by obtaining yarns with PAN and pure PEG ($M_n = 1000$, 4 wt %) (Fig. 2), which show a slight decrease in tensile strength (from 858 ± 103 MPa to 784 ± 77 MPa) and modulus (from 7.6 ± 1.0 GPa to 7.3 ± 1.1 GPa), a big increase in elongation at break (from 18.0 ± 1.6 % to 27 ± 2.5 %), and a slight increase in toughness (from 83 ± 12.2 J/g to 89 ± 15.0 J/g) after annealing. The yarns consisting of PAN and PEG (4 wt % but without azide groups) have almost the same elongation at break as yarns made from PAN and PEG-BA (4 wt % with azide groups), but they have lower strength. This suggests that the flexible oligomer PEG makes the yarns have higher elongation at break but lower strength than the PEG-BA yarns, due to the missing interaction between the fibrils. The interaction between cyano groups and PEG in the presence of azide groups was confirmed by $^1\text{H-NMR}$, $^{13}\text{C-NMR}$ (carbon-13 nuclear magnetic resonance), and ATR-FTIR (attenuated total reflectance-Fourier transform infrared spectroscopy) spectra (figs. S9 to S12). A new peak at about 4.2 parts per million (ppm) in $^1\text{H-NMR}$ and 162 ppm in $^{13}\text{C-NMR}$ spectra represents the carbon in the tetrazole after reaction between nitrile and azide groups. Further, a decreased intensity of the peak at 2100 cm^{-1} represents azide groups in the ATR-FTIR spectra, which suggests that the nitrile group in the PAN and azide groups in the PEG-BA can have a reaction in the yarns during the annealing process. i-EASYs are still soluble in N,N' -dimethylformamide and do not show any increase in molecular weight according to gel permeation chromatographic analysis, which strongly supports the idea that intermolecular cross-linking reactions of PAN molecules in the bulk of the fibrils did not occur. The most plausible explanation for these findings is that the reaction occurs only on the surface of the fibrils. Therefore, we postulate that under the presented conditions, interfibrillar reactions via PEG-BA are the dominating reaction.

A possible model for understanding the mechanical properties of i-EASY is shown in Fig. 3A. It highlights a reduction in the fractional-free volume after strain-induced crystallization and shrinking. As a result, PEG-BA macromolecules in the PAN matrix probably diffuse

to the fibril-free surface, which is the optimal position for efficient interfibrils reaction. Too much PEG-BA may lead to PEG microphases that represent defect structures that deteriorate the mechanical properties. Starting from pristine yarns, the PAN fibrils in the yarns begin to disentangle, resulting in a yield point. Beyond the yield point, the PEG-BA moieties bridging the PAN fibrils are responsible for stress transfer, impeding their ability to slide along and over each other. At a critical stress, the PEG-BA bridges might rupture, causing the yarns to break. This mechanism can be illustrated assuming the case of a single craze propagating ahead of the crack during stable crack growth. Then the local crack driving force (23, 24) is $\sim \frac{1}{\sqrt{E_1 E_2}}$, where, E_1 is the modulus in the fibril direction and E_2 is the modulus perpendicular to the fibrillar direction, which can be related to the PEG-BA elastic modulus. Thus, increasing E_2 should result in delaying the crack propagation. This mechanism is also supported by the fact that, at higher cross-linking density, the mechanical properties worsen.

To achieve the high strength and high toughness combination, annealing was required in addition to orientation and crystallization. Though single-polymer nanofibers could yield very high strength and high toughness, the handling difficulty of these single nanofibers has prevented their use in real-world applications. The presented process yields ultrafine electrospun yarns robust enough for practical use,

through a combination of thousands of fibrils with high alignment and interfibrillar reactions. We are convinced that ultrafine polymer yarns, as we show here, are not restricted to the present system. An important precondition for other systems is the extensibility of the yarn for orientation of the fibrils and reactive groups for interlinking of the fibrils.

REFERENCES AND NOTES

- R. O. Ritchie, *Nat. Mater.* **10**, 817–822 (2011).
- M. F. Ashby, *Materials Selection in Mechanical Design*, (Butterworth & Heinemann, ed. 2, 1999).
- D. C. Hofmann et al., *Nature* **451**, 1085–1089 (2008).
- H. Zhu et al., *Proc. Natl. Acad. Sci. U.S.A.* **112**, 8971–8976 (2015).
- M. D. Demetriou et al., *Nat. Mater.* **10**, 123–128 (2011).
- A. B. Dalton et al., *Nature* **423**, 703 (2003).
- M. Naraghi et al., *ACS Nano* **4**, 6463–6476 (2010).
- Z. Xu et al., *Adv. Mater.* **28**, 6449–6456 (2016).
- J. Cai, M. Naraghi, *Carbon* **137**, 242–251 (2018).
- A. Arinstein, M. Burman, O. Gendelman, E. Zussman, *Nat. Nanotechnol.* **2**, 59–62 (2007).
- D. Papkov et al., *ACS Nano* **7**, 3324–3331 (2013).
- Y. Ding, H. Hou, Y. Zhao, Z. Zhu, H. Fong, *Prog. Polym. Sci.* **61**, 67–103 (2016).
- J. H. Park, G. C. Rutledge, *J. Mater. Sci.* **53**, 3049–3063 (2018).
- D. Papkov et al., *ACS Nano* **13**, 4893–4927 (2019).
- D. A. Tirrell, *Science* **271**, 39–40 (1996).
- F. Vollrath, D. P. Knight, *Nature* **410**, 541–548 (2001).
- K. Spiess, A. Lammel, T. Scheibel, *Macromol. Biosci.* **10**, 998–1007 (2010).
- Z. P. Demko, K. B. Sharpless, *Angew. Chem. Int. Ed.* **41**, 2113–2116 (2002).
- N. Yusof, A. F. Ismail, *J. Anal. Appl. Pyrolysis* **93**, 1–13 (2012).
- For details of calculation, see supplementary materials.
- T. Shen, C. Li, B. Haley, S. Desai, A. Strachan, *Polymer* **155**, 13–26 (2018).
- Q. Ouyang et al., *J. Macromol. Sci. B* **50**, 2417–2427 (2011).
- H. R. Brown, *Macromolecules* **24**, 2752–2756 (1991).
- H. H. Kausch, C. J. G. Plummer, *Polymer (Guildf.)* **35**, 3848–3857 (1994).
- D. Zhu, X. Zhang, Y. Ou, M. Huang, *J. Compos. Mater.* **51**, 2449–2465 (2016).

ACKNOWLEDGMENTS

We thank R. Schneider for the GPC measurements, H. Schmalz and L. Benker for measurements of polarized Raman spectroscopy, P. Schmidt and T. Braun for support in construction of the yarn electrospinning set-up, S. Jiang for advice in electrospinning, and A. Wambach for technical support with figures and data arrangement. We acknowledge the use of the research facilities of the University of Bayreuth, the Bavarian Polymer Institute, the Institute of Physics - Martin-Luther-Universität Halle-Wittenberg, and the Forschungszentrum Jülich for this project. **Funding:** The work was supported by the University of Bayreuth (A.G.) and the Deutsche Forschungsgemeinschaft (WE4051/21-1 and 4051/22-1, to J.M.d.S.e.S.). **Author contributions:** A.G., X.L., and S.A. conceived and supervised the project. X.L. prepared the yarns; measured WAXS, TGA, NMR, and IR; and performed stress-strain tests. X.L., A.G., and S.A. wrote the manuscript. M.D. measured the crystal data and evaluated and discussed with S.F. X-ray computed tomography was performed by J.M.d.S.e.S. and was evaluated and discussed by J.M.d.S.e.S. and R.B.W. P.S. and H.H. evaluated and discussed the mechanical data of the yarns with X.L. and A.G. All authors contributed to the analysis and discussion of the data. The manuscript writing was led by A.G. with contributions from all other authors. **Competing interests:** The authors declare no competing interests. **Data and materials availability:** All data are available in the main text or the supplementary materials. Primary data are available from <https://myfiles.uni-bayreuth.de/ssf/s/readFile/share/31206/3130562511270201132/publicLink/Raw%20data%2020191018.zip>.

SUPPLEMENTARY MATERIALS

science.sciencemag.org/content/366/6471/1376/suppl/DC1
Materials and Methods
Figs. S1 to S12
Table S1
References (26–46)
Movies S1 to S4
27 July 2019; accepted 13 November 2019
10.1126/science.aay9033



science.sciencemag.org/content/366/6471/1376/suppl/DC1

Supplementary Materials for

High strength in combination with high toughness in robust and sustainable polymeric materials

Xiaojian Liao, Martin Dulle, Juliana Martins de Souza e Silva, Ralf B. Wehrspohn, Seema Agarwal, Stephan Förster, Haoqing Hou, Paul Smith, Andreas Greiner*

*Corresponding author. Email: greiner@uni-bayreuth.de

Published 13 December 2019, *Science* **366**, 1376 (2019)
DOI: 10.1126/science.aay9033

This PDF file includes:

Materials and Methods
Figs. S1 to S12
Table S1
References

Other Supplementary Material for this manuscript includes the following:
(available at science.sciencemag.org/content/366/6471/1376/suppl/DC1)

Movies S1 to S4 (.mp4)

Materials and Methods

Materials

Polyacrylonitrile (PAN, number average molar mass (M_n) of 120,000, \bar{D} : 2.79, co-polymer with about 4.18 mol% (6.35 wt%) methyl acrylate, Dolan, registry no. 26658-88-8h), poly(ethylene glycol) bisazide (PEG-BA; M_n of 1,100; Sigma-Aldrich), N,N'-dimethylformamide (DMF; Fisher Chemical, 99.99%) and acetone (technical grade) were used as received.

Yarn electrospinning

Continuous yarns were obtained by yarn electrospinning following a procedure as described in literature 26 with some minor modifications – see below). The solution (15 wt%) for electrospinning was prepared by dissolving 2.0 g PAN powder and 0.08 g poly(ethylene glycol) bisazide in 9.4 g DMF solution with 1.93 g acetone. The continuous yarns were fabricated using a homemade setup shown in fig. S1 comprising two syringe pumps, a high-voltage DC power supply, a poly(vinyl chloride) (PVC) funnel (8.0 cm in diameter) with a motor controller and a yarn winder collector with 2 cm in diameter. The solution was loaded into two syringes capped with metal needles, respectively (controllable feed rate of 0.5 mL/h by two syringe pumps), which were connected separately to the positive and negative electrodes of the DC power supply.

After adjusting the angle (13 degree of inclination), distance (40 cm) and altitude (perpendicular distance to the plane of the end of funnel: 2 cm) of these two syringes, high voltages (positive pole: +12 kV; negative pole: -12 kV) were applied to two needle tips respectively, resulting in positively and negatively charged continuous fibrils. At first, by the force of electric field, these two oppositely charged fibrils flew to the end of the funnel with 1,500 rpm rotation speed and a fibril membrane would be formed. Followed by switching on the winder collector of

13 rpm rotation speed, the membrane was dragged by a pre-suspended yarn which was connected with the winder collector. Then a rotodynamic fibril cone could be formed above the funnel. Simultaneously, helical form fibrils in the fibril cone were pulled up in a spiral path. Due to the cone maintained by the continuous helical form fibrils, a polymer yarn with continuous and twisted form was prepared from the apex of the fibril cone and wined around the collector. The whole electrospun yarn process was operated under infrared lamp (250 W) at about 45°C and with 10%-15% humidity.

Stretching and annealing process

To construct the continuously oriented hierarchical architecture, all as-spun yarns were stretched at high temperature by a homemade heat-stretching instrument consisting of three parts: a tubular furnace with one heat position zone (Heraeus, D6450 Hanau, Typ: RE 1.1, 400 mm in length, Germany), two rollers controlled by electronic motors and a laptop with “LV2016” software, which was used to precisely control the velocities of the motors. By adjusting the velocities of the two rollers in the LV2016 software, the yarns could be stretched continuously (fig. S1). The SR was calculated by the equation: $SR = v_f / v_s$, where v_f and v_s represent the velocities of fast roller and slow roller, respectively. To obtain a high SR (greater than six), the yarns were stretched repeatedly.

The subsequent annealing process was achieved by wrapping the curable stretched yarns around a glass tube, keeping the yarns under tension about 15 cN-20 cN. The cycloaddition reaction between PAN and PEG-BA was achieved by the azide-nitrile “click” reaction at a suitably high temperature. After being annealed at 130°C for 4 h, the final yarns were obtained and quickly transferred to a refrigerator at -4°C for 20 min.

NMR spectroscopy

The ^1H -NMR and ^{13}C -NMR spectroscopy was performed on a Bruker AMX-300 operating at 300 MHz. The deuterated dimethylsulfoxide was used as the solvent.

Scanning electron microscopy (SEM)

The morphology of all yarn samples was probed by a Zeiss LEO 1530 (Gemini, Germany) scanning electron microscope equipped with a field emission cathode and a secondary electron (SE2) detector. Before the measurements, for the surface SEM image measurements, all the yarn samples were attached to a sample holder with conductive double-sided tape; for the cross-sectional SEM image measurements, all the yarn samples were obtained by cutting them in liquid nitrogen after they had been emerged in ethanol and water for 0.5 h, respectively. Subsequently, all the yarn samples were sputter-coated with 2.0 nm of platinum by a Cressington 208HR high-resolution sputter coater equipped with a quartz crystal microbalance thickness controller (MTM-20). An SE2 detector was used for acquiring SE2 images at an acceleration voltage of 3 kV and a working distance of 5.0 mm. The SEM images were used to study the diameter and morphology of the fibrils and yarns. Quantitative analysis of the dimensional changes was carried out by ImageJ software. In addition, according to a previous literature report (27), the fibril alignment factors were calculated based on the following Eq. 1

$$d_{Fa} = (3\cos 2\theta - 1) / 2 \quad (1)$$

where d_{Fa} is the fibril alignment factor and θ is the angle between the individual fibrils and direction of the yarns. The given values were based on an average of 100 fibrils.

Linear density tests

The linear density of yarns was measured by the weighing method, which was calculated by the Eq. 2:

$$D = W / L \quad (2)$$

where the D is the linear density ($tex = g/km$), W is the weight of yarns and L is the length of yarns. All the yarn samples were washed by ethanol for 24 h to move the residue solvent and then dried in vacuum oven at 40°C for 24 h until to constant weight. The weight of dry yarns with a length of 30 cm was measured by an ultramicro balance (Sartorius MSE2.7S-000-DM Cubis, capacity of 2.1 g, readability of 0.0001 mg, Germany).

Mechanical properties tests

Tensile tests were performed using a tensile tester (zwickiLine Z0.5, BT1-FR0.5TN.D14, Zwick/Roell, Germany) with a clamping length of 10 mm, a crosshead rate of 5 mm/min at 25°C and a pre-tension of 0.005 N. The load cell was a Zwick/Roell KAF TC with a nominal load of 200 N. The two ends of yarn samples were fixed by double side tapes and loaded between the two clamp stages with the top clamp stage applying uniaxial tension on the yarns samples along the vertical direction. The yarn tensile tests were performed by a test programme of yarn shape for cross-section calculation, while the linear density and density of the specimen material were input parameters. After the tensile test measurement, quantitative analysis of the modulus and toughness was carried out by Origin 2016 software. The modulus was equal to the slope of the curves at 0-3% strain, and the toughness was calculated by integral area of the tensile curves divided by density of the specimen material.

For fatigue tests at maximum stress of 400 MPa for 5,000 cycles, the sequential tensile cycles were conducted by the tensile tester (zwickiLine Z0.5, BT1-FR0.5TN.D14, Zwick/Roell, Germany) with a clamping length of 10 mm and 200 N load cell (Zwick/Roell KAF TC). All curves were obtained at the strain ramp rate of 10 mm/min with 0 cN pre-tension. The test time, cycle number, stress, strain and the work per cycle were recorded. After 5,000th cycle, the final stress-strain tensile tests were performed automatically until the yarns ruptured.

Attenuated Total Reflectance Fourier Transform Infrared (ATR FT-IR) Spectroscopy

The ATR FT-IR studies were performed on a Digilab Excalibur 3000 system equipped with an ATR unit at a resolution of 2 cm⁻¹. A total of 16 measurements were averaged per sample to obtain higher signal-to-noise ratios.

Wide-angle X-ray diffraction (WAXS)

WAXS characterization was carried out using an anode X-ray generator (Bruker D8 ADVANCE, Karlsruhe, Germany) operating at 40 kV and 40 mA with Cu-K α radiation (wavelength $\lambda = 0.154$ nm). Before the measurement, the yarns were aligned into a yarn bundle with a width of 3 mm in a paper frame, which was then fixed in the instrument stage. XRD profiles were recorded in the 2 θ angle range from 8° to 36° at a scanning speed of 0.05°/min at 25°C. The acquired WAXS curves were analysed by DIFFRAC.EVA V4.0 software, while the degree of crystallinity and the crystallite size (L(100)) were calculated.

Measurement of crystallinity orientation

Crystallinity orientation was determined from 2D X-ray scattering patterns of yarns aligned perpendicular to the X-ray with respect to their drawing direction. The scattering patterns were recorded with the SAXS system “Ganesha-Air” from (SAXSLAB/XENOCs). The X-Ray source of this laboratory based system is a D2-MetalJet (Excillum) with a liquid metal anode operating at 70 kV and 3.57 mA with Ga-K α radiation (wavelength $\lambda = 0.1314$ nm) providing a very brilliant and a very small beam (<100 μ m). The beam is slightly focused with a focal length of 55 cm using a specially made X-Ray optic (Xenocs) to provide a very small and intense beam at the sample position. Two pairs of scatterless slits are used to adjust the beam size depending on the detector distance. For the measurements the yarns were aligned into a small bundle consisting of three yarns and fixed on a small paper frame which was fixed on a metal frame sample holder with double sided scotch tape. The bundles were aligned perpendicular to the primary beam and horizontally with respect to the detector at a sample detector distance of 152 mm. For the heat stretching experiment a single as-spun fibre was mounted in a Linkam Tensile Testing Stage (TST350) where the glass windows were replaced with X-ray transparent mica windows. The stage was placed such that the fiber was aligned as the ones in the paper frame. The heating block of the stage was heated to 160°C at a rate of 60°/min to keep the exposure to high temperature as small as possible. Upon reaching 160°C the fibre was stretched at a rate of 1 mm/s to the desired stretching ratios. As soon as stretching was finished the SAXS measurement was started and the sample was cooled down to room temperature.

In all measurements the scattering intensity was accumulated for 300 s. Background was always measured close to the respective sample position to minimize remnants of air scattering and shadows due to the sample holder and subtracted from the 2D image directly.

To determine the degree of orientation, first the subtracted 2D data were radially averaged to determine the radial peak width of the PAN (200) reflection. This width in q [nm⁻¹] was used to average the data azimuthally and obtain the $I(\varphi)$ vs. φ plots. One of the two peaks was then fitted with a Lorentz-peak function using the built in routine of Origin 2016 to obtain the *FWHM*. This was used to calculate the degree of orientation using Eq. 3 (22):

$$S = (180 - FWHM) / 180 \quad (3)$$

Polarized Raman Spectroscopy

For the polarized Raman measurements, a confocal WITec alpha 300 RA+ imaging system equipped with a UHTS 300 spectrometer and a back-illuminated Andor Newton 970 EMCCD camera was used. Raman spectra were acquired using an excitation wavelength of $\lambda = 532$ nm, a laser intensity of 5 mW and an integration time of 0.5 s (100x objective, NA = 0.9, 10 accumulations, WITec Control 5.1 software). Before the measurements, a single yarn was stuck on a glass plate with double-side tape applying a weak stress to prevent vibration.. All measurements focused on a single fibril in the yarns. All spectra were subjected to a cosmic ray removal routine and baseline correction.

The polarizer was used to rotate the angle between the direction of the yarns and the direction of the linearly polarized laser light. By adjusting the angle, the polarization direction of incident light could be parallel or perpendicular with respect to the long axis of the yarn. Therefore, two Raman spectra were acquired, with polarization parallel and perpendicular to the yarn long axis, respectively. According to previous literature reports (28,29) the molecular orientation factor (f) in the fibrils was calculated by the following Eq. 4:

$$f = 1 - I_{YY} / I_{XX} \quad (4)$$

where I_{XX} and I_{YY} are the absorption intensity of the 2245 cm^{-1} peak (-CN stretching vibration) in the XX and YY directions, respectively.

Three-dimensional X-ray transmission microscopy

Imaging experiments were performed in a Carl Zeiss Xradia Ultra 810, that is equipped with a chromium X-ray source (5.4 keV). The experiments were performed using phase-contrast imaging mode, thus, a gold phase-ring, with thickness designed to produce a phase-shift of $3\pi/2$ of the non-diffracted X-ray beam, was positioned near the back focal plane of the zone plate. Experiments were performed using high-resolution (800x magnification) and low-resolution (4200x magnification) modes. A small piece of the yarn was glued onto the tip of a metallic pin and inserted into the sample holder. A total of 901 projections were obtained over 180° with the exposure time of 60 s or 15 s (for high- and low-resolution modes, respectively) and detector binning of 2. Image reconstruction was performed by filtered back-projection algorithm using the software XMReconstructor (integrated into the Xradia 810 Ultra) which was also used to produce a stack of approximately 500 tiff images of ca. 500×500 pixels with voxel size of 128 nm or 32 nm (for low- and high-resolution modes, respectively). Commercial software arivis Vision4D (version 1.12.6) and Thermo Scientific Avizo (version 9.4.0) were used for image correction, segmentation, 3D renderings and movies presented here. Calculation of the orientation of the fibers was performed using Avizo after applying non-local means filter to the images, followed by a grey level threshold segmentation. Those three-dimensional images were used for the central path tortuosity calculation, which was used to obtain information of the alignment of the fibrils. The point of equilibrium of all fibrils in one single plane (x, y) is named centroid, and the path going through the centroid of all planes in z-direction is named the geodesic length. The tortuosity was

calculated as the ratio of the geodesic length to the shortest distance (Euclidean distance) between the centroids of planes in the two extremes (the starting and ending extremes of the geodesic path in z-direction). Thus, the tortuosity has a minimum value of 1, which correlates to a completely straight path.

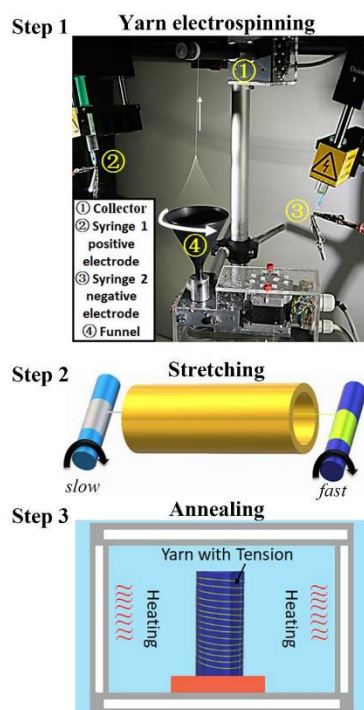


Fig. S1. Schematic diagram of the three fabrication steps of yarns.

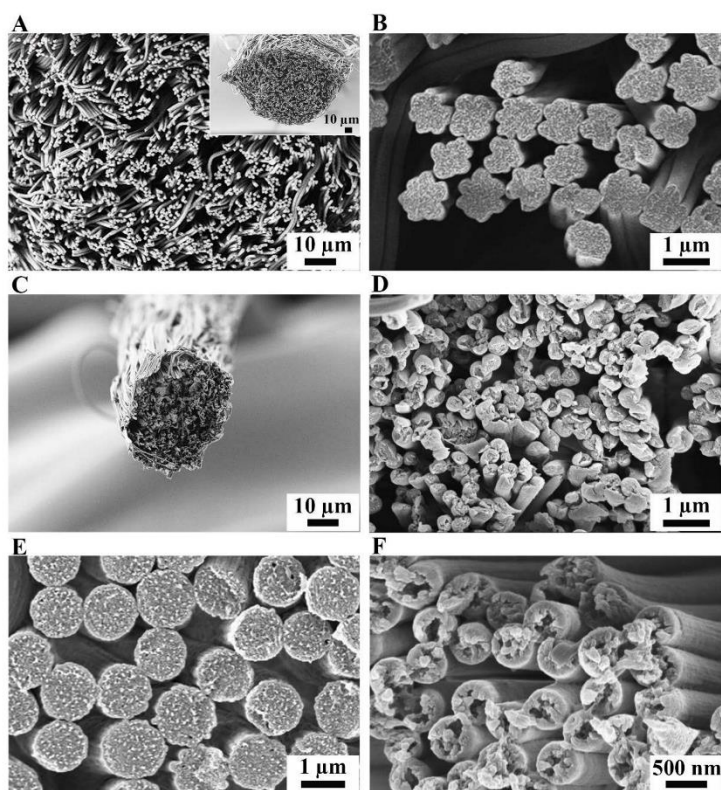


Fig. S2. Fibrils of yarns. **A** and **B**, Cross-sectional SEM micrographs of as-spun yarns at different magnifications. The inset in part **A** shows an image of as-spun yarns at low magnification. **C** and **D**, Images of yarns after stretching without annealing to a SR 9 at 160°C at different magnifications. **E**, Cross-sectional SEM images of as-spun yarns (with 3 wt% PEG-BA) at different magnifications. **F**, Cross-sectional SEM images of yarns (with 3 wt% PEG-BA) after stretching (SR 8 at 160°C) and annealing (130°C, 4h).

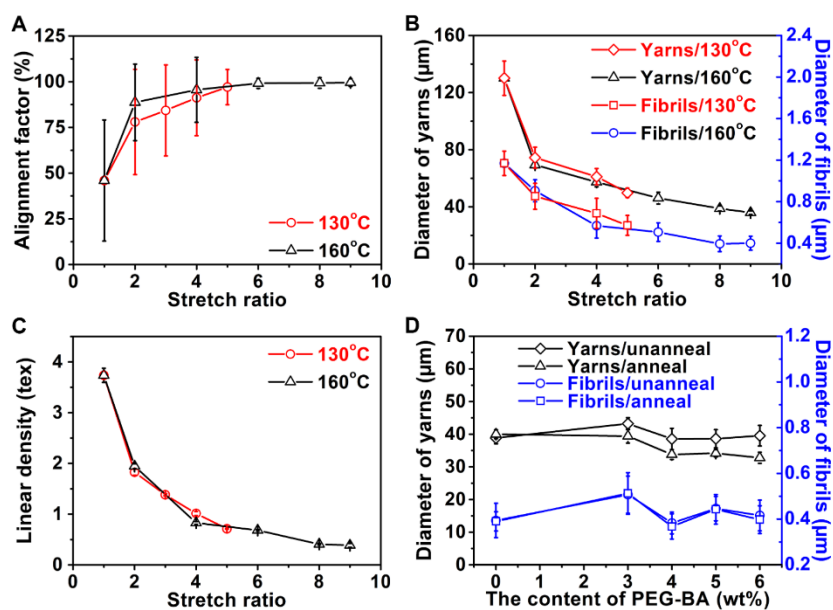


Fig. S3. Impact of stretching and annealing on the fibrils characteristics of yarns. **A**, Impact of stretching on the alignment factor of fibrils in the yarns at 130°C and 160°C. **B**, Impact of the SR on the diameter of yarns and fibrils at 160°C. **C**, Impact of stretching on the linear density of yarns at 130°C and 160°C. **D**, Effect of annealing at 130°C for 4 h on the diameter of stretched yarns (SR 8 at 160°C) with different contents of PEG-BA.

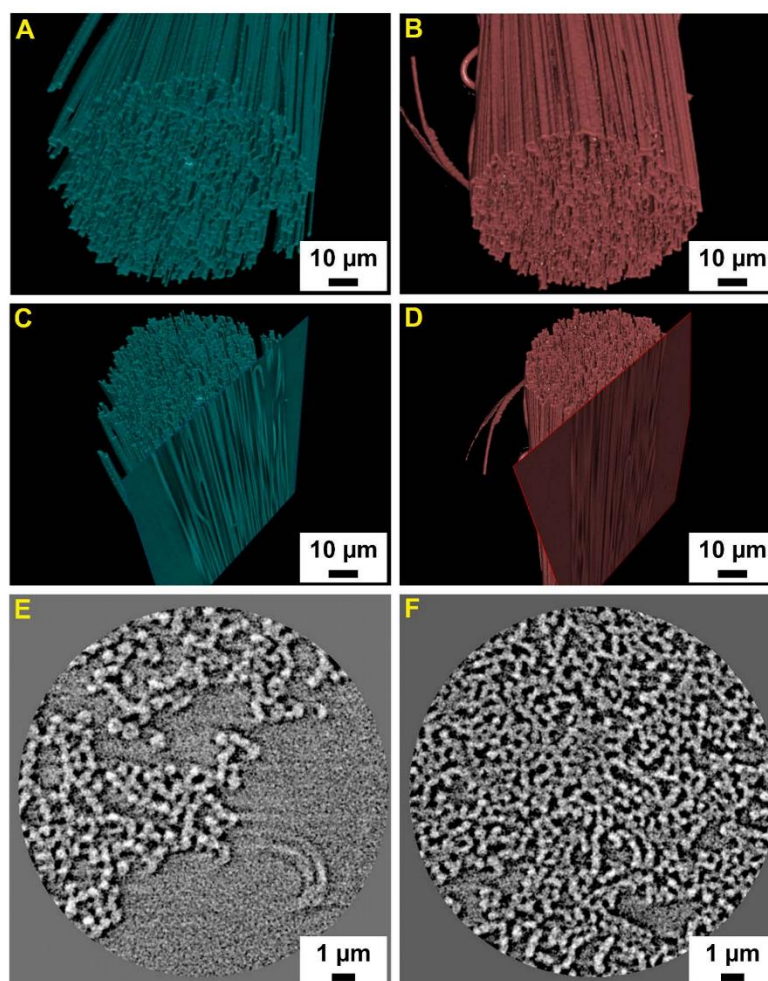


Fig. S4. Three-dimensional X-ray images of yarns. A and B, Volumetric images of stretched yarns (A) with 4 wt% PEG-BA after stretching without annealing to a SR 8 at 160°C and annealed yarns (B) with 4 wt% PEG-BA at 130°C for 4 h. C and D, Virtual cuts of yarns of A and B, respectively, to show the direction of the fibrils alignment. E and F, High-resolution X-ray

tomograms of stretched yarns (**E**) with 4 wt% PEG-BA after stretching without annealing to a SR 8 at 160°C and annealed yarns (**F**) with 4 wt% PEG-BA at 130°C for 4 h.

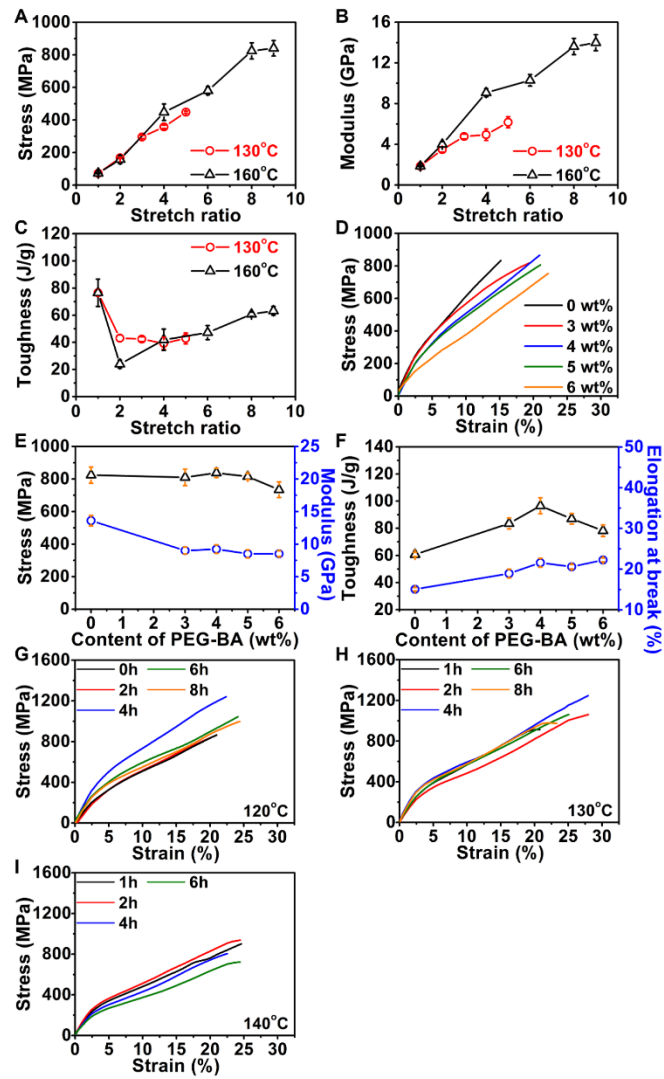


Fig. S5. Impact of processing parameters on the mechanical properties of yarns. A-C, Changes of tensile strength (A), modulus (B), and toughness (C) of yarns with 0 wt% PEG-BA

before annealing with different SR at different temperatures. **D** Stress/strain curves of yarns with different contents of PEG-BA before annealing with a SR 8 at 160°C. **E-F**, Changes of tensile strength, modulus (**E**), toughness and elongation at break (**F**) of yarns with different contents of PEG-BA before annealing with a SR 8 at 160°C. **G-I**, Stress/strain curves of yarns with 4 wt% PEG-BA and a SR 8 at 160°C annealed at 120°C (**G**), 130°C (**H**) and 140°C (**I**) for different periods.

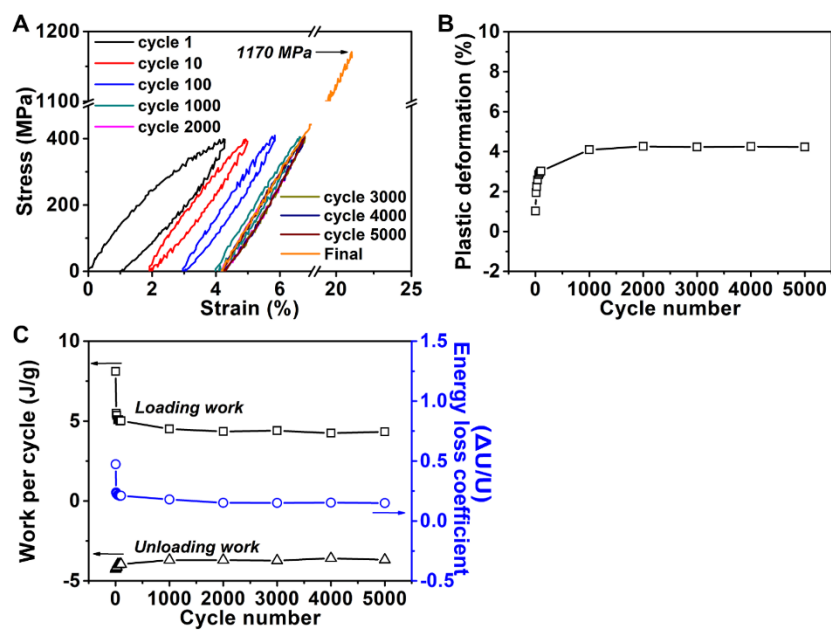


Fig. S6. The fatigue resistance behaviour of yarns. A, Stress versus strain curves of yarns (4 wt% PEG-BA and SR 8 at 160°C annealed at 130°C for 4 h) at maximum stress of 400 MPa for 5,000 cycles. B and C, Changes of plastic deformation (B) work per cycle (C) and energy loss coefficient (C) during this 5,000 cyclic tensile test, respectively.

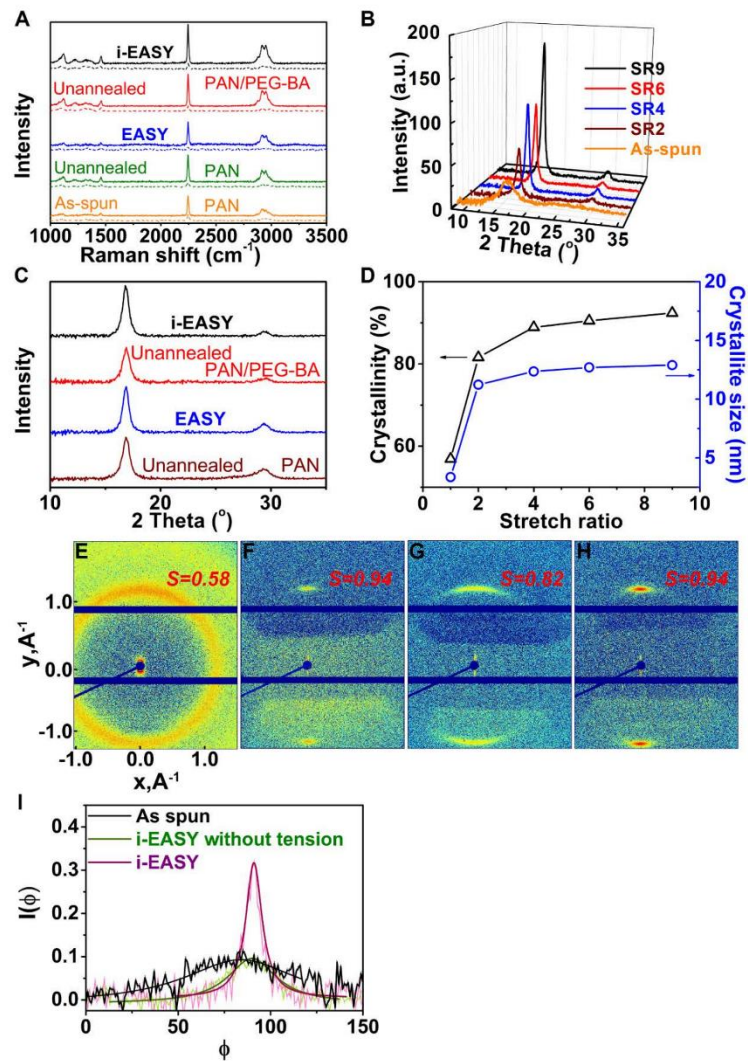


Fig. S7. Effect of annealing on yarns. A, Polarized Raman spectra of as-spun, unannealed and annealed (130°C, 4 h) yarns (SR 8) with 0 wt% and 4 wt% PEG-BA, respectively. solid line for

polarization parallel and dashed line for vertical to the fibre axis, respectively. **B**, WAXS analysis of yarns with different SR (stretched at 160°C, 0 wt% PEG-BA. **C**, WAXS analysis of yarns with 0 wt% and 4 wt% PEG-BA annealed at 130°C for 4 h, SR 8. **D**, Dependence of the degree of crystallinity and crystallite size of yarns (corresponding to fig. S7b) as a function of the SR. **E-H**, 2D scattering patterns of different yarns with 4 wt% PEG-BA: **E**, as spun yarns, **F**, stretched yarns, **G**, annealed yarns without tension, and **H**, annealed yarns with tension. It demonstrates that as-spun yarns have low orientational order with orientational order parameters in the range of $S = 0.37 - 0.58$. Stretching considerably increases the orientational order, reaching very high values of $S = 0.94$. Subsequent annealing has to be performed under tension to maintain the high degree of orientational order of $S = 0.94$. Without tension thermal motion reduces the degree of orientation to $S = 0.82$ leading to the deterioration of the mechanical properties. **I**, Representative $I(\phi)$ vs. ϕ plots. The bold lines are fits with a Lorentz peak function and from these the FWHM values were used to calculate the degree of order.

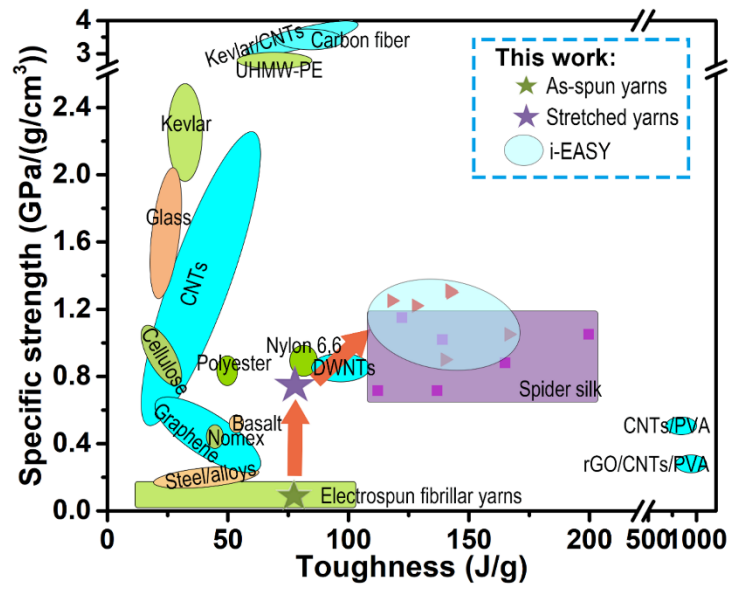


Fig. S8. Ashby plot of specific strength versus toughness for yarns, spider silk, electrospun fibrillar yarn, and other related materials. The data in the Ashby plot, which are shown in Supplementary Table S1, are taken from the literature.

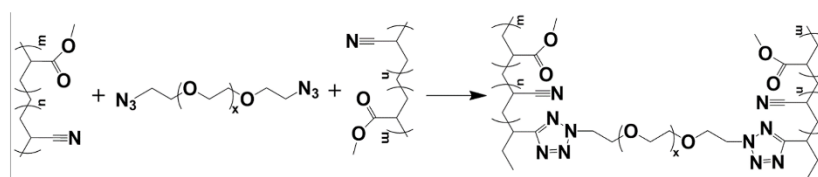


Fig. S9. The chemical reaction between PAN and PEG-BA.

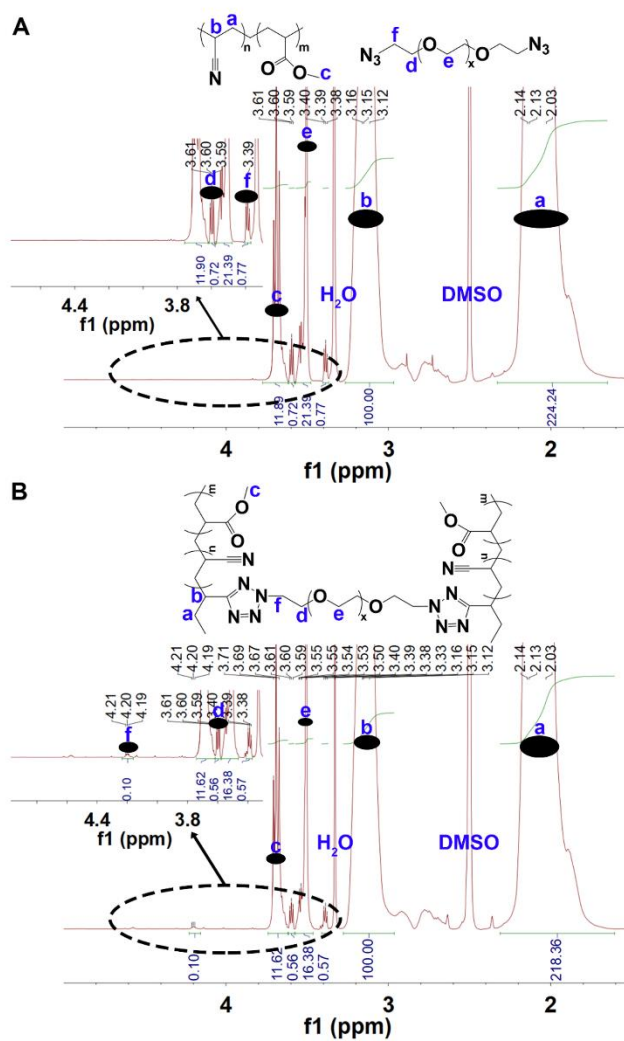


Fig. S10. $^1\text{H-NMR}$ spectra of yarn. The $^1\text{H-NMR}$ spectra of yarns (SR 8 at 160°C) consisting of PAN and PEG-BA (4 wt%) before (A) and after annealing (B) (130°C for 4 h), respectively.

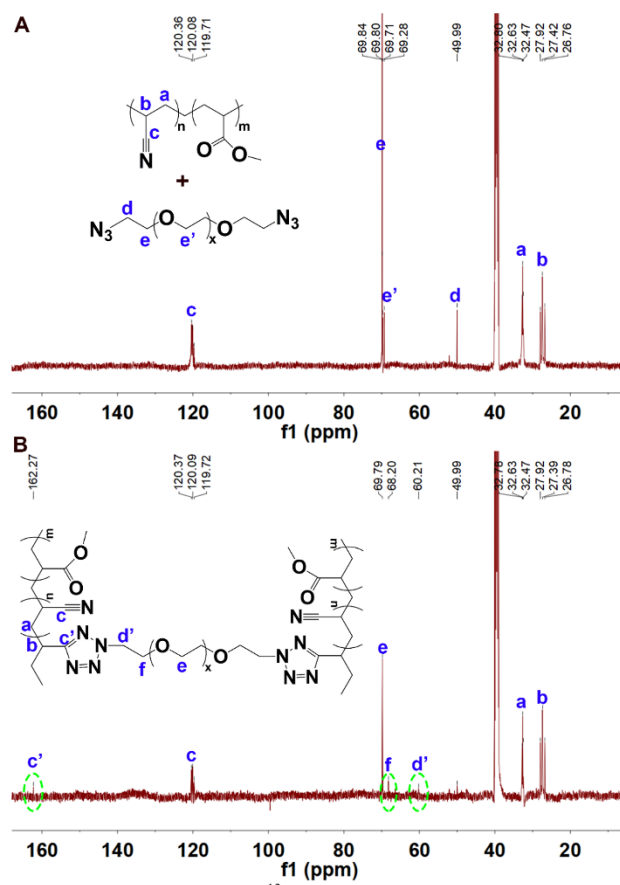


Fig. S11. ^{13}C -NMR spectra of yarn. The ^{13}C -NMR spectra of yarns (SR 8 at 160°C) consisting of PAN and PEG-BA (20 wt%) before (A) and after annealing (B) (130°C for 4 h), respectively.

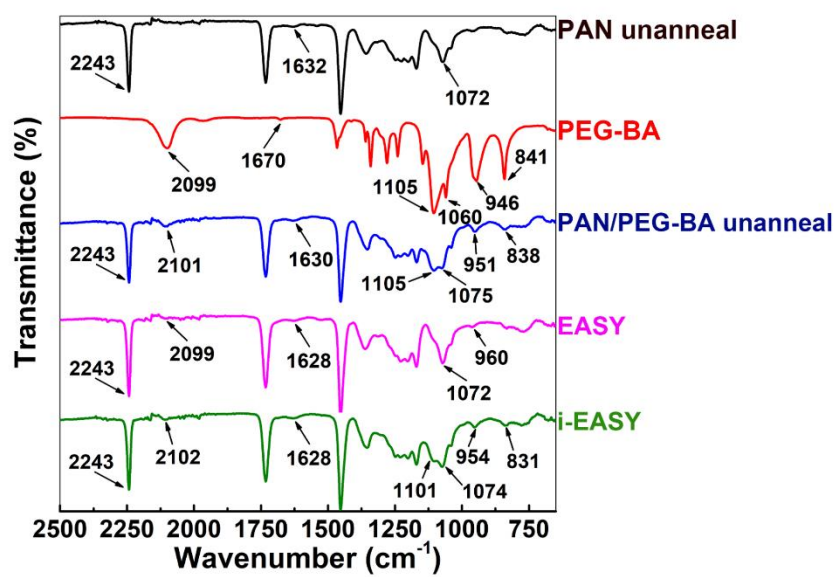


Fig. S12. ATR FT-IR spectra. The ATR FT-IR spectra of PEG-BA and yarns with (4 wt%) or without PEG-BA before and after anneal, respectively.

3 Publications

Table S1.

Comparisons of mechanical properties of our yarns with relevant literature values.

Materials	Specific strength	Toughness	Density	Strength	E-modulus	Specific E-modulus	Elongation at break	Ref.
	GPa/g·cm ³	J/g	g/cm ³	GPa	GPa	GPa/g·cm ³	%	
Spider silk	0.72-1.05	112.2-200	1.3	0.94-1.4	7-9	5.4-6.9	39	16,30 31
CNT yarn	0.31-0.58	11-20	0.8	0.25-0.46	--	--	3-13	32
DWNT yarn	0.89	100	1.575	1.4	--	--	20	7
Hot-drawn CNTs/PVA	0.5-1.38	40-870	1.3	0.6-1.8	--	--	6-430	33
CVD-grown CNT yarn	1.2-2.2	46-60	1.0	1.2-2.2	65-160	65-160	1.8-7.6	34

3 Publications

Reduced graphene oxide/CNTs/PVA	0.05-0.28	481-970	2.11	0.1-0.58	1.1-3.6	0.52-1.71	100-360	35
Graphene yarn	0.23-0.63	11.5-23.75	0.8	0.18-0.50	3.2-11.2	4-14	5.9-7.5	36
Graphene yarn	0.2-0.28	7.6-57.9	0.8	0.16-0.22	2.5-27	3.13-33.75	7.3-40	37
Carbon nanofiber	3.6	86	1.76	6.3	217	123	3.0	9
UHMW-PE	2.7	47-70	0.97	2.4	56-71	58-73	3.8-5.9	38
Kevlar 81	2.5	33	1.44	3.6	90	62.5	5	16
Kevlar 49	2.08	33	1.44	3.0	124	86.1	2.4	25
Kevlar/CNTs	3.13-3.93	63-99	1.5	4.7-5.9	115-207	77-138	4.0-5.4	39
27								
Nomex	0.43	44	1.38	0.6	17	12.3	22	11
E-glass	1.34	22	2.57	3.45	72	28.01	4.8	11
S-glass	1.99	27	2.46	4.89	88	35.77	5.7	11
Light steel	0.2-0.23	43.7-58	6.82	1.36-1.57	--	--	20-32	40
Tool steel	0.20-0.22	14-50	7.8	1.56-1.72	--	--	4.8-8.0	11,40
Basalt yarn	0.52	53.6	2.8	1.45	83	29.6	1.8	41
Cellulose nanofibre yarn	0.08-0.6	--	1.38	0.11-0.83	3.5-65.7	2.5-47.6	2.5-24.9	42
Cellulose nanofibrils	--	55 (MJ/m ³)	--	1.015	55	--	8-10	43

3 Publications

Cellulose nanofibrils	1.05	17.1-27.4	1.5	1.57	86	57.3	4-5	44
Nylon 6,6	0.92	80.5	1.14	1.05	--	--	--	11
Polyester	0.84	50	1.38	1.16	2.5	1.18	--	11
PMMA yarn	0.02-0.07	0.4-16.9	1.18	0.02-0.08	0.6-1.8	1.52	5-29	45
PVDF yarn	0.01-0.11	34-98.6	1.87	0.202	0.28	0.15	124-740	46
This work	0.76-1.27	118-166	1.18	0.9-1.5	11.4-15.4	9.7-13.1	23-30	

Movie S1.

Animations of a volumetric image of the yarn with 4 wt% PEG-BA after stretching without annealing to a SR 8 at 160 °C, with virtual planes sliding through the volume.

Movie S2.

Animations of a volumetric image of the stretched yarn (SR 8) with 4 wt% PEG-BA annealed at 130 °C for 4 h, with virtual planes sliding through the volume.

Movie S3.

The stretched yarn (SR 8) with 4 wt% PEG-BA annealed at 130 °C for 4 h (length 2.2 cm, weight 0.0008 mg) holds repeatedly a total a total weight of 30 g while raising.

Movie S4.

Manual buttoning of a common button on a shirt with the stretched yarn (SR 8) with 4 wt% PEG-BA annealed at 130 °C for 4 h.

References and Notes

1. R. O. Ritchie, The conflicts between strength and toughness. *Nat. Mater.* **10**, 817–822 (2011). [doi:10.1038/nmat3115](https://doi.org/10.1038/nmat3115) [Medline](#)
2. M. F. Ashby, *Materials Selection in Mechanical Design*, (Butterworth & Heinemann, ed. 2, 1999).
3. D. C. Hofmann, J.-Y. Suh, A. Wiest, G. Duan, M.-L. Lind, M. D. Demetriou, W. L. Johnson, Designing metallic glass matrix composites with high toughness and tensile ductility. *Nature* **451**, 1085–1089 (2008). [doi:10.1038/nature06598](https://doi.org/10.1038/nature06598) [Medline](#)
4. H. Zhu, S. Zhu, Z. Jia, S. Parvinian, Y. Li, O. Vaaland, L. Hu, T. Li, Anomalous scaling law of strength and toughness of cellulose nanopaper. *Proc. Natl. Acad. Sci. U.S.A.* **112**, 8971–8976 (2015). [doi:10.1073/pnas.1502870112](https://doi.org/10.1073/pnas.1502870112) [Medline](#)
5. M. D. Demetriou, M. E. Launey, G. Garrett, J. P. Schramm, D. C. Hofmann, W. L. Johnson, R. O. Ritchie, A damage-tolerant glass. *Nat. Mater.* **10**, 123–128 (2011). [doi:10.1038/nmat2930](https://doi.org/10.1038/nmat2930) [Medline](#)
6. A. B. Dalton, S. Collins, E. Muñoz, J. M. Razal, V. H. Ebron, J. P. Ferraris, J. N. Coleman, B. G. Kim, R. H. Baughman, Super-tough carbon-nanotube fibres. *Nature* **423**, 703 (2003). [doi:10.1038/423703a](https://doi.org/10.1038/423703a) [Medline](#)
7. M. Naraghi, T. Filletter, A. Moravsky, M. Locascio, R. O. Loutfy, H. D. Espinosa, A multiscale study of high performance double-walled nanotube-polymer fibers. *ACS Nano* **4**, 6463–6476 (2010). [doi:10.1021/nn101404u](https://doi.org/10.1021/nn101404u) [Medline](#)
8. Z. Xu, Y. Liu, X. Zhao, L. Peng, H. Sun, Y. Xu, X. Ren, C. Jin, P. Xu, M. Wang, C. Gao, Ultrastiff and strong graphene fibers via full-scale synergetic defect engineering. *Adv. Mater.* **28**, 6449–6456 (2016). [doi:10.1002/adma.201506426](https://doi.org/10.1002/adma.201506426) [Medline](#)
9. J. Cai, M. Naraghi, Non-intertwined graphitic domains leads to super strong and tough continuous 1D nanostructures. *Carbon* **137**, 242–251 (2018). [doi:10.1016/j.carbon.2018.05.030](https://doi.org/10.1016/j.carbon.2018.05.030)
10. A. Arinstein, M. Burman, O. Gendelman, E. Zussman, Effect of supramolecular structure on polymer nanofibre elasticity. *Nat. Nanotechnol.* **2**, 59–62 (2007). [doi:10.1038/nnano.2006.172](https://doi.org/10.1038/nnano.2006.172) [Medline](#)
11. D. Papkov, Y. Zou, M. N. Andalib, A. Goponenko, S. Z. D. Cheng, Y. A. Dzenis, Simultaneously strong and tough ultrafine continuous nanofibers. *ACS Nano* **7**, 3324–3331 (2013). [doi:10.1021/nn400028p](https://doi.org/10.1021/nn400028p) [Medline](#)
12. Y. Ding, H. Hou, Y. Zhao, Z. Zhu, H. Fong, Electrospun polyimide nanofibers and their applications. *Prog. Polym. Sci.* **61**, 67–103 (2016). [doi:10.1016/j.progpolymsci.2016.06.006](https://doi.org/10.1016/j.progpolymsci.2016.06.006)
13. J. H. Park, G. C. Rutledge, Ultrafine high performance polyethylene fibers. *J. Mater. Sci.* **53**, 3049–3063 (2018). [doi:10.1007/s10853-017-1724-z](https://doi.org/10.1007/s10853-017-1724-z)
14. D. Papkov, N. Delpouve, L. Delbreilh, S. Araujo, T. Stockdale, S. Mamedov, K. Maleckis, Y. Zou, M. N. Andalib, E. Dargent, V. P. Dravid, M. V. Holt, C. Pellerin, Y. A. Dzenis, Quantifying polymer chain orientation in strong and tough nanofibers with low

- crystallinity: Toward next generation nanostructured superfibers. *ACS Nano* **13**, 4893–4927 (2019). [doi:10.1021/acsnano.8b08725](https://doi.org/10.1021/acsnano.8b08725) [Medline](#)
15. D. A. Tirrell, Putting a new spin on spider silk. *Science* **271**, 39–40 (1996). [doi:10.1126/science.271.5245.39](https://doi.org/10.1126/science.271.5245.39) [Medline](#)
16. F. Vollrath, D. P. Knight, Liquid crystalline spinning of spider silk. *Nature* **410**, 541–548 (2001). [doi:10.1038/35069000](https://doi.org/10.1038/35069000) [Medline](#)
17. K. Spiess, A. Lammel, T. Scheibel, Recombinant spider silk proteins for applications in biomaterials. *Macromol. Biosci.* **10**, 998–1007 (2010). [doi:10.1002/mabi.201000071](https://doi.org/10.1002/mabi.201000071) [Medline](#)
18. Z. P. Demko, K. B. Sharpless, A click chemistry approach to tetrazoles by Huisgen 1,3-dipolar cycloaddition: Synthesis of 5-acyltetrazoles from azides and acyl cyanides. *Angew. Chem. Int. Ed.* **41**, 2113–2116 (2002). [doi:10.1002/1521-3773\(20020617\)41:12<2113::AID-ANIE2113>3.0.CO;2-Q](https://doi.org/10.1002/1521-3773(20020617)41:12<2113::AID-ANIE2113>3.0.CO;2-Q) [Medline](#)
19. N. Yusof, A. F. Ismail, Post spinning and pyrolysis processes of polyacrylonitrile (PAN)-based carbon fiber and activated carbon fiber: A review. *J. Anal. Appl. Pyrolysis* **93**, 1–13 (2012). [doi:10.1016/j.jaap.2011.10.001](https://doi.org/10.1016/j.jaap.2011.10.001)
20. For details of calculation, see supplementary materials.
21. T. Shen, C. Li, B. Haley, S. Desai, A. Strachan, Crystalline and pseudo-crystalline phases of polyacrylonitrile from molecular dynamics: Implications for carbon fiber precursors. *Polymer* **155**, 13–26 (2018). [doi:10.1016/j.polymer.2018.09.026](https://doi.org/10.1016/j.polymer.2018.09.026)
22. Q. Ouyang, Y. Chen, N. Zhang, G. Mo, D. Li, Q. Yan, Effect of jet swell and jet stretch on the structure of wet-spun polyacrylonitrile fiber. *J. Macromol. Sci. B* **50**, 2417–2427 (2011). [doi:10.1080/00222348.2011.564104](https://doi.org/10.1080/00222348.2011.564104)
23. H. R. Brown, A molecular interpretation of the toughness of glassy polymers. *Macromolecules* **24**, 2752–2756 (1991). [doi:10.1021/ma00010a018](https://doi.org/10.1021/ma00010a018)
24. H. H. Kausch, C. J. G. Plummer, The role of individual chains in polymer deformation. *Polymer (Guildf.)* **35**, 3848–3857 (1994). [doi:10.1016/0032-3861\(94\)90267-4](https://doi.org/10.1016/0032-3861(94)90267-4)
25. D. Zhu, X. Zhang, Y. Ou, M. Huang, Experimental and numerical study of multi-scale tensile behaviors of Kevlar[®] 49 fabric. *J. Compos. Mater.* **51**, 2449–2465 (2016). [doi:10.1177/0021998316671573](https://doi.org/10.1177/0021998316671573) 26. Z. Xie, H. Niu, T. Lin, Continuous polyacrylonitrile nanofiber yarns: Preparation and dry-drawing treatment for carbon nanofiber production. *RSC Advances* **5**, 15147–15153 (2015). [doi:10.1039/C4RA16247A](https://doi.org/10.1039/C4RA16247A)
27. R. Dersch, T. Liu, A. K. Schaper, A. Greiner, J. H. Wendorff, Electrospun nanofibers: Internal structure and intrinsic orientation. *J. Polym. Sci. Part A* **41**, 545–553 (2003). [doi:10.1002/pola.10609](https://doi.org/10.1002/pola.10609)
28. J. M. Citra, D. B. Chase, R. M. Ikeda, K. H. Gardner, Molecular orientation of high-density polyethylene fibers characterized by polarized Raman spectroscopy. *Macromolecules* **28**, 4007–4012 (1995). [doi:10.1021/ma00115a037](https://doi.org/10.1021/ma00115a037)

29. J. Wu, N. Mao, L. Xie, H. Xu, J. Zhang, Identifying the crystalline orientation of black phosphorus using angle-resolved polarized Raman spectroscopy. *Angew. Chem. Int. Ed.* **54**, 2366–2369 (2015). [doi:10.1002/anie.201410108](https://doi.org/10.1002/anie.201410108) [Medline](#)
30. B. Madsen, Z. Z. Shao, F. Vollrath, Variability in the mechanical properties of spider silks on three levels: Interspecific, intraspecific and intraindividual. *Int. J. Biol. Macromol.* **24**, 301–306 (1999). [doi:10.1016/S0141-8130\(98\)00094-4](https://doi.org/10.1016/S0141-8130(98)00094-4) [Medline](#)
31. F. Vollrath, B. Madsen, Z. Shao, The effect of spinning conditions on the mechanics of a spider's dragline silk. *Proc. R. Soc. London Ser. B* **268**, 2339–2346 (2001). [doi:10.1098/rspb.2001.1590](https://doi.org/10.1098/rspb.2001.1590) [Medline](#)
32. M. Zhang, K. R. Atkinson, R. H. Baughman, Multifunctional carbon nanotube yarns by downsizing an ancient technology. *Science* **306**, 1358–1361 (2004). [doi:10.1126/science.1104276](https://doi.org/10.1126/science.1104276) [Medline](#)
33. P. Miaudet, S. Badaire, M. Maugey, A. Derré, V. Pichot, P. Launois, P. Poulin, C. Zakri, Hot-drawing of single and multiwall carbon nanotube fibers for high toughness and alignment. *Nano Lett.* **5**, 2212–2215 (2005). [doi:10.1021/nl051419w](https://doi.org/10.1021/nl051419w) [Medline](#)
34. M. Motta, A. Moiala, I. A. Kinloch, A. H. Windle, High performance fibres from 'Dog Bone' carbon nanotubes. *Adv. Mater.* **19**, 3721–3726 (2007). [doi:10.1002/adma.200700516](https://doi.org/10.1002/adma.200700516)
35. M. K. Shin, B. Lee, S. H. Kim, J. A. Lee, G. M. Spinks, S. Gambhir, G. G. Wallace, M. E. Kozlov, R. H. Baughman, S. J. Kim, Synergistic toughening of composite fibres by self-alignment of reduced graphene oxide and carbon nanotubes. *Nat. Commun.* **3**, 650 (2012). [doi:10.1038/ncomms1661](https://doi.org/10.1038/ncomms1661) [Medline](#)
36. Z. Xu, H. Sun, X. Zhao, C. Gao, Ultrastrong fibers assembled from giant graphene oxide sheets. *Adv. Mater.* **25**, 188–193 (2013). [doi:10.1002/adma.201203448](https://doi.org/10.1002/adma.201203448) [Medline](#)
37. X. Xiang, Z. Yang, J. Di, W. Zhang, R. Li, L. Kang, Y. Zhang, H. Zhang, Q. Li, In situ twisting for stabilizing and toughening conductive graphene yarns. *Nanoscale* **9**, 11523–11529 (2017). [doi:10.1039/C7NR03305B](https://doi.org/10.1039/C7NR03305B) [Medline](#)
38. F. X. Kromm, T. Lorriot, B. Coutand, R. Harry, J. M. Quenisset, Tensile and creep properties of ultra high molecular weight PE fibres. *Polym. Test.* **22**, 463–470 (2003). [doi:10.1016/S0142-9418\(02\)00127-7](https://doi.org/10.1016/S0142-9418(02)00127-7)
39. I. O'Connor, H. Hayden, J. N. Coleman, Y. K. Gun'ko, High-strength, high-toughness composite fibers by swelling Kevlar in nanotube suspensions. *Small* **5**, 466–469 (2009). [doi:10.1002/sml.200801102](https://doi.org/10.1002/sml.200801102) [Medline](#)
40. S. H. Kim, H. Kim, N. J. Kim, Brittle intermetallic compound makes ultrastrong low-density steel with large ductility. *Nature* **518**, 77–79 (2015). [doi:10.1038/nature14144](https://doi.org/10.1038/nature14144) [Medline](#)
41. Y. Ou, D. Zhu, H. Li, Strain rate and temperature effects on the dynamic tensile behaviors of basalt fiber bundles and reinforced polymer composite. *J. Mater. Civ. Eng.* **28**, 04016101 (2016). [doi:10.1061/\(ASCE\)MT.1943-5533.0001615](https://doi.org/10.1061/(ASCE)MT.1943-5533.0001615)
42. S. Wang, F. Jiang, X. Xu, Y. Kuang, K. Fu, E. Hitz, L. Hu, Super-strong, super-stiff macrofibers with aligned, long bacterial cellulose nanofibers. *Adv. Mater.* **29**, 1702498 (2017). [doi:10.1002/adma.201702498](https://doi.org/10.1002/adma.201702498) [Medline](#)

43. N. Mittal, R. Jansson, M. Widhe, T. Benselfelt, K. M. O. Håkansson, F. Lundell, M. Hedhammar, L. D. Söderberg, Ultrastrong and bioactive nanostructured bio-based composites. *ACS Nano* **11**, 5148–5159 (2017). [doi:10.1021/acsnano.7b02305](https://doi.org/10.1021/acsnano.7b02305) [Medline](#)
44. N. Mittal, F. Ansari, V.K. Gowda, C. Brouzet, P. Chen, P. T. Larsson, S. V. Roth, F. Lundell, L. Wågberg, N. A. Kotov, L. D. Söderberg, Multiscale control of nanocellulose assembly: Transferring remarkable nanoscale fibril mechanics to macroscale fibers. *ACS Nano* **12**, 6378–6388 (2018). [doi:10.1021/acsnano.8b01084](https://doi.org/10.1021/acsnano.8b01084) [Medline](#)
45. X. Sui, E. Wiesel, H. D. Wagner, Mechanical properties of electrospun PMMA micro-yarns: Effects of NaCl mediation and yarn twist. *Polymer (Guildf.)* **53**, 5037–5044 (2012). [doi:10.1016/j.polymer.2012.08.062](https://doi.org/10.1016/j.polymer.2012.08.062)
46. M. Baniasadi, J. Huang, Z. Xu, S. Moreno, X. Yang, J. Chang, M. A. Quevedo-Lopez, M. Naraghi, M. Minary-Jolandan, High-performance coils and yarns of polymeric piezoelectric nanofibers. *ACS Appl. Mater. Interfaces* **7**, 5358–5366 (2015). [doi:10.1021/am508812a](https://doi.org/10.1021/am508812a) [Medline](#)

3.2 Impact of the Fiber Length Distribution on Porous Sponges Originating from Short Electrospun Fibers Made from Polymer Yarn

Xiaojian Liao, Pin Hu, Seema Agarwal, Andreas Greiner, Impact of the Fiber Length Distribution on Porous Sponges Originating from Short Electrospun Fibers Made from Polymer Yarn, *Macromolecular Materials and Engineering*, **2020**, 1900629.

Impact of the Fiber Length Distribution on Porous Sponges Originating from Short Electrospun Fibers Made from Polymer Yarn

Xiaojian Liao, Pin Hu, Seema Agarwal, and Andreas Greiner*

Ultralight highly porous sponges made of short electrospun polymer fibers have gained significant attention for a variety of applications. According to the established procedures, short electrospun fibers are obtained by cutting or homogenization of electrospun fibers in suspension, which yield fibers with inhomogeneous fiber length. The role of the fiber length distribution and the fiber length in the mechanical compressibility of the sponges is unknown. Therefore, as a model study, sponges made from suspensions of short electrospun poly(acrylonitrile) (PAN) fibers with controlled fiber length distribution are investigated, and the role of the fiber length distribution in the compressibility of the sponges is analyzed quantitatively. These sponges are also compared to the ones prepared by established procedure as a benchmark. It is found that the compression stress and modulus of ultralight sponges with monodisperse short fibers are respectively 32% and 45% higher than that made with polydisperse short fibers. The study also shows that sponges made from longer fibers have higher modulus in comparison to the sponges made from shorter fibers.

1. Introduction

Ultralight porous 3D materials, with unique integral properties of ultralow density,^[1,2] low thermal conductivity,^[3–5] high porosity,^[6,7] and good mechanical properties,^[8,9] exhibit a large range of applications as absorption materials, in thermal insulation, electronic equipment, as scaffolds for tissue engineering, and stimuli-responsive materials.^[10–13] Traditional inorganic aerogels, however, normally suffer from mechanical brittleness originating from rigid intrinsic quality of inorganic materials, which restricts their applications.^[11,14] The carbon aerogels based on carbon nanotube and graphene were considered as the promising elastic porous 3D materials. Unfortunately, the high-cost precursors hinder their practical applications.^[11,15]

X. Liao, P. Hu, Prof. S. Agarwal, Prof. A. Greiner
Macromolecular Chemistry and Bavarian Polymer Institute
University of Bayreuth
95440 Bayreuth, Germany
E-mail: greiner@uni-bayreuth.de

 The ORCID identification number(s) for the author(s) of this article can be found under <https://doi.org/10.1002/mame.201900629>.

© 2020 The Authors. Published by WILEY-VCH Verlag GmbH & Co. KGaA, Weinheim. This is an open access article under the terms of the Creative Commons Attribution License, which permits use, distribution and reproduction in any medium, provided the original work is properly cited.

DOI: 10.1002/mame.201900629

Recently, the potential of electrospun fibers was reported for the fabrication of novel electrospun fibrous sponges by the use of short electrospun fibers.^[4,6,14,16] Owing to flexible fabrication conditions and diversified electrospun fibers, the sponges displayed tunable densities, multifunctionality, and applicability for various applications, for instance, reversible manual compression,^[16] hydrophilic or super hydrophobic,^[17,18] electronics,^[19,20] respirable open cells,^[21] or scaffolds for tissue engineering.^[22,23] Thus, these sponges could perfectly overcome the mechanical brittleness of traditional inorganic aerogel and high cost of carbon aerogel problems, making them a perfect candidate for broad applications due to their high potential for functionalization.

So far, almost all the concepts to obtain ultralight sponges consist of fabrication of short electrospun fiber suspensions by mechanical cutting and processing by self-assembly, followed by freeze-drying.^[10] Normally, the short fibers obtained by using mechanical cutting devices, such as homogenizer, mixer, blender, grinder, exhibit uncontrollable length and broad length distribution represented by the high coefficient of variation (CV),^[3,24–26] which is defined as the ratio of the standard deviation to the mean length. Simultaneously, beyond several different reported methods, such as chemical treatment,^[27] ultrasonication,^[28] electric spark,^[29] concentrated polymer brush,^[30] and direct electrospinning,^[31–33] the patterned UV-crosslinking^[34] and microcutting method^[35,36] based on highly aligned fibers enable the production of quasi-monodisperse short fibers. Short fiber dispersions with low CV have not been used to the best of our knowledge for the preparation of sponges. Consequently, the role of CV and fiber length in the morphology and mechanical properties of the sponges is unknown, which is, however, very important for basic understanding and numerous applications.

Herein, we present a new method for the preparation of short electrospun fiber dispersions with controlled CV and use them for the preparation of the sponges in order to evaluate the microstructure and mechanical properties. We show the cryo-microcutting of multifibrillar highly oriented electrospun poly(acrylonitrile) (PAN) yarns which resulted finally in short individual PAN fibers of well-controlled length. Fiber dispersions of different CVs were obtained by mixing of short fibers of different lengths, which were used for the preparation of sponges following the established method. We could clearly

quantify the role of the fiber length distribution in the morphology and compression strength of sponges, which will be presented in detail in the following sections.

2. Experimental Section

2.1. Materials

PAN (M_n 120 000, co-polymer with 6 wt% methyl acrylate, Dolan), polyurethane (PU) synthesized in the authors' group according to the previous report (sample no. 8 in Lit.^[37] M_n of 50 000), dimethylformamide (DMF; Fisher Chemical, 99.99%), dimethylsulfoxide (DMSO; Fisher Chemical, 99.99%), dioxane (technical grade), ethanol (technical grade), and acetone (technical grade) were used as received.

2.2. Fabrication of High Aligned Electrospun Fibrillar Yarn

The electrospun fibrillar yarns were fabricated following with some modifications a previously published procedure.^[38] The solution for electrospinning was prepared by dissolving about 1 g of PAN powder in a mixed solvent of 4.7 g of DMF and 0.97 g of acetone. As shown in the **Figure 1**, the angle (13 degrees of inclination), distance (40 cm) and altitude (perpendicular distance to the plane of the end of funnel: 2 cm) of two syringes were fixed in the homemade syringe holder set-ups. The feed rate of solution was about 0.5 mL h^{-1} . The two needle tips of syringe were connected separately to the positive and negative electrodes of DC power supplies, respectively. After turning on the high voltages, firstly, two oppositely charged fibrils flew to the end of the funnel with 1500 rpm rotation speed and a fiber membrane would be formed. Followed by switching on the winder collector of 13 rpm rotation speed, the membrane was dragged by a pre-suspended yarn connected with the winder collector. Then a rotodynamic fibrillar cone could be formed above the funnel. Simultaneously, fibers on the fibrillar cone were

pulled up in a spiral path. The whole electrospun yarn process was operated under the light of an infrared lamp (250 W) at about $45 \text{ }^\circ\text{C}$ and with about 10–15% of humidity.

The subsequent stretching processes were performed by a homemade roll-to-roll heat-stretching instrument consisting of three parts: a tubular furnace with one heat position zone (Heraeus, D6450 Hanau, Typ: RE 1.1, 400 mm in length, Germany), two rollers with electronic motors, and a laptop with "LV2016" controlling software for controlling the velocities of the motors. By adjusting the velocities of the two rollers by the LV2016 software, the yarn could be stretched continuously. The stretch ratio (SR) was calculated by the equation: $\text{SR} = v_f/v_s$, where v_f and v_s represent the velocities of fast roller and slow roller, respectively.

2.3. Fabrication of Uniform Short Fibers from Yarns

First, the yarn was wound into an aligned yarn bundle, which was immersed in ethanol and water for 5 min each, respectively, followed by freezing in liquid nitrogen and cutting into a fixed length (0.4 mm or 1.0 mm) by a homemade cutting tool (Figure S1, Supporting Information). The obtained short segments of yarn were dispersed in dioxane (0.5 mg mL^{-1}). A dispersion of short individual fibers of uniform length were obtained after sonification (sonorex super AK 514 BH, working at 35 kHz, HF powder: 215 W eff). This dispersion was freeze-dried for 48 h, which resulted in powder-like fibers. For comparison, 1 g of the stretched yarn was cut in cooled dioxane (1 L) by a mixer (Robot Coupe Blixer 4, Rudolf Lange GmbH & Co. KG) at 4000 rpm for several minutes until it became short fibers. After that, the poly-disperse short fibers were obtained by freeze-drying for 48 h.

2.4. Fabrication of Sponges

In a typical experiment for the preparation of sponges with a density of about 7 mg cm^{-3} , firstly, 3 mg of PU was dissolved

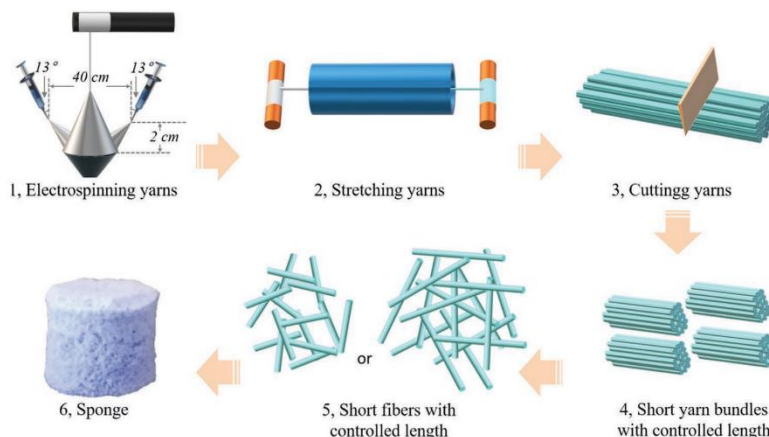


Figure 1. Schematic illustration of the fabrication process of sponge from short fibers with controlled length.

in 2.5 mL of dioxane, then 12 mg of short fibers were blended with the PU/dioxane solution. The obtained uniform dispersion was slowly cooled to $-20\text{ }^{\circ}\text{C}$, followed by freeze-drying for 48 h under 0.04 mbar. Finally, the sponges were annealed at $110\text{ }^{\circ}\text{C}$ for 2 h. The density of sponges was equal to the weight of sponge divided by the volume determination using radius and height of the cylindrical samples ($\pi r^2 h$). The sponges made of short fibers of controlled CV were obtained by mixing short fibers of 1.0 mm length and 0.4 mm length.

2.5. Characterization

Digital microscope (Smartzoom 5, Carl Zeiss AG) was used to observe the short fibers. The morphology of fibers, yarns, and sponges was studied by a Zeiss LEO 1530 (Gemini, Germany) scanning electron microscope (SEM). ImageJ software was used to measure the length of short fibers and the diameter of fibers and yarns based on an average of 100 fibers. According to a previous literature,^[9] the fiber alignment factors were calculated based on the equation: $d_{Fa} = (3\cos 2\theta - 1) / 2$, where d_{Fa} is the fiber alignment factor and θ is the angle between the individual fibers and direction of the yarns. The given values were measured by ImageJ software based on an average of 100 fibers. Recycle loading–unloading compression tests were performed by zwickiLine Z0.5, BT1-FR0.5TN.D14, Zwick/Roell, Germany material tester, using a crosshead rate of 10 mm min^{-1} in air at room temperature. The load cell was a Zwick/Roell KAF TC with a nominal load of 20 N

3. Results and Discussion

The overall concept for the preparation of sponges with fibers of different lengths and fiber length distribution is shown in Figure 1. Following this concept, electrospun PAN yarns (diameter = $130 \pm 22\text{ }\mu\text{m}$) consisting of about 3000 unaligned individual fibers (diameter = $1.19 \pm 0.08\text{ }\mu\text{m}$) were obtained by continuous yarn electrospinning, followed by roll-to-roll heat stretching at $160\text{ }^{\circ}\text{C}$ and alignment of the fibers (diameter = $0.51 \pm 0.09\text{ }\mu\text{m}$, alignment factor = 99% at a stretch ratio of 6). The as-spun yarn showed random deposition of fibers. The alignment of the fibers in the yarn upon heat stretching was dependent upon the stretch ratio. The alignment factor for fibers changed from $\approx 48\%$ at stretch ratio 1 to about 99% at stretch ratio 6. The high degree of fiber alignment was important for getting short fibers with narrow length distribution on cutting.

Short fibers of two different lengths (416 ± 83 and $1034 \pm 156\text{ }\mu\text{m}$) were obtained by cryo-microcutting of the stretched yarns (Figure 2; Table S1, Supporting Information) in liquid nitrogen with a specially designed cutter (Figure S1, Supporting Information) and followed by ultrasonication in dioxane.

Notably, these short fibers exhibit tunable aspect ratio and narrow fiber length distribution, represented by the low CV values 15.1% and 20.0%, respectively (Figure 2; Figure S2 and Table S1, Supporting Information). Furthermore, the control experiment of making short fibers by mechanical cutting in a mixer, show fibers with uncontrollable length (average length

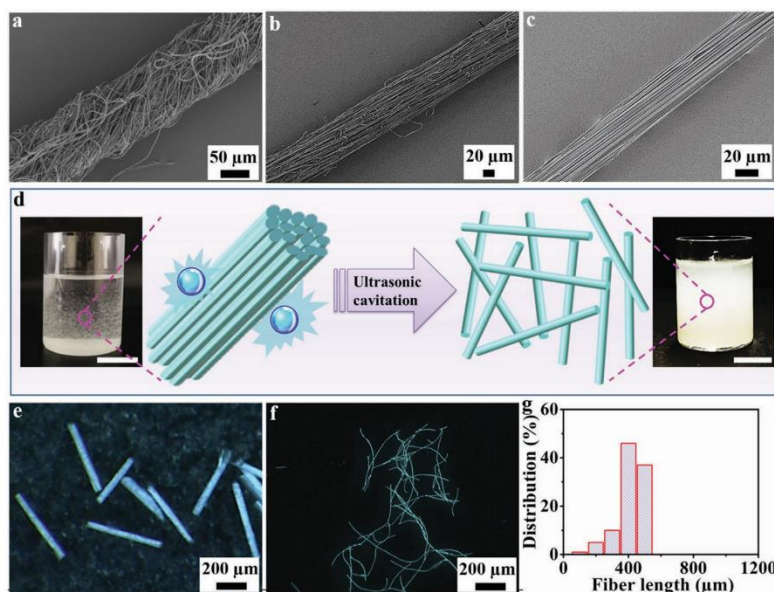


Figure 2. Microstructure and properties of yarns and fibers. SEM images of yarns with different stretch ratios: a) as-spun yarn, b) SR 3, and c) SR 6. d) Schematic representation of the ultrasonic cavitation process to produce individual fibers from short yarns. The inset digital pictures are dispersion of short yarns with 0.4 mm length (left) and corresponding dispersion of short fibers (right) in dioxane. The inset scale bar in the picture is 15 mm. Microscope pictures of: e) short yarns and f) fibers at 0.4 mm length. g) Fiber length distribution of short fibers made from cutter 0.4 mm.

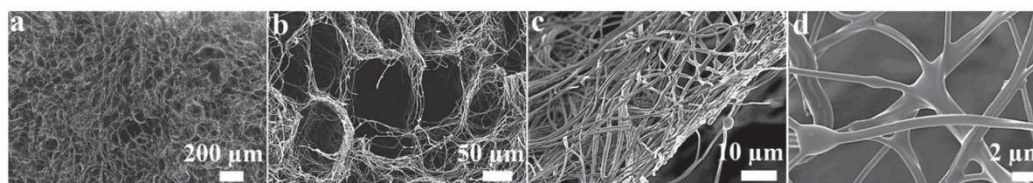


Figure 3. Cross-sectional SEM images of sponge made from short fibers of average length $416 \pm 83 \mu\text{m}$ in different magnifications. a) The whole cross-sectional image, b) the pore microstructure, c) the wall of pore, d) the glued individual fibers.

of $145 \pm 129 \mu\text{m}$) and broad length distribution with high CV of 89.0% (Figure S3 and Table S1, Supporting Information).

Short nanofibers (lengths 416 ± 83 and $1034 \pm 156 \mu\text{m}$) were dispersed in a dioxane solution of PU^[37] in different amounts for the preparation of the sponges. The addition of the particular PU was important due to its solubility in dioxane and its stickiness, which was required for binding of the fibers in the sponge. Different formulations made by dispersing short fibers and PU in dioxane were assembled into 3D porous sponges by freeze-drying process. **Figure 3** shows the typical cross-sectional SEM images of a sponge (density of $\approx 7.0 \text{ mg cm}^{-3}$) made from short fibers of average length $416 \pm 83 \mu\text{m}$. The sponge showed dual pore-structure with small (pores between the fibers) and big pores (pore size of about $112 \pm 18.3 \mu\text{m}$ formed by sublimation of ice during freeze-drying). The sponge had open-cellular structure with highly interconnected pores through triangular or quadrangle junctions. Unique fibrous cell walls (big pore walls) consist of small pores between the fibers created by overlaying of the individual fibers in a regular, usual criss-cross pattern. Simultaneously, the PU as glue, assembled on the surface of fibers, which could induce further physical gluing and reinforce the mechanical properties of sponges.

In order to understand the role of the fiber length and its CV in the pore size, pore morphology, and compression strength of the sponges were compared (Figures 4 and 5; Table S2, Supporting Information). The cross-sectional SEM images of the sponges showed the typical disordered open-cellular structures. All sponges showed similar average visual pore sizes in the range of 112–118 μm as shown in the Figure 4. Thus, it

suggested that the length and length distribution of short fibers hardly affect the pore size of sponges. Compression test was done for 100 cycles of loading–unloading at maximum strain of 50% (Figure 5; Figure S4, Supporting Information). Sponges with low CV showed enhancement in stress by 32% and in modulus by 45%, in comparison to sponges with high CV. Moreover, the longer fibers (1.0 mm length) could endow the sponge with higher modulus than the shorter fibers (0.4 mm length) (Figure 5a,b). The energy loss coefficient became almost constant after first compression cycle showing the work done in compression and the energy loss remained the same in each cycle (Figure 5c). Similar behaviors were described for low density carbon–graphene monolith materials^[9] and for electrospun nanofiber aerogels.^[16]

4. Conclusions

Cryo-microcutting of multifibrillar electrospun fibrillar yarns results in short fibers of well-controlled length. Dispersion of short fibers with well-controlled fiber length distribution was obtained by mixing of short fibers of different lengths in dispersion. Sponges obtained from these dispersions by freeze-drying showed similar pore size and pore size distribution, but significantly higher compression strength and modulus for sponges with low CV. Sponges with low CV showed clearly higher compression strength and modulus. From this, we postulate that the mechanical properties of sponges could be tailored over a wide range by adjustment of fiber length which provides an additional

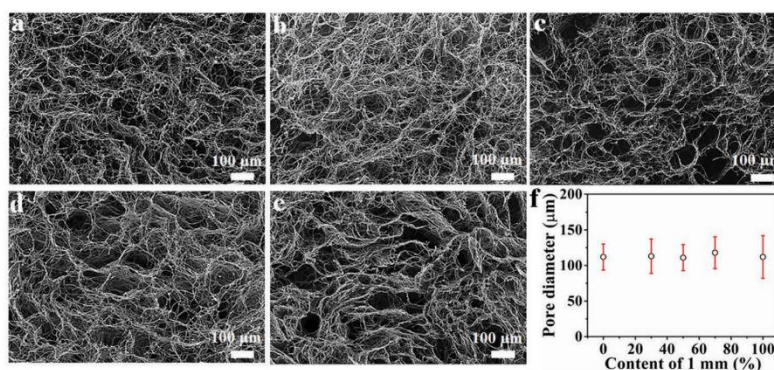


Figure 4. Microstructure of sponges. SEM cross-sectional images of sponges with different weight contents of 1 mm length short fibers: a) 0%, b) 30%, c) 50%, d) 70%, and e) 100%. f) Change of pore size in the sponge with different contents of 1 mm short fibers.

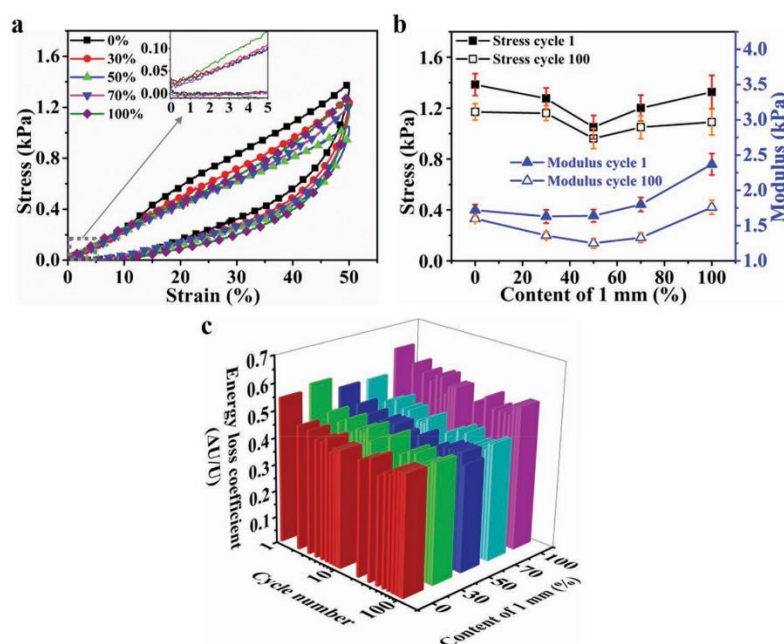


Figure 5. Microstructure and mechanical properties of sponges. a) Compression stress versus strain curves in compression test of sponges with different contents of 0.4 and 1.0 mm length short fibers. b) Changes of stress and modulus of sponges with different contents of 0.4 and 1 mm length short fibers during first and 100th cycle loading–unloading compression test. c) Changes of energy loss coefficient of the sponges with different contents of 0.4 and 1 mm length short fibers during 100 cycles compression test.

tool for tuning of sponge properties next to chemical treatments. Tailored mechanical properties will be of utmost importance for application of sponges, for example, in tissue engineering, sensors, electrodes, insulation materials, and textiles.

Received: September 19, 2019
Revised: November 3, 2019
Published online:

Supporting Information

Supporting Information is available from the Wiley Online Library or from the author.

Acknowledgements

The authors acknowledge DFG (SFB 840) for financial support. The authors thank Peter Schmidt, Thomas Braun, and their co-workers in the workshops for help, design and building of the electrospun yarn setup, roll-to-roll stretching device, and cutting tool.

Conflict of Interest

The authors declare no conflict of interest.

Keywords

electrospinning, fiber lengths, mechanical properties, sponges, yarns

- [1] S. S. Kistler, *Nature* **1931**, 127, 741.
- [2] A. Träger, A. Carlmark, L. Wågberg, *Macromol. Mater. Eng.* **2018**, *303*, 1700594.
- [3] S. Jiang, B. Uch, S. Agarwal, A. Greiner, *ACS Appl. Mater. Interfaces* **2017**, *9*, 32308.
- [4] J. Zhu, S. Jiang, H. Hou, S. Agarwal, A. Greiner, *Macromol. Mater. Eng.* **2018**, *303*, 1700615.
- [5] Y. Xiao, L. Li, S. Zhang, J. Feng, Y. Jiang, J. Feng, *Macromol. Mater. Eng.* **2019**, *304*, 1900137.
- [6] G. Hayase, K. Kanamori, G. Hasegawa, A. Maeno, H. Kaji, K. Nakanishi, *Angew. Chem., Int. Ed.* **2013**, *52*, 10788.
- [7] H. Sehaqui, Q. Zhou, L. A. Berglund, *Compos. Sci. Technol.* **2011**, *71*, 1593.
- [8] G. Duan, S. Jiang, V. Jérôme, J. H. Wendorff, A. Fathi, J. Uhm, V. Altstadt, M. Herling, J. Breu, R. Freitag, S. Agarwal, A. Greiner, *Adv. Funct. Mater.* **2015**, *25*, 2850.
- [9] H. Gao, Y. Zhu, L. Mao, F. Wang, X. Luo, Y. Liu, Y. Lu, Z. Pan, J. Ge, W. Shen, Y. Zheng, L. Xu, L. Wang, W. Xu, H. Wu, S. Yu, *Nat. Commun.* **2016**, *7*, 12920.
- [10] S. Jiang, S. Agarwal, A. Greiner, *Angew. Chem., Int. Ed.* **2017**, *56*, 15520.
- [11] Z. Qian, Z. Wang, N. Zhao, J. Xu, *Macromol. Rapid Commun.* **2018**, *39*, 1700724.



- [12] D. Lv, M. Zhu, Z. Jiang, S. Jiang, Q. Zhang, R. Xiong, C. Huang, *Macromol. Mater. Eng.* **2018**, *303*, 1800336.
- [13] S. Agarwal, S. Jiang, Y. Chen, *Macromol. Mater. Eng.* **2019**, *304*, 1800548.
- [14] S. S. Kistler, *J. Phys. Chem.* **1932**, *36*, 52.
- [15] H. Sun, Z. Xu, C. Gao, *Adv. Mater.* **2013**, *25*, 2554.
- [16] Y. Si, J. Yu, X. Tang, J. Ge, B. Ding, *Nat. Commun.* **2014**, *5*, 5802.
- [17] G. Duan, S. Jiang, T. Moss, S. Agarwal, A. Greiner, *Polym. Chem.* **2016**, *7*, 2759.
- [18] S. Jiang, N. Helfricht, G. Papastavrou, A. Greiner, S. Agarwal, *Macromol. Rapid Commun.* **2018**, *39*, 1700838.
- [19] T. Xu, Y. Ding, Z. Wang, Y. Zhao, W. Wu, H. Fong, Z. Zhu, *J. Mater. Chem. C* **2017**, *5*, 10288.
- [20] S. Jiang, S. Reich, B. Uch, P. Hu, S. Agarwal, A. Greiner, *ACS Appl. Mater. Interfaces* **2017**, *9*, 34286.
- [21] S. Jiang, V. Gruen, S. Rosenfeldt, A. S. Schenk, S. Agarwal, Z. Xu, A. Greiner, *Research* **2019**, *2019*, 1.
- [22] T. Xu, J. M. Miszuk, Y. Zhao, H. Sun, H. Fong, *Adv. Healthcare Mater.* **2015**, *4*, 2238.
- [23] M. Mader, V. Jerome, R. Freitag, S. Agarwal, A. Greiner, *Biomacromolecules* **2018**, *19*, 1663.
- [24] S. Jiang, G. Duan, J. Schöbel, S. Agarwal, A. Greiner, *Compos. Sci. Technol.* **2013**, *88*, 57.
- [25] W. Chen, J. Ma, L. Zhu, Y. Morsi, S. S. Al-Deyab, X. Mo, *Colloids Surf., B* **2016**, *142*, 165.
- [26] T. Xu, Z. Wang, Y. Ding, W. Xu, W. Wu, Z. Zhu, H. Fong, *Carbohydr. Polym.* **2018**, *179*, 164.
- [27] T. G. Kim, T. G. Park, *Macromol. Rapid Commun.* **2008**, *29*, 1231.
- [28] M. Sawawi, T. Y. Wang, D. R. Nisbet, G. P. Simon, *Polymer* **2013**, *54*, 4237.
- [29] I. W. Fathona, A. Yabuki, *J. Mater. Process. Technol.* **2013**, *213*, 1894.
- [30] C. F. Huang, C. Yoshikawa, K. Zhang, S. Hattori, T. Honda, E. Zawadzak, H. Kobayashi, *Adv. Mater. Res.* **2011**, *306-307*, 58.
- [31] I. W. Fathona, A. Yabuki, *J. Mater. Sci.* **2014**, *49*, 3519.
- [32] C. J. Luo, E. Stride, S. Stoyanov, E. Pelan, M. J. Edirisinghe, *J. Polym. Res.* **2011**, *18*, 2515.
- [33] S. Mahalingam, M. Edirisinghe, *Macromol. Rapid Commun.* **2013**, *34*, 1134.
- [34] A. Stoilkovic, S. Agarwal, *Macromol. Mater. Eng.* **2008**, *293*, 895.
- [35] A. Omidinia-Anarkoli, S. Boesveld, U. Tuvshindorj, J. C. Rose, T. Haraszti, L. De Laporte, *Small* **2017**, *13*, 1702207.
- [36] K. J. Lee, J. Yoon, S. Rahmani, S. Hwang, S. Bhaskar, S. Mitragotri, J. Lahann, *Proc. Natl. Acad. Sci. USA* **2012**, *109*, 16057.
- [37] P. Hu, A. Greiner, S. Agarwal, *J. Polym. Sci., Part A-1: Polym. Chem.* **2019**, *57*, 752.
- [38] X. Liao, M. Dulle, J. Martins de Souza Silva, R. B. Wehrspohn, S. Agarwal, S. Förster, H. Hou, P. Smith, A. Greiner, *Science* **2019**, *366*, 1376.
- [39] R. Dersch, T. Liu, A. K. Schaper, A. Greiner, J. H. Wendorff, *J. Polym. Sci., Part A-1: Polym. Chem.* **2003**, *41*, 545.

Copyright WILEY-VCH Verlag GmbH & Co. KGaA, 69469 Weinheim, Germany, 2020.



Supporting Information

for *Macromol. Mater. Eng.*, DOI: 10.1002/mame.201900629

**Impact of the Fiber Length Distribution on Porous Sponges
Originating from Short Electrospun Fibers Made from
Polymer Yarn**

Xiaojian Liao, Pin Hu, Seema Agarwal, and Andreas Greiner*

Xiaojian Liao, Pin Hu, Seema Agarwal and Andreas Greiner*

Copyright WILEY-VCH Verlag GmbH & Co. KGaA, 69469 Weinheim, Germany, 2019.

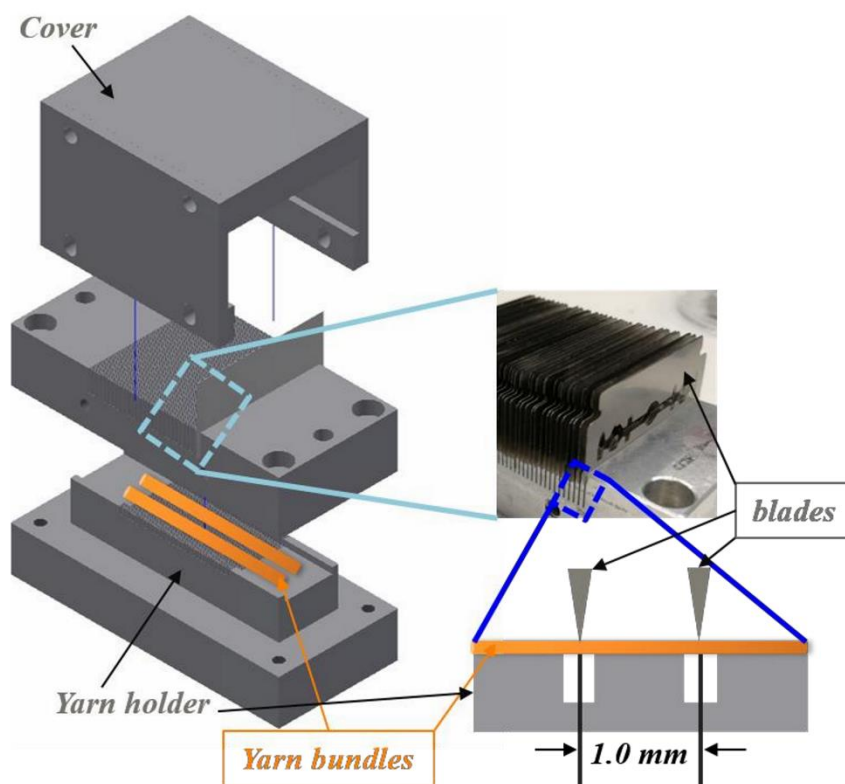
Supporting Information

The Supporting Information is available free of charge on the Wiley Online Library website at

DOI: 10.1002/mame.2019#####

Impact of the fiber length distribution on ultraporous sponges originating from short electrospun fibers made from polymer yarn

Xiaojian Liao, Pin Hu, Seema Agarwal and Andreas Greiner*



1

Figure S1. Schematic illustration of the home-made cutter with optional interval length of two blades.

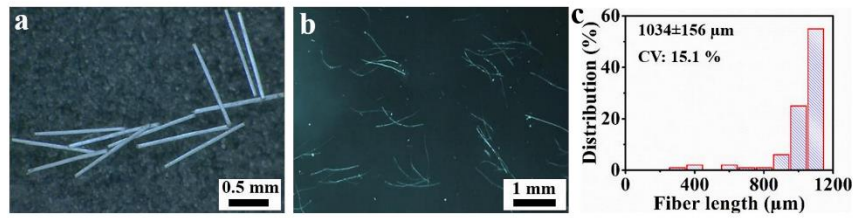


Figure S2. a and b, Microscope images of short yarns (a) and fibers (b) made from cutter 1.0, respectively. c, Fiber length distribution of short fibers made from cutter 1.0.

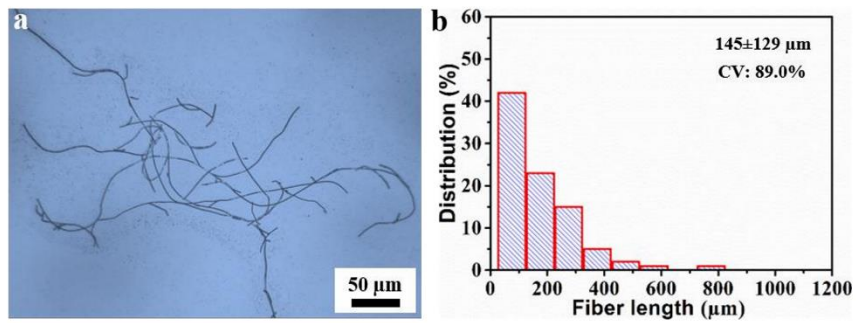


Figure S3. **a**, Microscope images of short fibers made from mixer. **b**, Fiber length distribution of short fibers made from mixer.

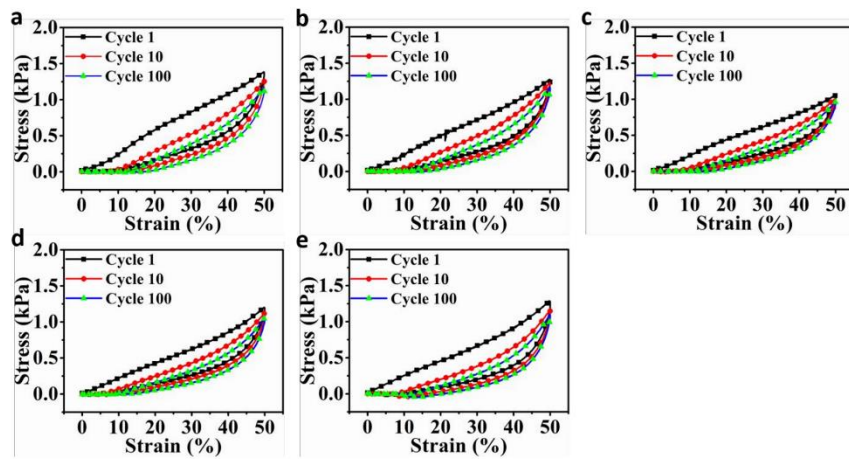


Figure S4. 100 cycles loading-unloading compression tests of sponges with different weight contents of 1 mm length short fibers in 0.4 mm length short fibers: a, 0 wt%; b, 30 wt%; c, 50 wt%; d, 70 wt% and e, 100 wt%.

Table S1. Information of short fibers cut by different methods.

Method	Average fiber length [μm]	Coefficient of Variance [CV, %]^a
Cutter 0.4 ^b	416 \pm 83	20.0
Cutter 1.0 ^c	1034 \pm 156	15.1
Mixer cutting	145 \pm 129	89.0

^a: The coefficient of variation (CV) is a measure of relative variability. It is the ratio of the standard deviation to the mean (average) length.

^b: the home-made cutter with option of cutting fibers to a length of 0.4 mm.

^c: the home-made cutter with option of cutting fibers to a length of 1.0 mm.

Table S2. Information of sponges with different content of 1.0 mm short fibers and 0.4 mm short fibers.

Content of 1 mm short fibers [wt%]	Sponge density [mg/cm³]	Sponge diameter [mm]	Sponge height [mm]	Sponge weight [mg]	Sponge volume [cm³]	Porosity [%]
100	6.61	14	6.9	7.02	1.06	99.44
70	6.62	14	6.9	7.03	1.06	99.44
50	6.46	14	6.8	6.78	1.05	99.45
30	6.88	14	7	7.43	1.08	99.42
0	6.78	14	6.7	6.98	1.03	99.43

3.3 Polarized blue photoluminescence of mesoscopically ordered electrospun non-conjugated polyacrylonitrile nanofibers

Xiaojian Liao, Frank-Julian Kahle, Bin Liu, Heinz Bässler, Xinghong Zhang, Anna Köhler, Andreas Greiner, Polarized blue photoluminescence of mesoscopically ordered electrospun non-conjugated polyacrylonitrile nanofibers, *Materials Horizons*, **2020**, 7(6), 1605-1612.

Please do not adjust margins



Materials Horizons

COMMUNICATION

Polarized blue photoluminescence of mesoscopically ordered electrospun non-conjugated polyacrylonitrile nanofiberst

Received 00th January 20xx,
Accepted 00th January 20xxXiaojian Liao^a, Frank-Julian Kahle^b, Bin Liu^{c, d}, Heinz Bässler^b, Xinghong Zhang^c, Anna Köhler^{*b},
Andreas Greiner^{*a}

DOI: 10.1039/x0xx00000x

Conjugated polymers and oligomers that emit polarized light are used as active materials in various optoelectronic device applications, notably organic light-emitting diodes (OLED). Here, we demonstrate the fabrication of electrospun polarized light-emitting fibers from the non-conjugated polymer that can be aligned by a simple heat-stretching process. Upon excitation at 340 nm ribbons made from the nanofibers show polarized deep blue luminescence with an anisotropy of 0.37 and a quantum yield of about 31%. Furthermore, they exhibit room temperature green phosphorescence with a lifetime of about 200 ms as well as a delayed deep blue fluorescence resulting from triplet-triplet annihilation (non-coherent photon upconversion) (TTA). Wide and small angle X-ray scattering experiments show that the stretched electrospun fibers are highly aligned with nearly perfect uniaxial orientation within the fabricated ribbons. This results in mechanically robust and flexible, with a high specific tensile strength (534±28) MPa*cm²/g and toughness (79±7) J/g. The combination of efficient polarized deep blue luminescence, room temperature phosphorescence, TTA, mechanically robustness and flexibility of these fibers opens up new avenues for applications of non-conjugated polymers.

An approach to reduce the power consumption in the next-generation display materials is to employ compounds that emit polarized light as this allows for the fabrication of high brightness displays with lower power consumption.¹ At the same time, the compounds should be solution-processable to

allow for low-cost processing methods such as spin-coating, ink-jet printing or roll-to-roll processing. The resulting materials should be mechanically flexible, lightweight and thin, so that they can be used in numerous applications — including foldable display screens and OLEDs.^{2,3} These applications call for the use of organic compounds such as π -conjugated oligomers or polymers. Obtaining polarized emission from solution-processed compounds can be challenging. Approaches include aligning a conjugated polymers, e.g. by applying a shear force through rubbing with a cloth or using a Teflon roller, by deposition onto nanogrooved substrates with subsequent heating of the film into a liquid crystalline phase followed by rapid quenching, or mechanically aligning fibres by stretching or imprinting a film.^{4,5} By combination of these methods, highly polarized blue electroluminescence could be achieved already yet the approach was not suitable for large scale technical use.⁶ More recently, aligning electrospun nanofibers has attracted attention as a possible approach.^{4,5,7} Electrospinning is an efficient technique to produce polymer nanofiber nonwovens and yarns by electrostatic charging on one of the electrodes and letting a jet of polymer solution propel towards the counter electrode.⁸⁻¹⁰ Typically, the conjugated polymer, for example (poly[(9,9-dioctylfluorenyl-2,7-diyl)-co-(1,4-benzo-(2,10-3);-thiadiazole)] (F8BT) or poly(9,9-dioctylfluorenyl-2,7-diyl) (PFO)) is mixed with a spinnable polymer such as poly(methyl methacrylate) or poly(ethylene oxide) (PEO).^{11,12} The 1D luminescent nanofibers that result from electrospinning tend to have a large aspect ratio and high surface area (compared to the corresponding bulk materials and 2D thin films), and they are reported to show enhanced mechanical properties, photoluminescence quantum yields (QY), radiative rates and anisotropy of photoluminescence.^{13,14,15} While the method of electrospinning is suitable for industrial scale-up, the use of conjugated polymers is expensive. Moreover, care needs to be taken in the design of novel polymers to avoid photoluminescence quenching upon aggregation, in particular when they are aligned.

^a University of Bayreuth, Macromolecular Chemistry, Bavarian Polymer Institute, Universitätsstrasse 30, 95440 Bayreuth, Germany. E-mail: greiner@uni-bayreuth.de

^b University of Bayreuth, Experimental Physics II, Bavarian Polymer Institute and BIMF, Universitätsstrasse 30, D-95440 Bayreuth, Germany. E-mail: anna.koehler@uni-bayreuth.de

^c MOE Key Laboratory of Macromolecular Synthesis and Functionalization, Department of Polymer Science and Engineering, Zhejiang University, Hangzhou 310027, P. R. China.

^d School of Energy and Power Engineering, North University of China, Taiyuan 030051, China

*E-mail: greiner@uni-bayreuth.de

*E-mail: anna.koehler@uni-bayreuth.de

† Electronic Supplementary Information (ESI) available: See DOI: 10.1039/x0xx00000x

Please do not adjust margins

Please do not adjust margins

ARTICLE

Journal Name

A different twist to this may be the use of non-conjugated polymers that show aggregation-induced emission. Some non-aromatic low-molecular weight organic units have been reported to show emission, and even room temperature phosphorescence, when aggregated, e.g. in a film.^{16–18} While the detailed mechanism is not yet fully understood, it seems that the interaction between adjacent cyano groups or carbonyl groups leads to the formation of a π -system with through-space conjugation, so that the emission of the interacting units is in the visible spectral range, quite in contrast to the non-interacting units for which emission is not observed. Such functional groups are easily incorporated into the backbone of non-conjugated polymers (NCPs) that can be electrospun. NCPs that show luminescence in the solid state caused by aggregation induced emission (AIE) are attracting increasing attention.^{16–18} In addition to being emissive, they are easily and cheaply made in comparatively large quantities, exhibit high molecular weight, mechanical flexibility, processability, diversified polymer backbones, additional stimuli responsiveness and biocompatibility.¹⁹ Some of the reported luminescent NCPs are low-cost commodity polymers like polyethylene terephthalate (PET)²⁰, polyacrylonitrile (PAN)¹⁶ and sulfonated polystyrene (PS)²¹.

In order to achieve polarized emission from such NCPs, two criteria need to be fulfilled. First, the NCP needs to have functional groups that show AIE, and second, the NCP needs to be macroscopically aligned.^{3,22,23} The latter is not trivial due to the commonly disordered packing of coiled, long non-conjugated polymeric chains. While the stretching forces during the process of electrospinning could be sufficient for the orientation of polymer chains along the nanofiber long axis of conjugated polymers,²⁴ this force is not strong enough to efficiently stretch the long coiled NCPs chains into a macroscopic alignment. Thus, it is still a challenge to achieve a polarized emitting system with facile processability and good reproducibility based on the emerging luminescent NCPs.

We report here the fabrication of polarized photoluminescence (PL) of mesoscopically ordered nanofiber ribbons (ENRs) from commercial non-conjugated PAN by electrospinning and high heat stretching above the glass transition temperature (T_g). (Fig. 1) The cyano groups in PAN are known to interact such as to show AIE with fluorescence as well as room temperature phosphorescence.¹⁶ The latter is attributed to admixtures of the $n-\pi^*$ transition derived from the nitrogen atoms in the cyano groups. The obtained ENRs are light-weight and show excellent mechanical strength and toughness. At room temperature, PL itself consists of prompt fluorescence, delayed fluorescence by triplet-triplet annihilation and phosphorescence. As a result, we show a very intriguing material with a unique property combination of emission, anisotropy and mechanical properties. The ENRS are stable as free-standing objects which facilitates potential applications.

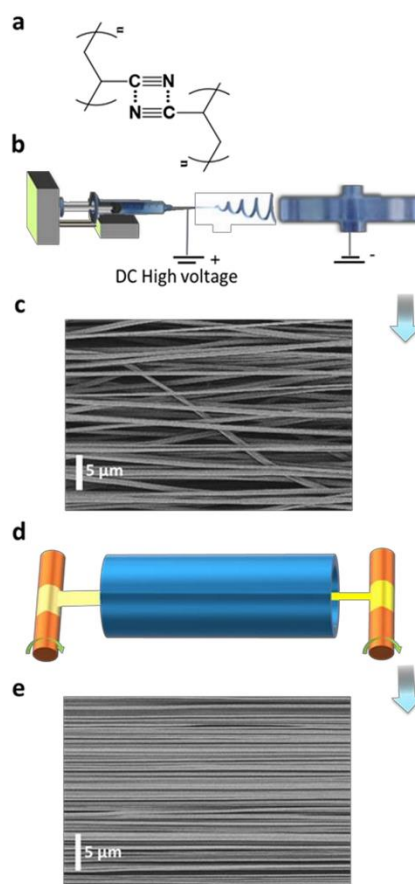


Fig. 1 Fabrication process and microstructure of ENRs. (a) Chemical structure of PAN with dipole-dipole attraction interactions. (b) Electrospinning setup. (c) A SEM image of the PAN as-spun ENRs. (d) Roll-to-roll heat-stretching setup. (e) A SEM image of the PAN ENRs after the heat-stretching process with stretch ratio at six.

PAN is a synthetic, semi-crystalline non-conjugated polymer (Fig. 1a). A high dipole moment of 3.9 Debye was reported for the substituent cyano group.^{25,26} This can induce strong attraction or repulsion between adjacent macromolecular chains which may even result in their orientation.^{25,26} We were able to obtain highly aligned chains using two sequential steps as shown in Fig. 1. First, we prepared as-spun ENRs from pure PAN solution by electrospinning using a conventional collector device with a narrow disc rotating at high speed (1,200 rpm) (Fig. 1b). These ENRs had an average width of about 10.0 mm

Please do not adjust margins

Please do not adjust margins

Journal Name

ARTICLE

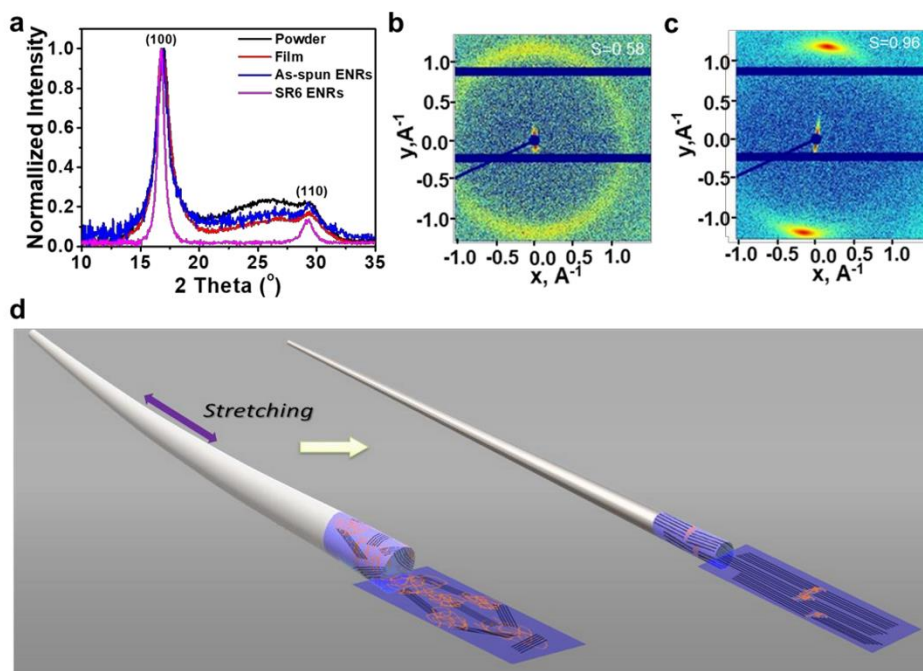


Fig. 2 Structural investigation on PAN films. (a) WAXS spectra of PAN in form of powder, drop-cast film, as-spun ENRs, and SR6 ENRs. (b and c) 2D SAXS scattering pattern images of ENRs before (as-spun ENR) (b) and after stretching (SR6) (c). (d) A schematic illustrating the envisaged molecular changes during the heat-stretching process from a semi-crystalline as-spun fibre to an aligned PAN fibre of highly aligned crystalline molecular chains.

with individual nanofibers having a diameter of (710 ± 160) nm (Fig. S1-3, ESI[†]). The nanofibers in the as-spun ENRs have an alignment factor of (92.6 ± 25.7) % (Fig. S2b, ESI[†]) along the ENRs main axis as assessed by the analysis of scanning electron microscopy (SEM) images (Fig. 1c). Due to the complex deposition path of the jets into nanofibers during electrospinning (Fig. 1b), there are, however, still unavoidable unaligned nanofibers (Fig. 1c, and Fig. S2, ESI[†]), which could have a negative effect on anisotropic photophysical properties. Therefore, in a second step, the obtained as-spun ENRs were stretched at 160 °C, i.e. above T_g of PAN ($T_g = 103$ °C), along the long axis of the ENRs using a roll-to-roll heat-stretching setup. In this setup the ENRs were conducted through a furnace while being stretched. We observed that stretching at temperatures above the T_g but below its onset of oxidation at 180 °C²⁷ could efficiently and homogeneously extend nanofibers along the axis of ENRs, as shown in Fig. 1d, S2b and S3 (ESI[†]). For this ENR system, the maximum stretching ratio could be up to six at 160 °C. By the heat stretching process, as shown in the ESI, Fig. S1, the width of ENRs decreased down from 10.0 mm to 2.5 mm at a stretching ratio of six. We refer to these stretched ribbons from now on as stretch ration (SR, stretched length divided by

original length) 6 ENRs. Not only the ribbons reduced in width through the stretching process, and the nanofiber diameters were also reduced down to (236 ± 62) nm (SR6 ENRs) (Fig. S2a, ESI[†]). Concomitantly, a nearly perfect uniaxial orientation of the nanofibers along the axis of ENRs could be achieved with an alignment factor of (99.97 ± 0.06) % (SR6 ENRs) (Fig. 1e and S2b, ESI[†]). This extension is irreversible and remains after the heat-stretching process is completed and the sample has cooled down to room temperature. In contrast, when stretching PAN fibers at temperatures below T_g , the reported extension of the fibre is up to 140 % (i.e. a SR1.4) and it is almost entirely reversible if the stress is removed. This extension is a response of PAN fibers to the stress without any changes of microstructure.²⁶ However, the high and irreversible extension of PAN nanofibers of up to 600 % (stretching at 160 °C) suggest that the stretching is accompanied with a re-arrangement of molecular chains in the nanofibers.

The orientation of molecular chains and packing patterns were investigated by wide-angle/small-angle X-ray scattering (WAXS/SAXS), as shown in Fig. 2, S4, S5 and Table S1 (ESI[†]). Comparing the WAXS diffractograms of PAN taken from

Please do not adjust margins

Please do not adjust margins

ARTICLE

Journal Name

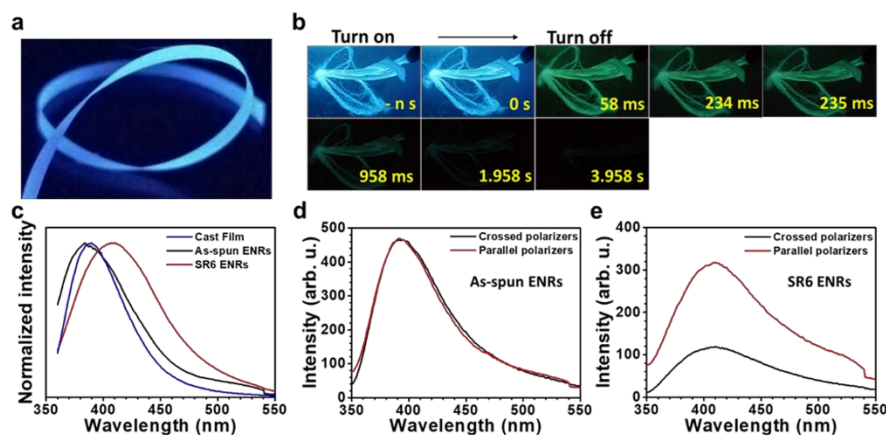


Fig. 3 Photoluminescence properties of ENRs. (a) Photograph of SR6 ENRs under UV light irradiation (365 nm). (b) Luminescence photographs of ENRs taken at 77 K under 365 nm UV irradiation and at different times after turning off the UV lamp. (c) Comparison of the PL spectra of film, as-spun ENRs and SR6 ENRs excited at 340 nm. (d and e) Polarization dependent emission spectra of as-spun ENRs (d) and SR6 ENRs (e) excited at 337 nm. The excitation light was linearly polarized parallel to the long axis of the ENRs.

powder, drop-cast film, and as-spun ENRs, we observed the same peaks at nearly the same positions: a sharp diffraction peak at $2\theta=16.9^\circ$ corresponding to the (100) crystal direction and a small diffraction peak at $2\theta=29.4^\circ$ associating with the (110) crystal direction. The interplanar spacings d corresponding to these two peaks are 5.25 Å and 3.03 Å, respectively. Apart from the crystal peaks, there is a broad feature that arises from the amorphous areas in the samples of powder, drop-cast film and as-spun ENRs (Fig. 2a). Interestingly, while nearly the same full width at half maximum (FWHM) of 1.35° was observed in the (100) peaks of the powder sample, the film and the as-spun ENRs, this FWHM reduced to nearly half of it for the heat-stretched SR6 ENRs. This implies high quality of the crystallites formed in the SR6 ENRs. In addition, the intensity of the broad features centred at about $2\theta = 25^\circ$ reduces from the powder and film samples to the as-spun ENR and almost disappears for the SR6 ENRs. A detailed peak analysis (see Fig. S4 and Table 1, ESI†) shows that the crystallinity increases drastically from 51% in the as-spun ribbon to 89% in the heat-stretched SR6 ENRs. At the same time, minor decreases in the value of the 2θ peaks (16.75° and 29.23° , respectively, for the (100) and (110) direction in the SR6 ENRs) were observed. This translates into small increases in the interplanar spacings d (5.29 Å and 3.05 Å, respectively, for the (100) and (110) direction in the SR6 ENRs).

Further structural information can be obtained from the 2D SAXS images of the as-spun ENRs and the SR6 ENRs (Fig. 2b and c). For the as-spun samples, we observe a ring, implying a near-isotropic orientation of the crystallites, whereas the SR6 ENRs show two sharp (200)-reflections, implying alignment accompanied by a high orientational order. The calculated

orientational order parameters are $S = 0.58$ for the as-spun ENRs and $S = 0.96$ for the SR6 ENRs (Fig. 2b and S5, ESI†). Thus, in summary, the process of heat-stretching leads to the formation of aligned, highly crystalline PAN ENRs. In contrast, in as-spun ENRs, crystallites have an isotropic orientation, lower crystal quality and the overall fraction of crystalline domains is reduced.

For applications, the mechanical properties of the ribbons can be relevant. The two key parameters of robustness and flexibility can be represented by the specific tensile strength and the toughness, respectively. The ENRs can support higher stresses and show a higher toughness when they are heat-stretched to higher stretching ratios (Fig. S6, ESI†). The results show that high values for specific tensile strength (534 ± 28.0 MPa \cdot cm 3 /g) and toughness (79 ± 7 J/g) of the ENRs are obtained with a stretching ratio of 6 at 160 °C. Evidently, the heat-stretching process and the associated alignment of the crystalline domains are beneficial for obtaining a high maximum tensile stress and for a high toughness.

Furthermore, we found that solid state samples of PAN like powders, films or ENRs showed bright blue emission under irradiation with UV-light (Fig. 3a, and S7-9, ESI†), while the acrylonitrile monomer itself did not give any detectable emission above 360 nm (Fig. S10, ESI†). After turning off the excitation, we observed a green afterglow that lasted for several seconds at 77K. The blue emission as well as the afterglow had already been reported for concentrated solutions of PAN.¹⁶ As the emission intensity has been shown to increase with concentration, this effect has been attributed to effects of

Please do not adjust margins

Please do not adjust margins

Journal Name

ARTICLE

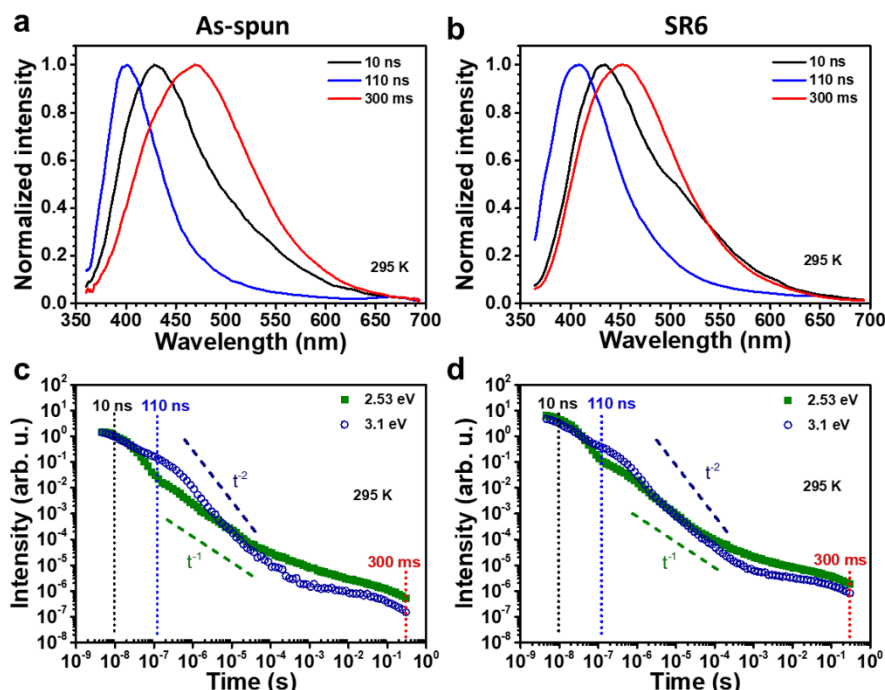


Fig. 4 (a and b) Comparison of room temperature PL spectra at different delay times after the excitation for (a) as-spun and (b) stretched SR6 ENRs. (c and d) Temporal PL decay at 295 K for (c) as-spun ENRs and (d) SR6 ENRs evaluated at 2.53 eV and 3.1 eV. Dashed vertical lines indicate the time corresponding to the spectra in (a) and (b). Also indicated are slopes corresponding to t^{-1} and t^{-2} for comparison. The gate width was half the delay time.

clustering of the cyano groups and has been referred to as aggregate induced emission (AIE).^{16,28}

In order to study the emission properties of the ribbons in more detail and to evaluate the influence of stretching the ribbons on their luminescence properties, we performed a range of additional photoluminescence (PL) measurements. They were conducted using unpolarized as well as polarized excitation light, and detecting in steady state mode as well as in a gated, time-resolved fashion. The steady state (PL) spectra of PAN films and ribbons displayed in Fig. 3c do not show any structure. While the films and the as-spun ENRs feature similar spectra with a maximum at around 394–388 nm, SR6 ENRs features a red shifted, broadened emission maximum at around 410 nm. The quantum yields of emission are similar for both ribbons and in the range of 30–32%, thus exceeding the value of 22% that we measure in a DMF solution at 80 mg/mL (Table S2, ESI†). When excited with linearly polarized light, the stretched ribbons feature a considerable anisotropy, $r = (I_{\parallel} - I_{\perp}) / (I_{\parallel} + 2I_{\perp})$, of 0.37 and a degree of polarization, $P = (I_{\parallel} - I_{\perp}) / (I_{\parallel} + I_{\perp})$, of 0.47 for the emission, whereas as-spun ENRs do not show a dependence of the emission intensity on

the position of the analyser (Fig. 3d and e). For the as-spun ENRs, both anisotropy and polarization are basically zero (Table S3, ESI†). Evidently, the polarization is induced by the heat-stretching process. Similarly, the increased weight in the red spectral range for the emission of SR6 ENRs as compared to the not stretched films is also associated with the stretching process.

To analyse the emission in more detail, we considered time-resolved measurements shown in Fig. 4. In the first 10 ns after the excitation pulse, we observe a broad emission centred at about 425 nm. The lower energy part of this distribution is more intense in the heat-stretched SR6 sample (seen as a higher initial intensity in Fig. 4d), consistent with the redshifted spectrum for continuous wave (CW) excitation (Fig. 3c). Evidently, there is a very wide energetic distribution of emitting states. After a few tens of ns, the emission from the lower-energy part of the distribution has decayed, leaving a significantly narrower spectrum of about half the previous FWHM that peaks around 400 nm. This blue emission decays on a μ s to ms timescale and a turquoise emission centred at 450–475 nm remains in the range of ms to s, both in as-spun ENRs

Please do not adjust margins

and in the stretch-oriented fibres. When exposing the fibers to oxygen, we find that the long-lived component is strongly reduced by oxygen, in contrast to the shorter lived components (Fig. S11, ESI†). Based on the long lifetime and sensitivity to oxygen, we can attribute the long components at room temperature to delayed fluorescence (centred at 3.1 eV, i.e. 400 nm) and phosphorescence (centred at about 2.7 eV, i.e. 460 nm). Room temperature delayed fluorescence (DF) and phosphorescence is unusual. It has been observed, however, in compounds with significant contributions from $n-\pi^*$ transitions to the emitting state, in particular when the molecule was rigidified, e.g. by aggregation, such as to suppress non-radiative decay channels.²⁸ The room temperature spectrum for CW excitation is not affected by oxygen, implying that it results mostly from prompt fluorescence. This is also consistent with the very similar photoluminescence QY and the very similar decay dynamics of the as-spun ENRs and the SR6 ENRs. If we consider intersystem crossing from the singlet to the triplet state as the dominant non-radiative decay process, and use the 1/e-decay time of 14 ns as a first approximation to the lifetime of the excited singlet states, then the PL QY of 31% implies a radiative decay rate of about $2 \times 10^7 \text{ s}^{-1}$ and an intersystem crossing (ISC) rate of about $5 \times 10^7 \text{ s}^{-1}$. Such high ISC rates are typical for compounds with a significant contribution from $n-\pi^*$ transitions.

The temporal decay of the long-lived emissions offers a clue for their assignment. Since it is virtually temperature-independent (see Fig. S12 in the ESI), thermally activated delayed fluorescence can be discarded as possible origin for the delayed blue component of the spectrum. Instead, it has to be identified as delayed fluorescence caused by recombination of either geminately bound electron-hole pairs or by triplet-triplet annihilation (TTA).^{29,30} The latter would be complementary to the work of Wohnhaas et al. who studied dye-sensitized TTA in electrospun poly(methyl methacrylate) fibres.³¹ Conventional kinetics predicts that the decay of triplets generated via ISC from the singlet state is governed by the interplay between monomolecular decay, described by the radiative (k_r) and non-radiative (k_{nr}) rate constants and bimolecular annihilation governed by the bimolecular rate constant γ , i.e.³²

$$\frac{d}{dt}[T(t)] = G - (k_r + k_{nr})[T(t)] - \gamma[T(t)]^2 \quad (1),$$

where G is the initial triplet generation rate, i.e. the product of the ISC yield times the singlet concentration, and $[T(t)]$ is the time-dependent concentration of triplets. A fraction f of TTA events gives rise to delayed fluorescence, i.e.

$$\frac{d}{dt}[DF(t)] \propto f\gamma[T(t)]^2 \quad (2),$$

where $[DF(t)]$ denotes the concentration of singlets available to give delayed fluorescence. In systems with long triplet lifetime TTA usually controls triplet decay, i.e. $\gamma[T(t)]^2 \gg (k_r + k_{nr})[T(t)]$. By solving the rate equation (1) one obtains the temporal decay of the reservoir of triplet

excitations and, therefore, the temporal decay of the phosphorescence.

$$I_{ph} \propto \frac{k_r}{k_r + k_{nr}} \frac{[T_0]}{1 + \gamma[T_0]t} \quad (3),$$

where $[T_0]$ is the initial concentration of triplets. Eq. 3 predicts that in an intermediate time regime, i.e. $(\gamma[T_0])^{-1} < t \ll (k_r + k_{nr})^{-1}$ the phosphorescence should decay in a power law fashion, i.e. $I_{ph} \propto t^{-1}$. Ultimately, the phosphorescence is limited by the intrinsic triplet lifetime. Combining eqs. 2 and 3, predicts that in the intermediate time regime the DF should decay as t^{-2} . From the fact that in the intermediate time regime the blue component closely follows a t^{-2} decay over four orders of magnitude while in the same time regime the phosphorescence decays as t^{-1} we conclude that the DF is caused by TTA. In passing we note that the fact that the emission right after the decay of the prompt fluorescence is not time independent (as it should, according to eq. 3) is a common signature of dispersive triplet transport.

It is noteworthy that the stretched PAN-fibres show polarized emission also for the phosphorescence part of the spectrum, while the monomer acrylonitrile does not show any phosphorescence.

Summarizing the results of the photoluminescence spectroscopy, we observe a delayed blue fluorescence as well as green phosphorescence at room temperature in addition to the prompt fluorescence. The DF results from TTA, also referred to as triplet upconversion (UC). The observation of TTA implies that triplet excitons are remarkably mobile in these non-conjugated materials. This opens up a new perspective for electrospun fibers. Non-coherent triplet upconversion is frequently thought after for biomedical applications and usually requires the use of a sensitizer in addition to the emitter. In electrospun nanofibers, TTA-UC has so far only been achieved when sensitizer and emitter were included in a colloidal nanocapsule inside the electrospun fiber.^{31,33}

In our ENRs, the CW emission is efficient and with about 31% similar in the as-spun and stretched samples. However, the stretched samples show highly polarized emission with an anisotropy of 0.37. The lack of polarization in the as-spun sample, as well as the high degree of orientation order found in SR6 after the heat-stretching are in excellent agreement, respectively, with the isotropic orientation found for the crystallites by 2D SAXS in the as-spun samples and the high orientation observed in SR6 after stretching.

Conclusions

We present a concise and efficient fabrication approach to achieve polarized emission PAN ENRs by mesoscopic order. The ribbons are lightweight and have a high strength and toughness. From our analysis we are able to identify three important molecular design rules to achieve polarized emission in non-conjugated polymers: i) electrospinning the non-conjugated

Please do not adjust margins

Journal Name

ARTICLE

polymer into nanofibers, ii) aligned crystal arrangement by sufficient heat-stretching at high temperatures above T_g , and iii) using functional groups that show AIE when interactions between adjacent groups lead to the formation of a more extended π -system.

PAN ENRs satisfy these design requirements by forming a highly ordered macroscopically aligned structure upon stretching at temperatures above T_g . Interactions between adjacent cyano side groups result in the formation of an extended π -system and the occurrence of aggregate induced polarized deep blue emission. They exhibit a photoluminescence quantum yield of 30–32%, which is remarkable for a simple non-conjugated polymer (not particularly designed for light emission). Due to the contribution of $n-\pi^*$ transitions resulting from the nitrogen atoms in the cyano groups, intersystem crossing occurs that leads to the formation of highly mobile triplet states with quantum energy of about 2.5 eV and lifetime up to 1s. These triplets give rise to delayed fluorescence via TTA and to phosphorescence.

Conflicts of interest

There are no conflicts to declare.

Acknowledgements

We gratefully acknowledge the financial support of SFB 840, project B8.

Notes and references

- L. Wan, J. Wade, F. Salerno, O. Arteaga, B. Laidlaw, X. Wang, T. Penfold, M. J. Fuchter and A. J. Campbell, *ACS Nano*, 2019, **13**, 8099–8105.
- X. Ai, E. W. Evans, S. Dong, A. J. Gillett, H. Guo, Y. Chen, T. J. Hele, R. H. Friend and F. Li, *Nature*, 2018, **563**, 536–540.
- B. G. Kim, E. J. Jeong, J. W. Chung, S. Seo, B. Koo and J. Kim, *Nat. Mater.*, 2013, **12**, 659–664.
- K. Chung, Y. Yu, M. S. Kwon, J. Swets, J. Kim and J. H. Youk, *MRS Commun.*, 2015, **5**, 169–189.
- K. Chung, D. S. Yang, W.-H. Sul, B.-G. Kim, J. Kim, G. Jang, M. S. Kwon, M. Barló, T. S. Lee, S.-Y. Park, M. Al-Hashimi and J. Kim, *Macromolecules*, 2019, **52**, 6485–6494.
- K. S. Whitehead, M. Grell, D. D. C. Bradley, M. Jandke and P. Strohriegel, *Appl. Phys. Lett.*, 2000, **76**, 2946–2948.
- K. Yin, L. Zhang, C. Lai, L. Zhong, S. Smith, H. Fong and Z. Zhu, *J. Mater. Chem.*, 2011, **21**, 444–448.
- S. Agarwal, A. Greiner and J. H. Wendorff, *Prog. Polym. Sci.*, 2013, **38**, 963–991.
- Y. Ding, H. Hou, Y. Zhao, Z. Zhu and H. Fong, *Prog. Polym. Sci.*, 2016, **61**, 67–103.
- X. Liao, M. Dulle, J. Martins, R. B. Wehrspohn, S. Agarwal, S. Förster, H. Hou, P. Smith, A. Greiner, *Science*, 2019, **366**, 1376–1379.
- S. Pagliara, M. S. Vitiello, A. Camposeo, A. Polini, R. Cingolani, G. Scamarcio and D. Pisignano, *J. Phys. Chem. C*, 2011, **115**, 20399–20405.
- C. C. Kuo, C. T. Wang and W. C. Chen, *Macromol. Mater. Eng.*, 2008, **293**, 999–1008.
- A. Macagnano, E. Zampetti and E. Kny, *Electrospinning for high performance sensors*, Berlin, Germany: Springer, 2015.
- A. Camposeo, L. Persano and D. Pisignano, *Macromol. Mater. Eng.*, 2013, **298**, 487–503.
- W. Han, F. Cui, Y. Si, X. Mao, B. Ding and H. Kim, *Small*, 2018, **14**, 1801963.
- Q. Zhou, B. Cao, C. Zhu, S. Xu, Y. Gong, W. Z. Yuan and Y. Zhang, *Small*, 2016, **12**, 6586–6592.
- L. Song, T. Zhu, L. Yuan, J. Zhou, Y. Zhang, Z. Wang and C. Tang, *Nat. Commun.*, 2019, **10**, 1315.
- Q. Li, Y. Tang, W. Hu and Z. Li, *Small*, 2018, **14**, e1801560.
- T. L. Mako, J. M. Racicot and M. Levine, *Chem. Rev.*, 2019, **119**, 322–477.
- X. Chen, Z. He, F. Kausar, G. Chen, Y. Zhang and W. Z. Yuan, *Macromolecules*, 2018, **51**, 9035–9042.
- T. Ogoshi, H. Tsuchida, T. Kakuta, T.-a. Yamagishi, A. Taema, T. Ono, M. Sugimoto and M. Mizuno, *Adv. Funct. Mater.*, 2018, **28**, 1707369.
- X. Ma, C. Xu, J. Wang and H. Tian, *Angew. Chem., Int. Ed. Engl.*, 2018, **57**, 10854–10858.
- J. Yang, X. Zhen, B. Wang, X. Gao, Z. Ren, J. Wang, Y. Xie, J. Li, Q. Peng and K. Pu, *Nat. Commun.*, 2018, **9**, 840.
- R. Dersch, T. Liu, A. Schaper, A. Greiner and J. Wendorff, *J. Polym. Sci., Part A: Polym. Chem.*, 2003, **41**, 545–553.
- L. D. R., *CRC handbook of chemistry and physics: a ready-reference book of chemical and physical data*, CRC press, 1995.
- G. Henrici-Olivé and S. Olivé, in *Chemistry*, Springer, 1979, 123–152.
- N. Yusof and A. F. Ismail, *J. Anal. Appl. Pyrolysis*, 2012, **93**, 1–13.
- Z. An, C. Zheng, Y. Tao, R. Chen, H. Shi, T. Chen, Z. Wang, H. Li, R. Deng, X. Liu and W. Huang, *Nat. Mater.*, 2015, **14**, 685–690.
- K. Hong and J. Noolandi, *J. Chem. Phys.*, 1978, **68**, 5163–5171.
- Y. V. Romanovskii, V. Arkhipov and H. Bässler, *Phys. Rev. B*, 2001, **64**, 033104.
- C. Wohnhaas, K. Friedemann, D. Busko, K. Landfester, S. Balushev, D. Crespy and A. Turshatov, *ACS Macro Lett.*, 2013, **2**, 446–450.
- A. Köhler and H. Bässler, *Electronic processes in organic semiconductors: An introduction*, John Wiley & Sons, 2015.
- S. Balushev, K. Katta, Y. Avlasevich and K. Landfester, *Mater. Horiz.*, 2016, **3**, 478–486.

This journal is © The Royal Society of Chemistry 20xx

J. Name., 2013, **00**, 1–3 | 7

Please do not adjust margins

Polarized blue photoluminescence of mesoscopically ordered electrospun non-conjugated polyacrylonitrile nanofibers

Supplementary Information

Xiaojian Liao^a, Frank-Julian Kahle^b, Bin Liu^{c, d}, Heinz Bäessler^b, Xinghong Zhang^c, Anna Köhler^{*b}, Andreas Greiner ^{*a}

^a University of Bayreuth, Macromolecular Chemistry, Bavarian Polymer Institute, Universitätsstrasse 30, 95440 Bayreuth, Germany. E-mail: greiner@uni-bayreuth.de

^b University of Bayreuth, Experimental Physics II, Bavarian Polymer Institute and BIMF, Universitätsstrasse 30, D-95440 Bayreuth, Germany. E-mail: anna.koehler@uni-bayreuth.de

^c MOE Key Laboratory of Macromolecular Synthesis and Functionalization, Department of Polymer Science and Engineering, Zhejiang University, Hangzhou 310027, P. R. China.

^d School of Energy and Power Engineering, North University of China, Taiyuan 030051, China

*E-mail: greiner@uni-bayreuth.de

*E-mail: anna.koehler@uni-bayreuth.de

Materials

Poly(acrylonitrile) (PAN, M_n 120,000, co-polymer with 6 wt% methyl acrylate, Dolan; without any dye certified by Dolan). Acrylonitrile (>99.9%; Acros Organic), *N,N'*-dimethylformamide (DMF) and Aceton were purified by distillation.

Characterizations

Steady-state and polarization dependent PL spectra as well as PL quantum yield measurements were performed with a FP-8600 (JASCO) luminescence spectrometer using a Xe lamp as an excitation source. Confocal laser scanning microscope images were recorded using a confocal

1

microscope Leica TCS SP8 (Model DMI 6000, HyD Hybrid-Detector; PMT-Detector) with an argon-laser (405 nm, Live/Dead). Tensile tests were performed using a tensile tester (zwickiLine Z0.5, BT1-FR0.5TN.D14, Zwick/Roell, Germany) with a clamping length of 10 mm, a crosshead rate of 10 mm/min at 25 °C and a pre-tension of 0.001 N. The load cell was a Zwick/Roell KAF TC with a nominal load of 200 N. The morphology of all ENRs samples was probed by a Zeiss LEO 1530 (Gemini, Germany) scanning electron microscope equipped with a field emission cathode and an SE2 detector. In addition, according to a previous literature report¹, the fibril alignment factors were calculated based on the following formula: $d_{f\alpha} = (3\cos^2\vartheta - 1)/2$, where $d_{f\alpha}$ is the fibril alignment factor and ϑ is the angle between the individual fibrils and the direction of the ENRs. The values reported here are based on an average of 100 fibrils. WAXS characterization was carried out using an anode X-ray generator (Bruker D8 ADVANCE, Karlsruhe, Germany) operating at 40 kV and 40 mA with Cu-K α radiation (wavelength $\lambda = 0.154$ nm). The scattering patterns were recorded with the SAXS system "Ganesha-Air" from (SAXSLAB/XENOCSS) at 70 kV and 3.57 mA with Ga-K α radiation (wavelength $\lambda = 0.1314$ nm).

Methods

Preparation of electrospun nanofiber ribbons

The typical solution used in electrospinning was prepared by dissolving 2.00 g PAN powder in 9.40 g DMF and 1.93 g acetone. Then, the solution was loaded into a syringe capped with a metal needle (0.6 mm in diameter). The feed rate of 0.8 mL/h was controlled by a syringe pump. After a positive direct current voltage of 15 kV was applied to the syringe needle, a continuous electrospun fiber

was deposited on a grounded metal disc collector (diameter of 30.0 cm, disc rim of 1.0 cm) at a high speed of 1,200 rpm. The distance between the spinneret and the metal disc collector was adjusted to 30 cm. The electrospinning process was performed under illumination with an infrared lamp (250 W) at about 45 °C and with 10-15% humidity. After electrospinning, the ribbon was wet by ethanol and was shifted on a roller of diameter at 20 mm with helix paths. The ENRs was obtained by drying at 60 °C under vacuum to a constant weight.

Preparation of stretched ENRs

A homemade heat-stretching instrument consisting of a tubular furnace including one heat position zone (Heracus, D6450 Hanau, Typ: RE 1.1, 400 mm in length, Germany), two rollers (20 mm in diameter) controlled by electronic motors and a laptop with "LV2016" software used to precisely control the velocities of the rollers was used to stretch the ribbons. By adjusting the velocities of the two rollers in the LV2016 software, the obtained ENRs were stretched continuously at 160 °C. The stretch ratio (SR) was calculated by the equation: $SR = v_f / v_s$, where v_f and v_s represent the velocities of fast roller and slow roller, respectively. To obtain a high SR, the ENRs were stretched repeatedly.

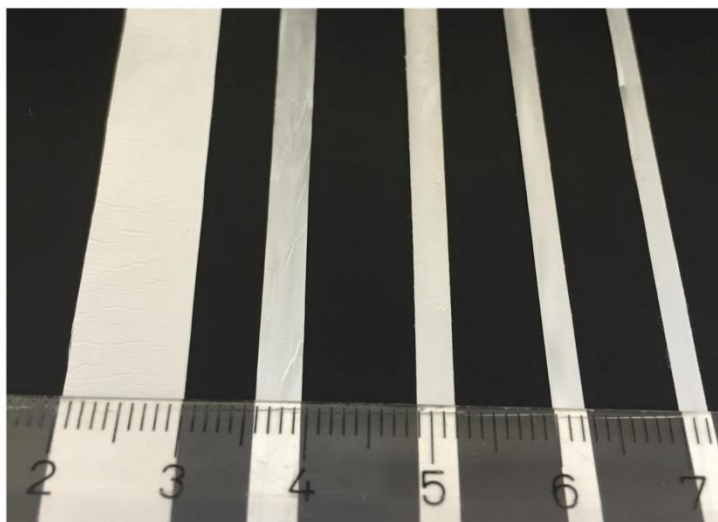


Figure S1 Digital photograph of ENRs with different stretching ratios. left to right: as spun, SR3, SR4, SR5 and SR6 ribbon. ("SRx" is the abbreviation of a stretch ratio x)

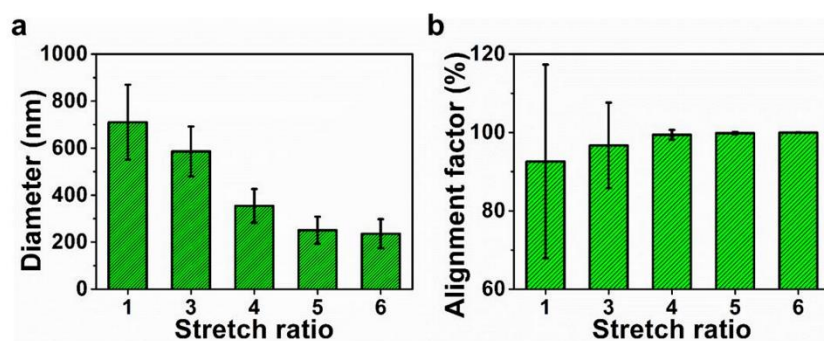


Figure S2 Changes of diameter of nanofiber (a) and alignment factors (b) of nanofibers along the ENRs with stretch ratio during heat-stretching process.

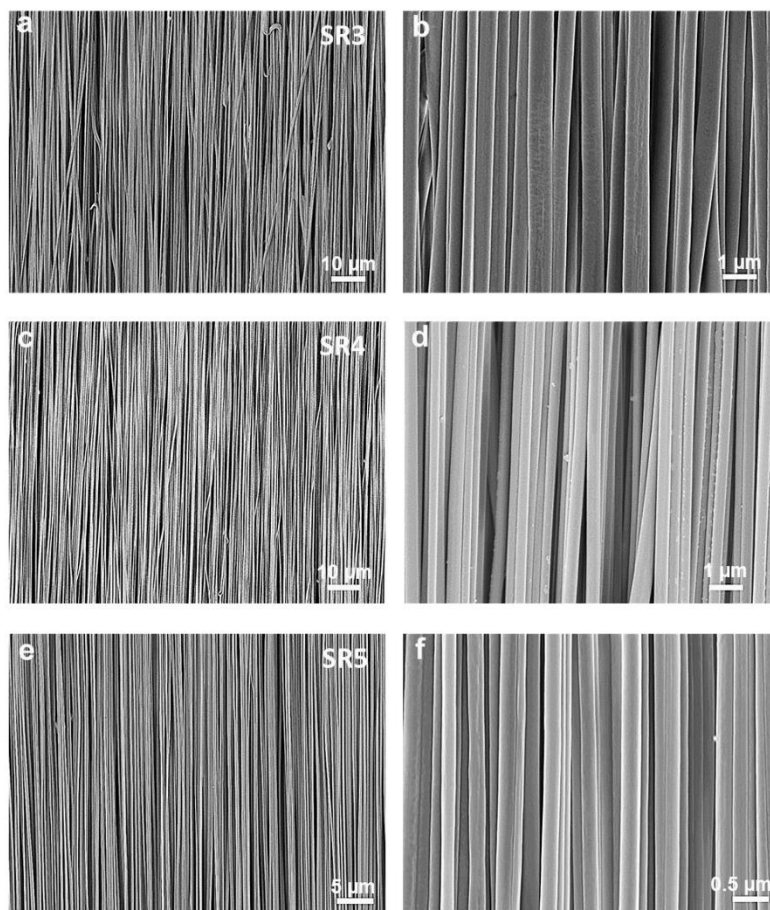


Figure S3 SEM micrographs of ENRs after stretching to stretch ratio of 3 (**a** and **b**), 4 (**c** and **d**) and 5 (**e** and **f**) at different magnifications.

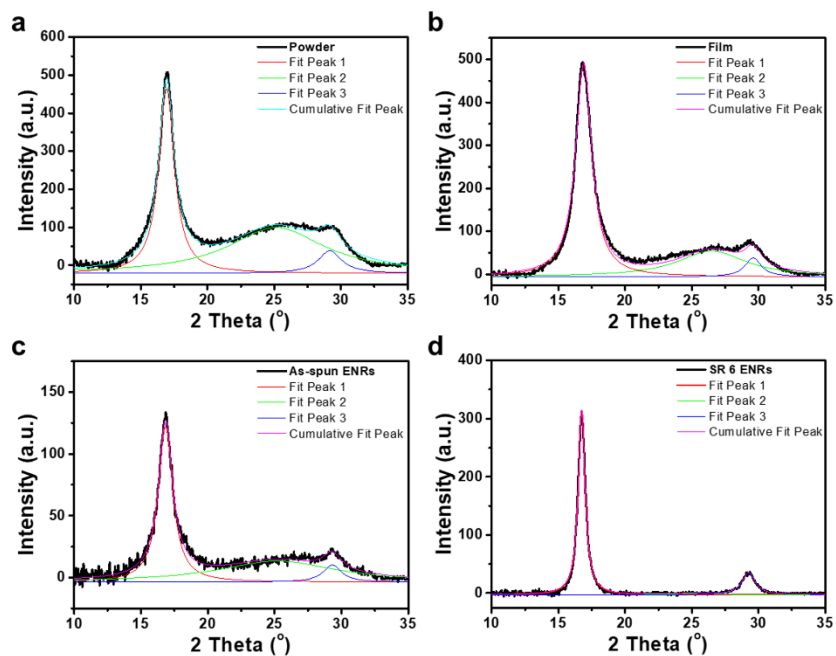


Figure S4 WAXS spectra of PAN in different solid state: powder (a), film (b), as-spun ENRs (c) and SR6 ENRs (d). The fits were performed using Lorentz peak functions.

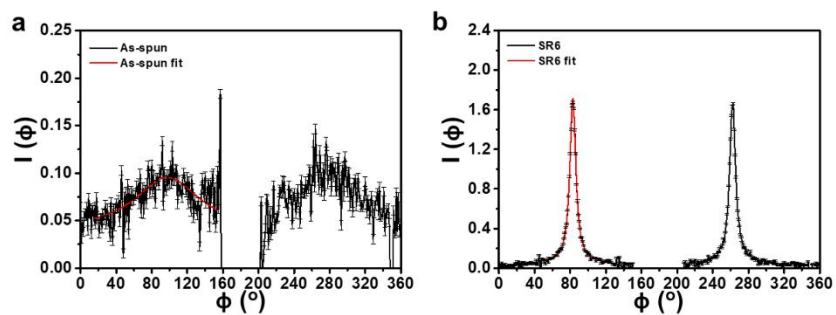


Figure S5 Representative $I(\phi)$ vs. ϕ plots from 2D scattering patterns SAXS of as-spun ENRs (a) and SR6 ENRs (b). The red lines fits using a Lorentz peak function, the corresponding FWHM values were used to calculate the degree of order.

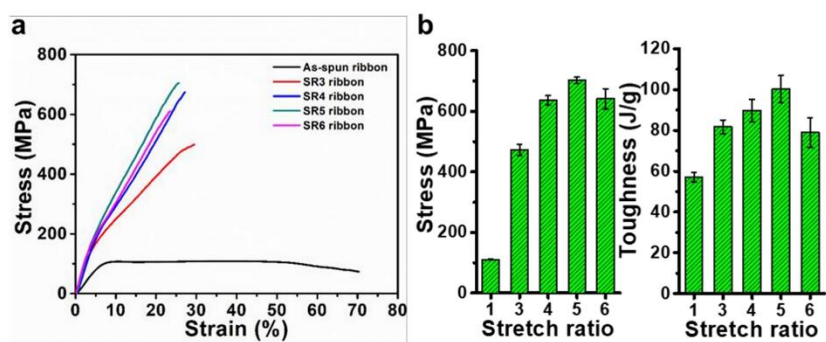


Figure S6 Mechanical properties of ENRs. a) Tensile stress test curves of ENRs with different stretch ratios. b) Evolution of maximum tensile stress supported by the ribbons and toughness of the ribbons with the stretching ratios.

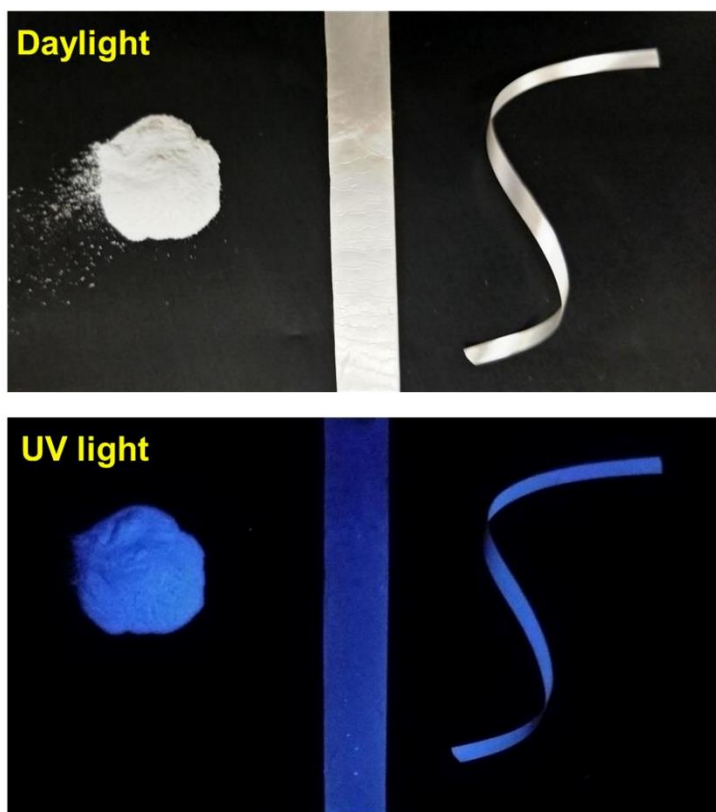


Figure S7 Digital photographs of PAN powder, as spun ENRs and SR6 ENRs (from left to right) under daylight (up) and UV light (below, 365 nm).

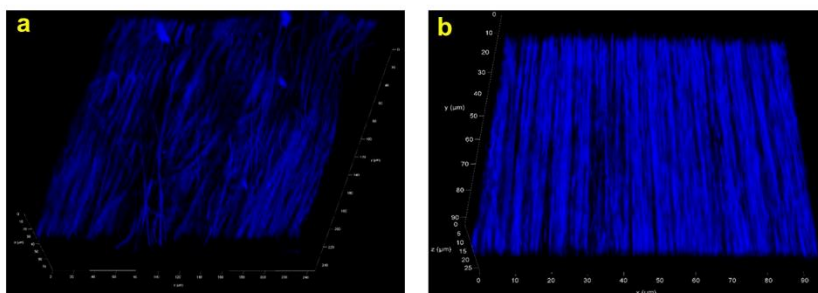


Figure S8 Confocal microscope images of as-spun ENRs (a) and SR6 ENRs (b), respectively ($\lambda_{ex}=405$ nm).

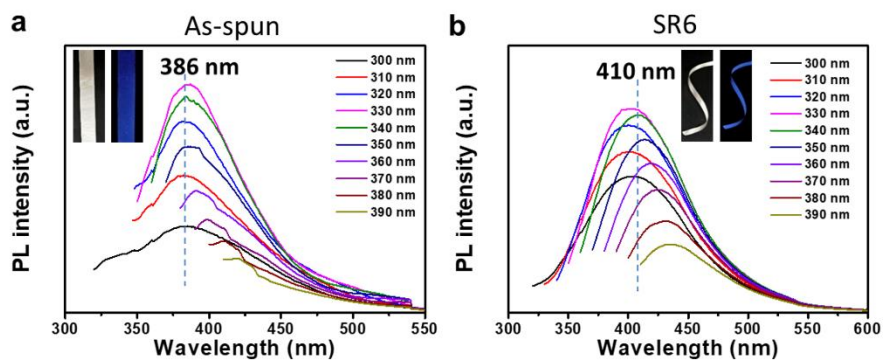


Figure S9 PL spectra of as-spun ENRs (a) and SR6 ENRs (b) irradiated with different excitation wavelengths. The insert white and blue images are ENRs under daylight and UV light (wavelength at 365 nm), respectively.

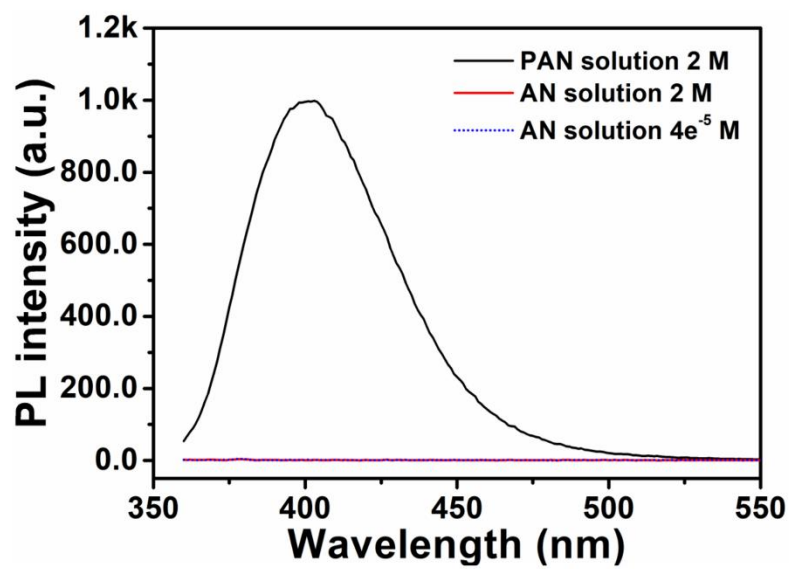


Figure S10 PL spectra of the monomer acrylonitrile at different concentrations of $4e^{-5}$ and 2 M and a PAN solution with a concentration of 2 M, respectively ($\lambda_{ex}=340$ nm).

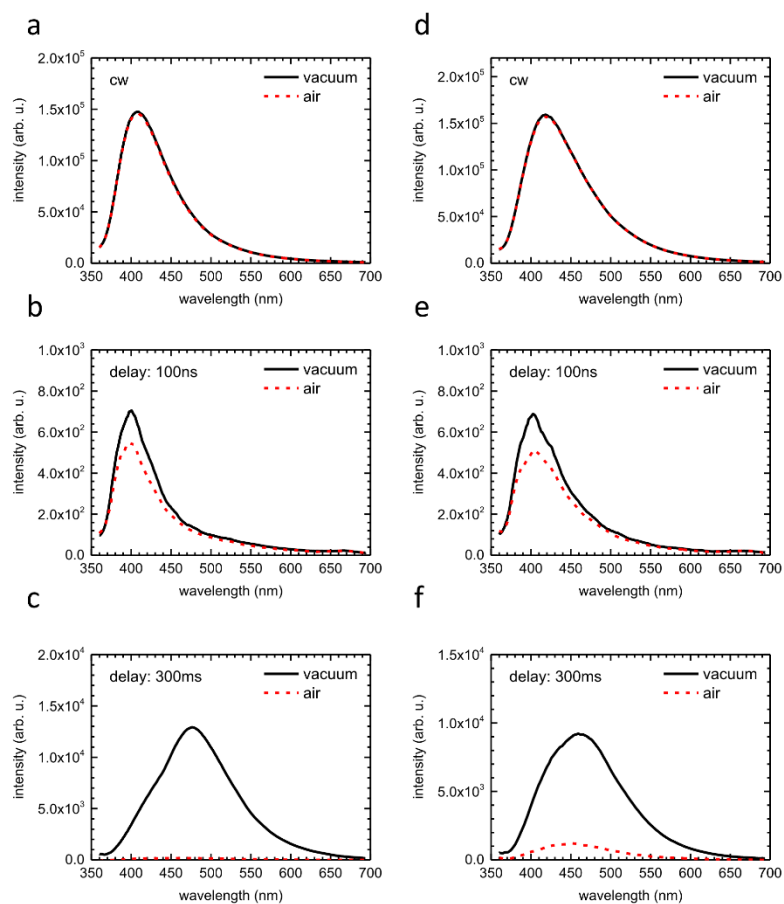


Figure S11 PL spectra of as-spun (a-c) and stretched SR6 ribbons (d-f) measured at room temperature under vacuum and in air recorded under cw conditions (a,d) and for a delay time of 100ns (b,e) and 300ms (c,f) after the excitation pulse.

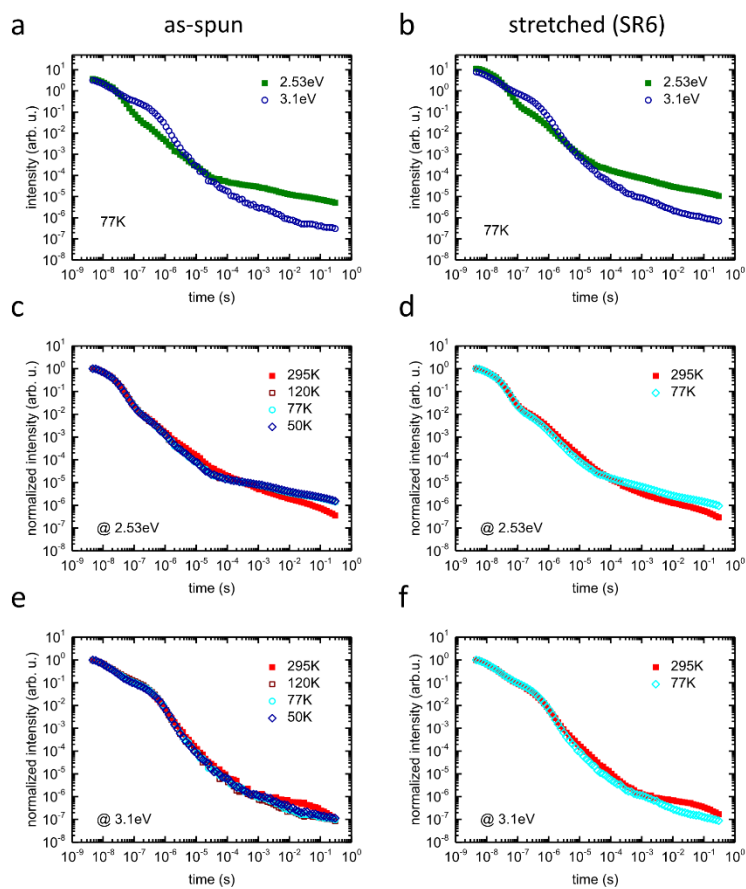


Figure S12 Temporal PL decay at 77K for (a) as-spun and (b) SR6 ENRs evaluated at 2.53 eV and 3.1 eV. c,d) Comparison of the normalized temporal PL decay at 2.53 eV and different temperatures for (c) as-spun and (d) SR6 ENRs. e,f) Comparison of the normalized temporal PL decay at 3.1 eV and different temperatures for (e) as-spun and (f) SR6 ENRs.

Table S1 The parameters of WAXS spectra in different samples correspond with the Fig. 2a and S4.

	Powder		Film		As spun ENRs		SR6 ENRs	
2θ (°)	17.00	29.43	16.85	29.39	16.85	29.34	16.75	29.23
d (Å)	5.210	3.031	5.255	3.035	5.255	3.040	5.287	3.052
Crystallinity	44%		55%		51%		89%	

Table S2 Photoluminescence quantum yield for PAN solution, as-spun ENRs and SR6 ENRs excited at 340 nm.

Samples of PAN	PLQY (%)
Solution (80 mg/mL)	22.0
As-spun ribbon	30.2
SR6 ribbon	32.8

Table S3 Anisotropy r and polarization p for SR6 and as-spun ENRs derived from polarization dependent measurements.

	I_{\parallel} / arb.u.	I_{\perp} / arb.u.	PL anisotropy (r) ^a	polarization (P) ^b
SR6	35020	12554	0.37	0.47
As-spun	38885	39357	-0.004	-0.006

$$a: r = \frac{I_{\parallel} - I_{\perp}}{I_{\parallel} + 2I_{\perp}}$$

$$b: P = \frac{I_{\parallel} - I_{\perp}}{I_{\parallel} + I_{\perp}}$$

Notes and references

- 1 R. Dersch, T. Liu, A. K. Schaper, A. Greiner, and J. H. Wendorff, *J. Polym. Sci. Part A*, 2003, **41**, 545-553.

4 Acknowledgements

Sincerely, I would like to express my thanks to all the people who have helped me during my Ph.D. period.

The first and deepest appreciation to my supervisor **Prof. Andreas Greiner**. Due to my poor English and limited knowledge at the beginning of my Ph.D. period, I went through rough days. However, he has been guiding me patiently and generously. Following his teaching, I began to walk on the road of scientific researching. I have learned a great deal in these years under his guidance, encouragement, supporting, trust and patience. Meanwhile, he is also my mentor in life. With his suggestions and teaching, I learned how to face and overcome failures, obtained numerous valuable tips of social skills, broadened my horizon and improved my logical thinking pattern. Deeply and sincerely, I appreciate his teaching, trust and supporting.

Next, I appreciate **Prof. Seema Agarwal** sufficient care, guidance in researching work, and her high efficiency while proofreading my manuscripts. She is also very supportive of my works. She gave me a lot of valuable suggestions on my projects and helped me to develop a logical way of thinking as well. Her dedication to science and caring for her students and the whole MC II group made me a very deep impression. When I'm depressed sometimes, but fortunately her encouragement could cheer me up.

I would like to present my thanks to **Prof. Haoqing Hou** in Jiangxi Normal University, for suggesting and recommending me to the Mc II group for pursuing my Ph.D. degree. I very appreciate his guidance and supporting during my master's degree. I am deeply impressed by his diligence and knowledge.

My sincere thanks go to **Prof. Paul Smith** for his valuable suggestion and discussion on the multifibrillar fibers work and proofreading of the manuscript. He offered me a lot of valuable expert advice on the mechanical properties of multifibrillar fibers and the polarized photo luminescent fibers. He also shared many of his funny stories in life. I enjoyed working and talking with him. Meanwhile, my sincere thanks go to **Prof. Anna Köhler** for her professional and kindly help during our cooperation work in the photo luminescent fibers. I am very impressed by her meticulous spirit and attitude of scientific research. She shared her professional manuscript writing skills with me and encouraged me. And I also appreciate **Prof. Hans-Werner Schmidt** rigorous approach

and valuable suggestion while proofreading my manuscripts. Many people have helped me a lot in the high strength and toughness multifibrillar fiber and photo luminescent fiber projects. Here, I would like to thank **Dr. Martin Dulle** and **Prof. Stephan Förster** for SAXS measurements and scientific discussion, **Dr. Juliana Martins de Souza e Silva** and **Prof. Ralf B. Wehrspohn** for the X-ray computed tomography, evaluation and scientific discussion, **Prof. Eyal Zussman** for the valuable expert scientific discussion on the mechanical properties of multifibrillar fibers, **Dr. Frank-Julian Kahle** and **Dr. Bin Liu** for the photo luminescent measurements, analysis, scientific discussion and manuscript proofreading, **Prof. Heinz Bässler** and **Prof. Xinghong Zhang** for their valuable suggestion, discussion and proofreading of the manuscript on photo luminescent fiber project, **Dr. Holger Schmalz** and **Dr. Lothar Benker** for measurements of polarized Raman spectroscopy, **Mr. P. Schmidt**, **Mr. M. Gaag** and **Mr. T. Braun** for supporting in construction of the yarn electrospinning of related set-ups, **Prof. Shaohua Jiang** for advice in electrospinning, and **Adrian Wambach** for technical support with figures and data arrangement. Without their contribution and kindly help, these projects could never have achieved a high level.

I'd like to thank all my dear colleagues in the MC II group for their useful discussions, suggestions and enjoyment during and after work. Firstly, I thank former colleagues, **Dr. Judith Schöbel**, **Dr. Gaigai Duan**, **Dr. Markus Langner**, **Dr. Jian Zhu**, **Dr. Oliver Hauenstein**, **Dr. Ziyin Fan**, **Dr. Li Liu**, **Dr. Steffen Reich**, **Dr. Ling Peng**, **Dr. Roland Dersch**, **Dr. Hui Wang** and **Dr. Matthias Burgard**, for their valuable scientific discussion and knowledge exchange of related topics. Besides, I very much appreciate **Rika Schneider's** assistance with polymer synthesis, GPC measurements and many help in laboratory works. And appreciations to **Martin Pretscher** for helping me translate the summary of my Ph.D. thesis, and many valuable suggestions in my study and life as well. I also would like to thank current colleagues, **Michael Mader**, **Lu Chen**, **Stefan Feth**, **Yuanhu Zhang**, **Benedict Petran**, **Qiang Gao**, **Christian Hils**, **Amir Reza Bagheri**, **Julia Kronawitt**, **Chen Liang**, **Xue Lin**, **Mina Heidari**, **Mahsa Mafi**, **Chengzhang Xu**, **Simon Neumann**, **Pin Hu**, **Sören Schumacher**, **Anil Kumar**, **Nikola Majstorovic**, and **Elmar Sehl**, who have been providing many kindly help, suggestions, and nice atmosphere around me. Thanks also go to **Annette Krökel** for solving lots of laboratory related problems. Moreover, secretary **Ms. Gaby Rösner-Oliver** and **Mr. Niko Plocher** have been assisting me in all the complex administrative work, which I very much

appreciate.

My thanks also go to the **University of Bayreuth Graduate School** for supporting me to attend the 4th international conference (NANOFIBERS, APPLICATIONS AND RELATED TECHNOLOGIES) at the Technical University of Liberec in Liberec, the Czech Republic in 2019.

I am very much thankful for the family education and unconditional support from **my mother and father**. Although they are not highly educated, they always teach me to be humble in victory and gracious in defeat, and offer me a good environment and atmosphere for learning. Their unconditional love and supporting gave me the impetus to move forward.

At last, I'd like to express my sincere appreciation to my beautiful wife **Meizhen**. This kindly lady and I went through lots of toughness together and have the crystal of our love finally – our lovely angel **Xinyue**. I am very grateful that my wife understands and supports me, takes care of my daily life, and gives me so sweet daughter.

5 (Eidesstattliche) Versicherungen und Erklärungen

(§ 9 Satz 2 Nr. 3 PromO BayNAT)

Hiermit versichere ich eidesstattlich, dass ich die Arbeit selbstständig verfasst und keine anderen als die von mir angegebenen Quellen und Hilfsmittel benutzt habe (vgl. Art. 64 Abs. 1 Satz 6 BayHSchG).

(§ 9 Satz 2 Nr. 3 PromO BayNAT)

Hiermit erkläre ich, dass ich die Dissertation nicht bereits zur Erlangung eines akademischen Grades eingereicht habe und dass ich nicht bereits diese oder eine gleichartige Doktorprüfung endgültig nicht bestanden habe.

(§ 9 Satz 2 Nr. 4 PromO BayNAT)

Hiermit erkläre ich, dass ich Hilfe von gewerblichen Promotionsberatern bzw. -vermittlern oder ähnlichen Dienstleistern weder bisher in Anspruch genommen habe noch künftig in Anspruch nehmen werde.

(§ 9 Satz 2 Nr. 7 PromO BayNAT)

Hiermit erkläre ich mein Einverständnis, dass die elektronische Fassung meiner Dissertation unter Wahrung meiner Urheberrechte und des Datenschutzes einer gesonderten Überprüfung unterzogen werden kann.

(§ 9 Satz 2 Nr. 8 PromO BayNAT)

Hiermit erkläre ich mein Einverständnis, dass bei Verdacht wissenschaftlichen Fehlverhaltens Ermittlungen durch universitätsinterne Organe der wissenschaftlichen Selbstkontrolle stattfinden können.

.....
Ort, Datum, Unterschrift